Macromolecular Materials and Engineering
www.mame-journal.de

# Materials Requirements in Fused Filament Fabrication: A Framework for the Design of Next-Generation 3D Printable Thermoplastics and Composites

*Antonella Sola*

**Fused filament fabrication (FFF), also known as fused deposition modeling, is the leading technology for polymer-based additive manufacturing. The simplicity, along with the cleanness, the affordability, and the multi-material capability, are some of the main advantages that have prompted this success. Nonetheless, the uptake of FFF in industry is hampered by the limited functionality of commercial filaments, that are often based on plain thermoplastics. The future growth of FFF into new markets needs a significant improvement of available materials. However, materials requirements in FFF are complicated and often mutually conflicting. Whereas heuristic approaches to materials design imply significant costs in terms of time, energy, and materials, a critical survey of the main requirements that a new material should fulfill in order to be printable and suitable for commercial adoption is still missing. In order to bridge this gap, the present paper analyzes the workflow from filament production to end-of-life disposal of printed objects, and, for each step, brings to light the governing materials properties. Wherever possible, practical guidelines are given on acceptable values. Existing lacks of knowledge are identified to direct future studies. The ultimate goal is to provide a road map to making materials development in FFF more efficient.**

## 1. Introduction

Fused filament fabrication (FFF), also known as fused deposition modeling (FDM, which is the original trademark by Stratasys), is currently one of the most popular additive manufacturing (AM) techniques.[1] According to the classification in ISO/ASTM 52900,[2] FFF belongs to the "material extrusion" group, as the functioning mechanism of this technique relies on the feedstock material, typically a thermoplastic or a thermoplastic-matrix composite, being heated until soft and forced to flow (namely, extruded) through the print nozzle. As the "fused filament fabrication" name suggests, the feedstock must be a filament, intuitively resembling a long string. For this reason, the material needs to be thermally processed at least two times, once from pellets to filament and then from filament to printed object.

Nowadays, many review papers in the literature provide the reader with exhaustive information about the properties of existing and emerging materials in FFF.[3–22] The scope of this article is different, since it specifically explores the requisites that a material should satisfy to be printable in FFF. The question "what makes a material printable" (in FFF) has already been put forward by Duty et al.[23] and then elaborated by Das et al.,[24] with an emphasis on rheology. However, a survey that encompasses the whole FFF process, from feedstock preparation to printing to finishing, is still missing.

After a summary of the main advantages that justify the increasing popularity of FFF, the following sections discuss the critical importance of understanding materials requirements in FFF. The printing process is then analyzed in order to identify the materials properties that govern each step. To conclude, an overarching table helps materials scientists and developers navigate themselves through the challenging task of merging printability and functionality.

## 2. Competitive Advantages of FFF

The success of FFF with scientists, developers, and even hobbyists depends on several synergistic factors.

Firstly, a key advantage of FFF is its simplicity. In principle, the functioning mechanism is straightforward. As shown in **Figure 1**, parts are printed layer-upon-layer starting from a filament, typically made of a thermoplastic material or a thermoplastic-matrix composite.

The filament is fed into the printhead by the action of two counter-rotating wheels (sometimes, rollers) actioned by a

A. Sola
Commonwealth Scientific and Industrial Research Organisation (CSIRO)—Advanced Materials and Processing Program
Manufacturing Business Unit
Clayton VIC 3168, Australia
E-mail: antonella.sola@csiro.au

The ORCID identification number(s) for the author(s) of this article can be found under https://doi.org/10.1002/mame.202200197



**DOI: 10.1002/mame.202200197**

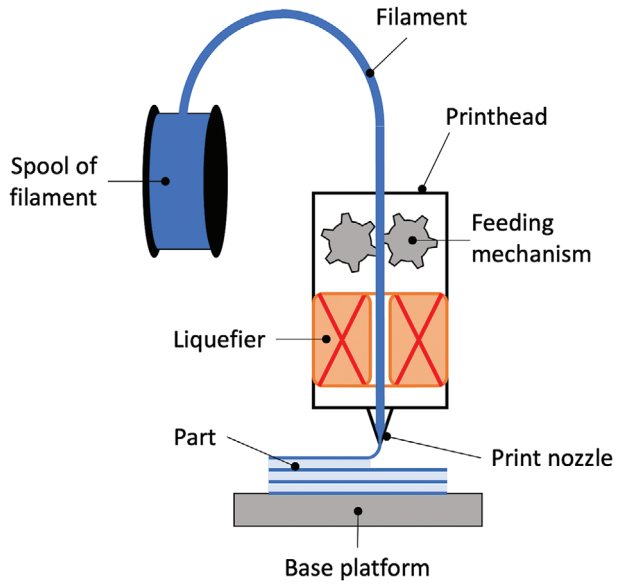


**Figure 1.** Schematic representation of the printing process by FFF. The feedstock material in filament form is fed into the liquefier by two counter-rotating gears, and then heated until soft in the liquefier, and deposited on the base platform (or on the previous layers) through the print nozzle. The 3D part is built layer-upon-layer. (Note: drawing not in scale.)

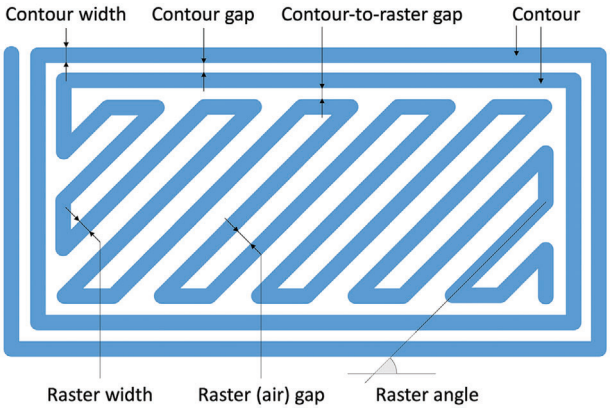


**Figure 2.** Basic structure of a single layer in FFF, comprised of internal rasters and contours.

stepper motor. In standard FFF systems, the filament enters the feeding mechanism tangentially to the surface of the wheels. As discussed in Section 5.1, at least one of the wheels has teeth that actually cut onto the surface of the filament thus preventing slippage, but leaving marks on the filament. The pinch wheel is mounted on a spring arm that applies a normal force against the filament to maintain traction with the drive wheel. Ideally, perfect (slip-free) traction is established between the filament and the wheels. The core of the printhead is the liquefier (heater), where the material is heated. The material softens more as the temperature increases, to the point that it can flow under the force applied by the colder and stiffer filament a. Working like a piston, the filament at the entrance of the liquefier pushes the softened material out of the print nozzle. Simultaneously, the printhead swipes across the base platform (in the *X*–*Y* plane) following a computer-controlled toolpath, and selectively deposits the material where it is needed to draw the part's geometry. As illustrated in **Figure 2**, each layer is built up by the progressive addition of neighboring rasters (also known as roads or beads), generally surrounded by contours along the perimeter. After completing the first layer, the base platform moves downward (or, depending on the printer, the printhead moves upward) along the growth direction (*Z*-axis) and the printhead lays down a second layer of material on top of the previous one. The process is repeated until completion of the desired 3D shape.[25,26] In common FFF printers, the printhead sits on a *X*–*Y* gantry that translates along the *Z*-axis. Otherwise, in Delta printers the printhead may be hinged to three or more arms that slide along vertical rails. Quite often, the base platform is round. This enables the fabrication of small and tall parts. In selective compliance assembly robot arm (SCARA) printers, the printhead is linked to a robotic arm and there is no in-built base platform. While these models are based on Cartesian coordinates, in polar printers the build volume is mapped out according to a polar coordinate system and the printhead is connected to a curved arm that swings on a spinning circular base platform.[27]

Secondly, printing by FFF is relatively clean. Since the feedstock material is a filament, FFF mitigates the potential safety, occupational and environmental issues related to working with powders, especially micron- and sub-micron-sized ones[10,28,29] (however, powders and additives may be required in experimental materials and composite filaments. Additional detail regarding safety issues in FFF is provided below in a dedicated section—Section 7.3). Moreover, FFF does not require organic solvents, nor does it involve the presence of sticky resins or inks. If the object is properly designed for FFF printing, the waste material originated from removable supports is limited and, in principle, defective parts from failed jobs can be recycled.[30–32] The assessment of particulate emission and volatile organic compounds (VOCs) is presently the subject of research, since additives may lead to the release of noxious substances in the temperature range typically required for printing by FFF.[33] However, for most feedstock materials, especially poly(lactic acid) (PLA) which is bio-based and low melting (thus requiring a relatively low printing temperature), a well-ventilated place may suffice to work safely, although the safe operating instructions are different for each material and should be carefully considered before printing.[34,35]

FFF is very versatile, since it is compatible with a wide range of thermoplastic-based materials.[36] Although this requires additional equipment, FFF can also be the starting point to obtaining fully inorganic parts.[37] To this aim, an FFF printer is used to print a green part starting from a composite feedstock material with a very high filler loading ("shaping"). Then, the polymer matrix is removed by thermal, chemical, or catalytic routes ("debinding") and, finally, the green object is "sintered" to consolidate the inorganic filler into a solid part. Accordingly, this three-step workflow is often called "shaping, debinding, and sintering" (SDS). However, it is worth mentioning that SDS is a very general term that encompasses all different shaping techniques that can include injection molding (e.g., ref. [38]) and profile extrusion (e.g., ref. [39]) when dealing with thermoplastics, as well as other material extrusion-based AM methods leading to fully

 

inorganic parts,[40] or even AM techniques based on photosensitive resins like vat photopolymerization (VPP),[41] and binder jetting.[42] Historically, the names "fused deposition of ceramics" (FDC) and "fused deposition of metals" (FDMet) have been very common in the literature regarding FFF,[40] and the term "metal fused filament fabrication" (MFFF, MF3, or MF$^3$) is also gaining popularity to describe FDMet (e.g., refs. [43, 44]).

FFF is suitable for multi-material printing.[45,46] Nowadays, most professional printers, as well as many desktop printers, come with two (or more) nozzles, which makes it possible to simultaneously process two (or more) feedstock materials. For example, one nozzle can be dedicated to the main structural material, and the second one to the support material. Otherwise, two structural materials can be co-printed in order to impart different colors or different functional properties (e.g., electrical conduction/insulation) to selected areas of the same object. Advanced equipment may also come with multiple nozzles for extended materials options.[47,48]

Recently, FFF has proved to be a viable technique for 4D printing, which, according to the original definition formulated by Prof. Tibbits, is a "new process that demonstrates a radical shift in additive manufacturing. It entails multi-material prints with the capability to transform over time, or a customized material system that can change from one shape to another, directly off the print bed".[49] In practice, time is the fourth dimension (hence, the name "4D printing") that adds a new degree of freedom over conventional 3D printing[50,51] and imparts new stimuli-activated functional properties.[52] Many routes have been successfully attempted to enable responsiveness over time of FFF parts, including printing of smart polymers and composites, multi-material printing of materials having a controlled thermo-dilatometric mismatch, and single-material printing of specially designed architectures whereby the local response is controlled through the raster orientation.[53]

Generally speaking, 3D printing is revolutionizing the existing paradigms in manufacturing because building up a part by means of the selective addition of material paves the way for unprecedented freedom in geometry and customization.[54] On top of this, FFF is one of the few AM techniques capable of fabricating hollow parts.[55] Although very large or complicated cavities may require support structures,[56] the ability to print hollow parts is key to producing advanced components that leverage the presence of engineered cavities, such as the honeycomb of lightweight sandwich structures.[57] Also, inter-connected pores are fundamental structural features of scaffolds for biomedical applications, especially for bone tissue engineering. Scaffolds are highly porous structures intended to support the spontaneous healing processes of natural tissues, or to create a 3D environment for in vitro tests and cultures. Large (around 300 μm) and interconnected pores are needed to allow for cell migration, revascularization, and removal of physiological by-product.[58,59] Whereas conventional processing methods control the scaffold's porosity on average terms (average porosity, average pore size, average pore-to-pore opening size), the adoption of AM makes it possible to produce and consistently repeat the exact porous structure that is needed for a given application and, if required, to mimic the anatomy of the patient.[60]

The capability of FFF to deal with hollow structures is conducive to the development of parts with a sparse infill pattern.

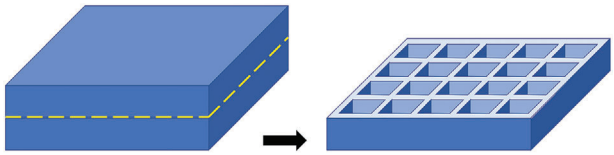

**Figure 3.** Example of a part printed with a sparse infill pattern. While the object looks fully solid as seen from outside, the interior is mostly hollow, with few internal walls that bridge the external surfaces and give strength to the structure.

Whereas structural components should be fully solid to withstand load-bearing functions, non-structural parts can be printed leaving a gap between adjacent rasters or even with internal void patterns, which is helpful to reducing material's usage, part's weight, and residual stresses, while maintaining the visual appearance of the printed object. **Figure 3** shows an example of a simple part printed with a sparse infill pattern. Reducing the infill degree lowers the tensile properties, including tensile stiffness and strength, of the printed part.[61,62] However, according to experimental results reported under flexural load,[63] there is not a linear correlation between infill degree and flexural strength, which means that the properties of a part printed with, for example, a 60% infill degree will likely exceed 60% of the properties of the same part built with a 100% infill degree. Moreover, it has also been observed that working with infill degrees lower than 100% and combining them with solid layers with 100% infill degree on top and below (thus obtaining sandwich panel-like structures) allow designers to keep the weight down and simultaneously maintain the flexural strength of FFF printed specimens.[64] According to the results of the combined analytical–experimental model developed by Phan et al.,[65] the apparent bending strength of FFF parts, namely the bending strength calculated as a function of the nominal cross sectional area, is deeply affected by the infill degree. Intuitively, the apparent bending strength becomes lower as the raster gap is increased (which corresponds to having lower infill degree). However, although this may seem counterintuitive, the strength of the bond established between subsequent layers increases as the raster gap is increased. This means that, if the raster gap is increased, the contact area between subsequent layers is reduced, but the intrinsic strength of the bond developed within this contact area is improved as a consequence of the different thermal history experienced by the printed rasters.[65] Last, the strength of FFF parts can be enhanced through the appropriate design of the raster pattern.[66] In other terms, the correct choice of the infill degree (which defines how much material is printed) and pattern (which dictates where the material is printed) allows the performance-to-weight ratio to be maximized.

An additional advantage is that FFF is comparatively affordable with respect to other AM systems. For example, a selective laser sintering (SLS) printer for polymer-based feedstock typically exceeds 40000 USD, whereas a desktop FFF printer may cost just a few hundred dollars.[67] FFF printers for industrial usage are more expensive than do-it-yourself (DIY) ones and the investment cost conceivably increases with the introduction of special features such as a heated base platform or an enclosed build volume. However, it has been proven that, if the printing parameters are properly tuned, the quality (e.g., tensile properties) of polymer parts built under normal conditions with prosumer printers may

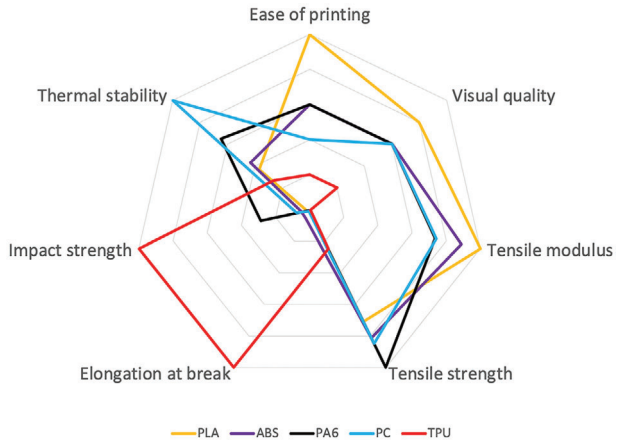


**Figure 4.** Radar chart comparing relevant features of some common FFF materials, including poly(lactic acid) (PLA), acrylonitrile-butadiene-styrene (ABS), polyamide 6 (PA6, or nylon 6), polycarbonate (PC), thermoplastic polyurethane (TPU). The graph accounts for printing-related properties (ease of printing and visual quality), tensile behavior (tensile modulus, ultimate stress, and elongation at break), impact resistance, and thermal stability (through the heat deflection temperature, HDT, at 66 psi = 0.46 MPa).

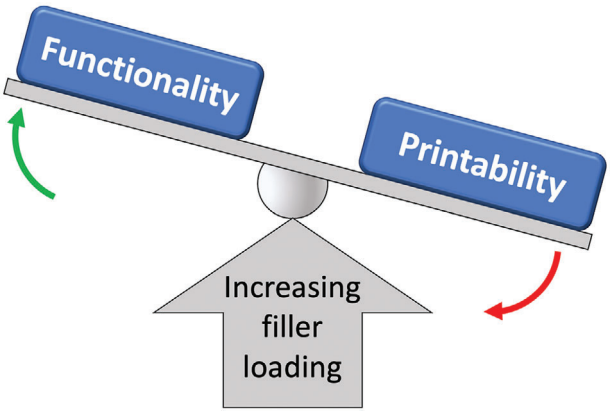


**Figure 5.** Oftentimes, printing requirements and functional needs follow opposite trends and a delicate balance must be reached. For composite materials, increasing the filler loading may help to potentiate the targeted functionality (for example, electrical conductivity), but it may also hamper the original printability of the thermoplastic matrix.

compete with industrial benchmarks produced with professional equipment.[68–70]

## 3. Materials Development for the Advancement of FFF

AM is widely recognized as a driving force of the Industry 4.0 revolution, as it sits at the intersection of smart production systems and virtual prototyping.[71] In particular, owing to its numerous advantages, nowadays FFF is very common both in academia and in industry, where it is progressively transforming the approach to manufacturing. Even hobbyists appreciate it. However, the advancement of FFF from being a "rapid prototyping tool" to becoming an "industrial manufacturing method" is being delayed by the limited functionality of thermoplastic materials that are conventionally processed in FFF.[72] The radar chart in **Figure 4**, which has been completed according to the material data sheets of commercial FFF feedstock materials[73] and according to information available online[74–76] and in published scientific papers,[15,77,78] provides a comparison of the main features of some common FFF materials, including PLA, acrylonitrile-butadiene-styrene (ABS), polyamide 6 (PA6, or nylon 6), polycarbonate (PC), and thermoplastic polyurethane (TPU). Information about other thermoplastics that are processed by FFF can be found in other sections (for example, polycaprolactone (PCL) in Section 5.4, poly-ether ether ketone (PEEK) and poly-ether ketone ketone (PEKK) in the same Section 5.4, and polyhydroxyalkanoate (PHA) bioplastics in Section 6.6), whilst Figure 18 in Section 6.3 summarizes the tensile stiffness and strength of parts fabricated with numerous commercial filaments.

For example, PLA is the easiest material to print by FFF and, apart from technical polymers such as PEEK or PEKK, is also one of the stiffest, having a Young's modulus around 3 GPa.[79] However, PLA is very brittle, which prevents it from being applied for structural purposes. Also, like the greatest part of thermoplastics, PLA is not electrically conductive, which is a hindrance to the development of 3D printed circuitry, electronic, and robotic devices. PLA is not thermally conductive, and this impedes the production of thermal exchangers or other components, such as molding tools, that require efficient heat dissipation.[80] Although it has been "generally recognized as safe" (GRAS) by the American Food and Drug Administration (FDA),[81] PLA is not able to promote bone growth, which would be required for the development of bone implants and porous scaffolds for bone tissue engineering.[82] This explains the attention that scientists and researchers are paying to composite feedstock materials, whereby the addition of appropriate fillers may impart new functionality. For example, the addition of bioactive fillers to a PLA-based matrix is a well-established procedure to prepare bioactive composites,[83] with an ever-increasing number of examples in relation to 3D printing.[84–86]

The adoption of FFF in areas of strategic importance like biomedicine, defence, robotics, aerospace and aeronautics, transport, and civil engineering is thus jeopardized by the deficiency of adequate materials for the industrial manufacturing of devices capable of real-world functionality.[10,72,87–89] Driven by growing industrial needs and prompted by the expiry of relevant patents in 2009,[90] research in novel materials for FFF has been flourishing over the past 10 years, with hundreds of papers being published annually. Great attention has been paid to advanced polymers, polymer blends, and polymer-matrix composites with embedded functionality.[91] However, the development of new printable materials remains very challenging because, in spite of its apparent easiness, FFF actually poses numerous, and often conflicting, materials requirements. In this regard, it is important to point out that, in order to be appealing to the market, any new feedstock material should be compatible with standard FFF printers or, at least, should require minimum adjustment of the printing hardware.[19] However, as sketched in **Figure 5**, in many cases printability and functionality follow opposite trends. For example, the electrical conductivity of thermoplastic-matrix composites usually increases with higher filler loadings, whilst the

 

printability decreases due to the altered mechanical and rheological properties of the matrix (with the ratio between compressive modulus and viscosity playing a critical role for printability as further discussed in Section 5.2), and due to the higher risk of clogging the print nozzle upon printing.

Ultimately, a clear understanding of materials requirements in FFF is crucial to directing research in new materials that are easy to print and, at the same time, apt to address specific functional needs.

## 4. Filament Production

Commercial feedstock for FFF is available in filament form, with the standard diameter being either 1.75 or 2.85 mm. Filaments come as spools typically weighing between 300 g and 2 kg. In order to compete with existing products, new materials for FFF should be easily processed into filaments having similar properties. However, this poses numerous challenges in terms of production volume, extrudability, filament size (diameter and length), and spoolability.

### 4.1. Production Volume

Upon developing a new material for FFF, the first issue to tackle is the production volume. Whereas experimental materials are often formulated in small batches, the fabrication route should be affordable and viable for industrial scale-up. This may be relatively straightforward for neat polymers, but becomes more challenging for advanced materials and especially for composites. This also results in different costs. For example, PLA filaments for DIY generally cost between 25 and 50 USD $kg^{-1}$, but high end-use materials (for example, special electrically conductive PLA-matrix composites) may be much more expensive and exceed 2000 USD $kg^{-1}$.

Presently, there are two main methods for obtaining continuous fiber reinforced parts. According to the dual nozzle method, a neat polymer filament and a polymer-impregnated fiber-reinforced filament are fed and printed through two separate nozzles (or printheads). According to the in-nozzle impregnation method, the fibers are fed into the liquefier, where they become impregnated with the molten polymer and then printed. In both cases, special extrusion and printing equipment is required for processing continuous fiber-reinforced filaments.[13,92,93]

Conversely, filaments with discrete fillers, if properly fabricated, can be processed on any standard printer. There are three main approaches to producing thermoplastic-matrix composites with discrete fillers, namely: i) in situ polymerization, ii) solvent mixing, and iii) melt compounding.[94,95] The in situ polymerization method implies to disperse the filler in the liquid monomer, and then to initiate and drive the polymerization reaction in the presence of the filler's particles, that may act as catalyzers for the on-going reaction. In solvent mixing, the polymer matrix is dissolved in an appropriate solvent that does not affect the filler. The filler is then added into the polymer solution. The filler can be either in the dry state or, more commonly, preliminarily dispersed in a liquid medium that may be or may be not the same solvent used for the matrix. As for melt compounding, the filler is mixed into the molten (or, strictly speaking, heated until soft, if the thermoplastic is amorphous) matrix by shear stresses exerted by the action of an extruder or of an internal mixer.[95]

Out of these three possible approaches, in situ polymerization is most rarely seen in the literature regarding FFF, because controlling the polymerization reaction in large volumes may be cumbersome.[82] Owing to the presence of the solvent acting as liquid carrier, solvent mixing, especially if assisted by (ultra)sonication, can be extremely effective in breaking down aggregates and achieving a uniform filler distribution.[96,97] However, substantial amounts of solvent would be required for large scale production. Also, the complete removal of any residue of solvent after mixing is an energy-consuming process. As a consequence, solvent mixing is mainly used in FFF for the production of masterbatches.[82] According to the masterbatch technique, a small volume of composite having a high filler loading is first obtained by solvent mixing or by melt-compounding and then diluted to the targeted (lower) concentration by melt compounding with additional neat polymer matrix. This approach has been demonstrated both with micron-sized fillers (for example, ZnO micro-particles[98]) and with nano-sized fillers (for example, carbon nanotubes, CNTs[99]). In order to improve this two-stage process, it is a good practice to start with a low viscosity grade of the thermoplastic matrix, and then dilute this with a higher viscosity grade of the same thermoplastic.[100]

Melt compounding is ultimately the preferred way of producing composite feedstock for FFF. Since the material must be extruded into a filament, the easiest option is to melt compound filler and matrix inside the extruder directly, so that compounding and extrusion can be completed in a single step. Twin-screw extruders are typically run to this purpose on account of their good mixing ability.[101] Sometimes, dry polymer and filler can be physically pre-mixed in a low energy stirring mixer or in a plastic bag.[102] However, this may be not sufficient to break down the aggregates and distribute the filler properly. The mechanical processing of powder mixtures by ball milling is known to be very effective to induce intimate mixing through repetitive plastic deformation and to reduce the size of particle aggregates.[103] The effectiveness of ball milling prior to extrusion has been demonstrated, for example, by the flexible strain sensors printed by Yang et al.[104] Matrix and filler can also be pre-mixed by solvent mixing,[102] as seen before. Alternatively, pre-mixing can be completed by melt compounding in an internal mixer, whose chamber is designed to promote a very fine and even distribution of the filler.[105] Although it has been proven that the mixing ability of twin screw extruders may exceed that of internal mixers,[106] pre-mixing in an internal mixer may be convenient if the twin screw extruder does not have feeding units for all the ingredients used in the compound. Critical materials that are difficult to compound may be extruded two (or more) times, with the first extrusion cycle(s) acting as pre-mixing step(s).[107]

Sometimes, unfavorable reactions may take place between the filler and the matrix upon mixing. For example, some fillers such as ZnO are known to trigger the thermal degradation of PLA.[98] Whilst the easiest option would be to change the matrix or the filler, sometimes this is not possible, because composite materials are conceived for combining specific attributes of each constituent phase to meet demanding service requirements (for example, the antimicrobial properties of ZnO with the biocompatibility and ease of printing of PLA[82,108] in order to produce

patient-specific biomedical devices with limited risk of infection transmission). Under these circumstances, special measures (for example, adjusted processing parameters to minimize the residence time at high temperature, or a surface treatment of the filler's particles[82]) should be put in place on a case-by-case basis to mitigate the side effects.

### 4.2. Extrudability

The key step in the manufacturing of FFF feedstock is producing a filament with the correct diameter over a sufficient length. This point is sometimes overlooked in the literature, maybe because it is considered trivial, however, the capability of being formed into a filament is actually a crucial requirement that significantly narrows down the range of materials suitable for FFF. For example, thermoplastic-based materials can be extruded into filaments, whereas common thermosets cannot. Metal filaments can be easily produced by wire drawing. Conversely, most ceramics are not capable of being formed into very long filaments, although there are some exceptions. For example, glass-based optical fibres may be hundreds of metres long, but the diameter is usually some tens of microns,[109] which is therefore around one order of magnitude smaller than the standard diameter of filaments for FFF.

Thermoplastic-based filaments are typically produced via extrusion. Piston extrusion, which allows for fabricating filaments in small quantities, is used for trial runs only. Screw extrusion, either with a single-screw extruder or with a twin-screw extruder, is used for continuous filament production. Twin-screw extruders are more efficient in mixing, whereas single-screw extruders exert a higher extrusion pressure that enables a high and constant throughput.[15,101,110–112]

In order to be extrudable, thermoplastic materials should fulfil some basic requirements. First of all, they should be capable of being melt processed. As for the processing temperature, the extrusion temperature for most polymers should be around 20–40 °C higher than the glass transition temperature. The polymer should be able to withstand the processing temperature without degrading for the whole duration of extruding.[113] Another important parameter is the so-called melt strength, which is the maximum stress required to break the extruded strand of material. In practice, melt strength is an engineering measure of the resistance to stretching (extension). For this reason, melt strength is often assimilated to extensional viscosity,[114] as they similarly depend on the resistance to untangling under strain.[115] The properties that govern the resistance to untangling are the molecular weight, the molecular weight distribution, and the molecular branching of the polymer. As each property increases, the melt strength also increases.[116,117] Branching is particularly important, as linear chains can disentangle more easily than branched ones when a strain is applied.[116,118] Having a high melt strength is key for extruding, as it avoids drawdown and sagging at the spinneret exit[116] and enables the material to be stretched more and result in a stronger extruded part.[118]

Whilst extruding neat polymers is a well-established procedure, the presence of a filler unavoidably changes the thermal and rheological properties of the matrix, sometimes with contrasting effects.[10] Much attention should be paid to prevent the filler from aggregating and to promote a uniform distribution, which are pre-requisites for achieving high-quality printed composites.[119] Although the diameter of the spinneret required for extruding FFF filaments is relatively large, in principle filler aggregates, if bulky, may cause blockage.[120] Other issues that may occur upon extruding composite filaments for FFF include the wear of the screws, the barrel and the spinneret due to the abrasive action of hard fillers, the fracture of brittle fillers having a high aspect ratio, and the loss of material because of the filler being thermally decomposed (especially vegetable fillers) or stuck onto the internal surfaces of the extruder (especially inorganic fillers).[107,121–124]

### 4.3. Filament Geometry: Diameter and Length

To be printable, filaments must have a perfectly round cross section with a consistent diameter, ideally corresponding to the standard sizes available in the marketplace.

Due to shear-induced molecular orientation, extruded polymers may experience a differential shrinkage, which may ultimately lead to an oval cross section of the filament. Especially in experimental settings, a filament that does not have a perfectly round cross section may be still printable, but the quality of the printed part will suffer if the cross section is not constant throughout the length of the filament, as this may cause inhomogeneous deposition of material upon printing, or even interrupt the printing job.[125]

The scientific literature is accomodating in terms of filament diameter, since large variations may be accepted for small-scale production and proof-of-concept research, with deviations that may reach 19% from the nominal value.[126] However, if industrial filaments are considered, the tolerance is very tight, since commercial printers use filaments with a diameter of either 1.75 $\pm$ 0.1 or 2.85 $\pm$ 0.1 mm.[127] If the filament is too thin, the feeding mechanism is unable to pinch it properly and, once the filament is inside the printhead, the mismatch between filament and liquefier wall creates a gap that hinders heat transfer. Conversely, if the filament is too thick, the feeding mechanism is likely to clog. Also, changes in the filament diameter cause under- or overfeeding and, ultimately, impair the print quality.[128,129]

The obtainment of a consistent diameter corresponding to the nominal value largely depends on the correct set-up of the extruding apparatus, including any potential ancillary units like the water (or ice) bath or fans utilized to cool down the filament at the exit of the spinneret, or the winding system run to spool the filament and, at the same time, to draw it to the desired size.[126] However, the intrinsic properties of the material being extruded are equally important. A fundamental requirement is that the material must be heated to the right viscosity to smoothly flow through the spinneret. Although the viscosity limits should be exactly defined for individual systems as a function of the specific equipment and materials in use, a viscosity of 10000 Pa s can be considered as the upper limit for screw-based extruders. Above this threshold, the torque may become excessive and damage the extruder.[124] On the opposite end, Zavrel et al.[124] observed that PCL-hydroxyapatite composite filaments became too sticky and unable to hold their shape after leaving the spinneret when the viscosity became lower than 5000 Pa s.

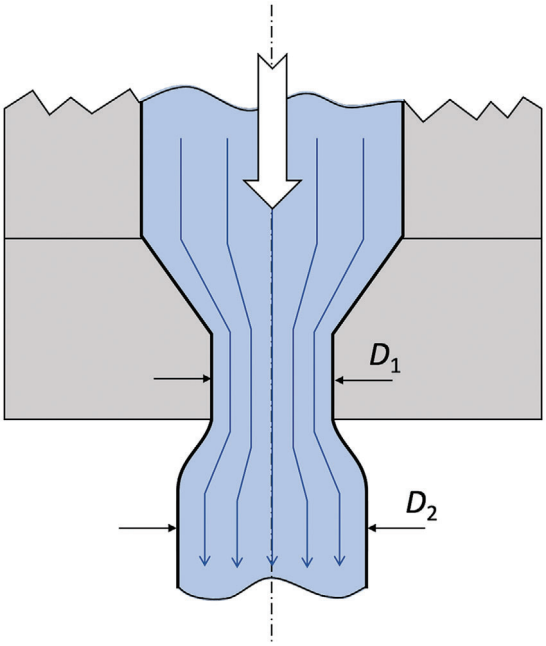


**Figure 6.** After leaving the nozzle tip, the diameter of the extrudate, $D_2$, increases over the nominal diameter of the orifice, $D_1$, due to the recovery of the elastic deformation. This phenomenon is generally known as "die swelling" effect.

At the exit of the extruder tip, all materials experience the so-called "die swelling effect," which is an increment in diameter as a consequence of the recovery of the elastic component of the deformation that the material receives while transitioning through the die.[130] According to the symbols in **Figure 6**, the actual diameter of the filament, $D_2$, is thus larger than the nominal opening of the die, $D_1$, and the swelling ratio, $S$, quantifies this difference as:

$$S = \frac{D_2}{D_1} \tag{1}$$

Polymers with a high degree of branching and a high molecular weight are more "elastic," meaning that they have higher relaxation times, and this leads to more pronounced die swelling.[131] The swelling ratio typically ranges between 1.05 and 1.30 for the greatest part of thermoplastic materials relevant to FFF.[129] In this regard, it is interesting to note that the addition of a filler, especially if inorganic, is expected to limit the polymer chain mobility and hence the elastic recovery. This stabilizes the diameter of the extrudate, reduces the swelling ratio and facilitates the production a tightly controlled filament.[132,133] Intuitively, a longer residence time in the die will help relax the stored deformation energy. For this reason, the swell ratio may be reduced by reducing the shear stress and shear rate. Similarly, the swell ratio decreases with a rise of temperature. If the applied load and temperature cannot be changed, the die swelling effect decreases if the die diameter is reduced, or if the die length-to-diameter ratio is increased.[134] Working with a spinneret diameter smaller than the targeted diameter may be a practical strategy to counteract the die swelling effect. Otherwise, the diameter of the extrudate can be monitored and corrected through calibration units, adjusting haul off and winding speed.

Whereas this stabilizing effect is certainly advantageous, a processing issue with composite feedstocks may come from the so-called "wall slip phenomenon." Even if the mixing action of the extruder produces a homogeneous distribution of the filler in the barrel, the rigid filler is unable to adapt to the wall of the nozzle tip as effectively as the neat polymer does. The filler's particles are pushed back to the core of the filament, while a slip layer of neat polymer appears at the wall boundary. Wall slip has been defined as "ubiquitous" in rigid particle dispersions.[135] Though not ideal for the achievement of parts with a uniform filler distribution, the wall slip phenomenon (which occurs again through the print nozzle) may be tolerated for FFF purposes, provided that the inter-bead and inter-layer bonding mechanisms in the printed part are not impaired.[136]

The filament length is another critical feature. For example, the length of a standard 2 kg spool of PLA (density: 1.25 g $cm^{-3}$ [137]) is nearly 670 m. As a prime requirement, this entails the ability of the material to be consistently extruded into a hundreds-of-metres long filament without breaking or clogging. Additionally, the successful fabrication of a commercial filament also depends on the ability of the filament to be bent and wound on a reel, namely on its "spoolability" (sometimes, also referred to as "windability"). Otherwise, handling the filament would be unpractical.

### 4.4. Spoolability and Mechanical Behavior of the Filament

For the sake of practicality, commercial filaments are available as spools, which can be either loose spools for small-scale printers or spool-like cartridges for large-scale (industrial) printers.[129] At the exit of the spinneret, the freshly extruded filament is usually cooled down to "freeze" its diameter and then immediately wound on a reel. On professional extrusion lines, the winding unit is often coupled with a laser calliper and the spooling speed/traction force are continuously adjusted to control the filament diameter.

Although standard thermoplastics like PLA and ABS are relatively easy to handle, special polymers and composite materials may become brittle due to the presence of additives and fillers, and hence prone to breaking upon spooling and de-spooling. Whereas the standard size (internal diameter) of commercial spools can range from 5 to 10 cm, sometimes larger spools can be used to accomodate special filaments that are easy to break.[10] For research purposes, filaments that are too brittle to be spooled can be fed manually into the printer, one segment at time.[138] However, this procedure is incompatible with the need for automation that is a driving force in modern manufacturing. Also, the physical gap between subsequent segments is likely to trigger print defects. As a rule of thumb, it has been suggested that a material should have a minimum strain at yield of around 5% under tensile load in order for the filament to be spoolable.[139]

Spoolability becomes critical for composite filaments with a high filler loading, especially those for SDS, since the presence of a very high concentration of inorganic particles drastically limits the pliability of the filament. Achieving an even distribution of the filler in the polymer matrix is generally recognized as a

pre-requisite for enabling the extrudability as well as the spoolability of composite filaments for SDS.[140] The pre-mixing strategy plays a key role in this regard. For example, Hasib et al.[102] investigated the behavior of feedstock materials for SDS made of pulverized PLA pellets and Ni-Cu gas-atomized powders. The pulverized polymer and the inorganic filler were either physically preblended in a plastic bag, or solvent mixed in dichloromethane, and then extruded in a single screw extruder. After solvent mixing, the composite material could be extruded and spooled until the filler loading reached a maximum value of 62 vol%. Increasing the filler loading above this threshold led to extrudable but not spoolable materials. Above 63.4 vol% the composite could not be extruded anymore. As a term of comparison, physically pre-mixed materials could be extruded and spooled up to 43 vol% of filler loading, and remained extrudable but not spoolable up to 54 vol%.[102] This substantial difference was tentatively attributed to the fact that the physically pre-mixed feedstocks are prone to slippage at the high shear rate experienced while flowing through the extrusion die, which undermines the extrusion quality. Conversely, it was postulated that the action of dichloromethane in the solvent mixing step may weaken the secondary bonds between the macromolecules of the PLA matrix, which makes it possible for the polymer chains to disentangle more easily under shear and, thus, to form a larger contact area to the extruder walls with better adhesion.[102] In addition to this flow-related mechanism, another possible reason for the limited extrudability and spoolability observed after physical pre-mixing may be the different particle size of the pulverized polymer pellets (in the 2–4 mm range) and the gas atomized metal powders (having a median particle size of 62.4 μm) causing a size-driven separation upon shaking due to granular convection (Brazilian nut effect).[141]

Although this may cause a lower stiffness, the addition of plasticizers or thermoplastic elastomer (TPE) compounds may be necessary for improving the handleability of highly-loaded filaments.[119] In their investigation for new materials for the 3D printing of battery cells, Maurel et al.[142] observed that the total amount of filler within the filament should not exceed about 30 vol% when neat PLA is used as the matrix, whereas the filler loading may be increased to about 50 vol% with the introduction of a convenient plasticizer.

In order to mitigate the potential issue of breaking upon unspooling, commercial filaments for SDS often need to be preheated prior to printing. Increasing the temperature to a value close to the glass transition temperature of the main component of the polymer binder enhances the molecular chain mobility and augments the filament flexibility.

At present, there exists no standard method for quantifying the spoolability of a filament. Hasib et al.[102] defined the spoolability of a 2.85 mm filament as the "ability to wind at least 12 ft long uniform filaments in a 100 mm diameter spool without any breakage due to brittleness/stiffness," but they recommended to adjust this criterion according to the spool diameter and to the temperature of the filament during winding. Alternatively, bending tests may be useful to investigate the ability of the filament to be bent without breaking, which is informative about its spoolability.[143] In this regard, Wu et al.[143] designed a special testing equipment to measure the ability of the filament to be bent and thus to be coiled/uncoiled. The functioning mechanism is explained in **Figure 7**. Wu et al.[143] observed that commercial ABS filaments are

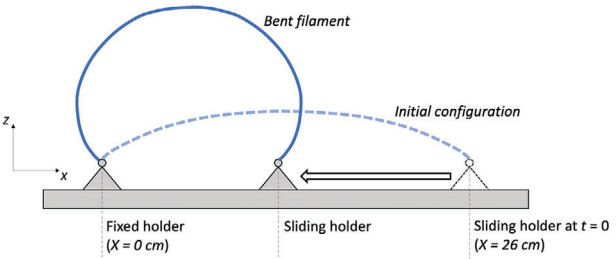


**Figure 7.** Experimental rig to compare the spoolability of experimental FFF filaments to commercial ones, as proposed by Wu et al.[143]

usually supplied on a spool with an internal radius of 4.5 cm. In order to verify whether experimental filaments may be able to match the ability to be bent of commercial reference filaments, Wu et al.[143] prepared 26.5 ± 0.5 cm long filament samples, and then clamped the ends of each sample in two holders that enabled the rotation in the vertical (*X*–*Z*) plane as the only permitted degree of freedom. Then, one holder was fixed as the "origin" at $X = 0$ cm, whereas the other holder was moved smoothly along a rail in the *X* direction from the $X = 26$ cm coordinate toward the origin. The sliding speed was kept constant at 4.7 cm $s^{-1}$. Upon testing, as the sliding holder approached the fixed holder, the filament sample progressively bent in the vertical plane until failure. The process was digitally filmed normal to the vertical plane and the frame at the point of failure was elaborated to determine the radius of curvature, *R*, by best fitting the sample's shape to a dome and applying the equation

$$R = \frac{\left(\frac{d}{2}\right)^2 + h^2}{2h} \tag{2}$$

where *d* is the diameter of the dome and *h* is the distance from the base to the highest point of the dome. Wu et al.[143] recommended to compare the curvature radius to that of commercial ABS filaments, which was around 4.5 cm.

In addition to spoolability tests, various mechanical characterizations have been proposed in the literature as a tool for preliminarily screening the printability of new materials for FFF. This topic is extensively discussed in the area of "3D pharming," which explores the feasibility and potential benefits of applying 3D printing to personalized therapeutics.[1,16,144–146] As pointed out by Naserredin et al.,[147] extrusion has long been used in the fabrication of traditional oral dosage forms, such as tablets. However, according to the traditional procedure, the extrudate must be broken down to pellets, or to fine particles, for subsequent processing, which is typically accomplished by compression. For this reason, extrudable materials for pharmaceutical applications are often brittle, because this reduces the time and energy required for milling them. However, brittle materials are unsuitable for FFF, since they are likely to break when handled or fed into the printer.[147] Predicting whether a filament can be printed or not before actually feeding it into the printer is particularly important in 3D pharming, since filaments are often loaded with expensive pharmaceutical ingredients and any blockages in the printhead may cause substantial material waste. Moreover, the feedstock material may become contaminated.[147,148]

Naserredin et al.[147] run mechanical tests on a custom-made texture analyzer that measured the filament's response under a compress-and-release cycle, and recorded a plot of the force (due to the filament opposing the applied deformation) as a function of the compression distance. After normalizing the data, it was possible to observe a close correlation between the filament's behavior under axial compression and its printability, since all the filaments that experienced brittle failure upon testing could not be printed ("brittle filaments"). Vice versa, all printable materials deformed under compression, but then recovered when the axial force was removed ("pliable filaments"). Interestingly, Naserredin et al.[147] also pointed out the existence of a third class of filaments, that could not be either tested or printed because too flexible and prone to collapse under their own weight ("string-like filaments").

Zhang et al.[149] proposed to verify the "stiffness" (defined as the "breaking stress"[149]) and the "brittleness" (defined as the "breaking distance"[149]) of filaments for FFF on a small-scale 3-point bending test apparatus, using 5 cm long filament segments as the test specimens. According to a modified testing protocol named "Repka–Zhang method", the "flexibility" (namely, "the tolerance of the filament to bending without breaking"[150]) and the "toughness/brittleness" (namely, "the breaking of the filament without significant plastic deformation, when the filament is subjecte to loading"[150]) of the filaments were measured with the same small-scale bending test system used by Zhang et al.,[149] whilst the "stiffness" (namely, "the load required to achieve a certain deformation"[150]) was determined with a slightly different experimental set-up, where the supporting blades were replaced with a flat metal surface and the moving blade gradually penetrated the filament sample until the deformation reached a maximum value of 35%.[150] Following the original terminology of the Repka–Zhang method, Zhang et al.[150] observed that, if intended for standard usage in a variety of FFF printers, filaments should have adequate flexibility (breaking distance: 0.61 mm), toughness (breaking stress: 635.5 g $mm^{-2}$), and stiffness (20,758.3 g $mm^{-2}$).

Ultimately, Xu et al.[148] combined the methodologies already proposed by Naserredin et al.[147] and by Repka–Zhang[150] and reached the conclusion that the "toughness/brittleness" of a filament is the most accurate parameter for predicting its printability. It was demonstrated that a minimum toughness of 80 kg $mm^{-2}$% was required for printing on a Prusa I3 MK3S machine, thus identifying the process window of this printer.

Though interesting to the aim of filaments' screening, unfortunately the approaches described by Naserredin et al.,[147] Zhang et al.,[149,150] and Xu et al.,[148] require the usage of special testing rigs, whereas conventional measurement systems, such as universal testing machines or bending systems, might be more readily accessible. As further discussed in Section 5.2, some equations are available that predict the printability of a material as a function of its compressive elastic modulus and its viscosity at the printing temperature. This avoids the need for special rigs, since a universal testing machine to perform mechanical tests and a rheometer, preferably a capillary one, to determine the rheological behavior may suffice to acquire the required experimental input (as demonstrated, for example, in the contribution by Leng et al.[151]).

Besides the mechanical requirements mentioned so far, also surface roughness becomes critical when experimental materials come into play.[149] For example, individual fillers or aggregates may cause bulges on the filament surface,[143] or sharkskin instabilities may occur especially under high shear rates.[152] Some authors advice that having a smooth surface, as typically observed with commercial filaments, is important to ensure the correct functioning of the feeding mechanism, which relies on the filament-gears contact, and the smooth sliding of the filament through the liquefier entrance.[153] However, there is not a consensus in the literature regarding the roughness level that can be acceptable for printing. In future studies, it would be interesting to understand if a roughness limit exists, above which filaments are not printable anymore, and, in case, if this threshold value is different for different materials.

### 4.5. Other Considerations Relevant to Filaments for FFF

It is generally recognized that producing high-quality filaments is key to printing high-quality parts.[119] As previously mentioned, for research purposes, filaments can be cut down and extruded again to remove air bubbles and homogenize the material, especially if fillers are present.[107] However, multiple extrusion cycles increase the production time and cost. Also, the repeated action of heat and mechanical stresses within the extruder is likely to degrade the polymer and, in case the filament is a composite material, damage the filler.[154] This typically results in fiber lengths that are around one order of magnitude lower than the critical length required for effective stress transfer from the matrix to the reinforcement.[155] Additional damage to the filler may also be induced by the printing process itself, due to the composite feedstock being forced to flow through the nozzle.[10]

After extruding and spooling, the filament must be conveniently stored to preserve its pristine properties. Most polymers, such as ABS, are sensitive to light and become brittle if exposed to ultraviolet (UV) rays.[156,157] Many polymers frequently used in FFF, like PLA and PA, are also prone to absorb moisture from the environment. When hydrophilic matrices like PLA and PA absorb water and are melt processed, their degradation will accelerate due to hydrolysis (polymer chains break).[158–161] Absorbed water molecules have a strong plasticizing effect, thus changing the properties of the filament,[162] and may be released upon printing and cause bubbling at the print nozzle exit, thus resulting in major defects.[163] In this regard, it is important to remark that, if the filament is a composite system, fillers may affect the long-term stability of the polymer matrix, for example, promoting moisture uptake (this is the case with many vegetable fillers, which are also sensitive to humidity[164]) or catalyzing ageing processes.[165,166] Ultimately, the shelf-life is typically longer for filaments for FFF than for polymer feedstocks used in other AM technologies such as PolyJet,[167] however, this largely depends on the exact material formulation, as well as on the storage conditions, since some additives may be prone to exude or evaporate from the base polymer.[168]

## 5. Feeding and Flowing Through the Hot-End

As summarized in the following paragraphs, various analytical models have been proposed in the literature to describe the

 

material flowing through the printhead and thus to predict the printability of new filaments. Most of them were originally formulated to outline the behavior of materials for SDS, since the high filler loading typically required to produce fully inorganic parts pushes the limits of printability. However, these models can often be extended to neat polymer filaments and to polymer-matrix composites with a relatively low filler loading, thus offering a valuable aid in directing research in new materials for FFF and reducing the experimental burden associated to trial-and-error methodologies.

More accurate information on printability can be obtained by finite element (FE) simulations and other computational approaches, with comprehensiveness being the main advantage of these models. For example, the FE analysis published by Ramanath et al.[169] provides a thorough mapping of the temperature distribution, of the pressure drop and of the fluid velocity along the flow channel for $\epsilon$-PCL, and accounts for varying nozzle angle and nozzle diameter values. However, the exploration of several design and working conditions may be cumbersome, is spite of the continuous growth of computational power.[170] Moreover, the outcomes of computational simulations are case-specific, meaning that detailed geometric variables and material properties must be introduced as input data and the predictivity of the model depends on the accuracy of this information.[169] As such, computational approaches provide precise information on the system's behavior under certain conditions, but it may be difficult to quantitatively translate the results to different geometries and materials.

Consequently, combining analytical models and computational simulations is often required to better understand how the feedstock material is fed into the hot-end, heated to the right viscosity, and eventually extruded out of the nozzle.[171] In future, artificial intelligence is expected to enable a deeper comprehension of the mechanisms and of the influencing parameters in FFF.[172,173]

### 5.1. Interaction between Filament and Feeding Mechanism

Based on the feeding mechanism, FFF printers can be grouped into two main classes. In direct drive printers, the feeding mechanism is integral to the printhead. Conversely, in Bowden drive systems, the filament feed unit is placed away, typically at the rear of the printer.[174] The printhead of Bowden drive printers is thus smaller and lighter, which makes it suitable for working on a larger build surface. Also, the lower inertial forces of Bowden drive systems significantly reduce the surface waviness that is often encountered in parts produced with direct drive printers as a consequence of vibrations (a phenomenon known as "rippling" or "ghosting" or "ringing"[175]). However, in Bowden drive printers the filament has to travel a long distance from the rear of the printer to the printhead. For this reason, Bowden drive printers are not the optimal choice for processing very flexible and soft materials like TPEs or highly drug-loaded materials for therapeutics.[148] For the same reason, filaments for Bowden drive printers often have a diameter of 2.85 mm.[176]

Regardless of the specific configuration of the feeding mechanism of the printer, the filament must possess the right geometry (roundness and diameter) and the right mechanical properties to be pinched without breaking between the feeding gears. In more detail, the feedstock material should not deform plastically (although minor indents are routinely generated by the contact between knurled gears and filament[43,177]) nor fracture.[178] The combination of "longitudinal resistance" and "transverse resistance" to applied loads is sometimes referred to as the "mechanical resilience" of the filament and is useful to comprehensively assess the resistance to pinching.[149,179]

Since the filament at the entrance of the liquefier works like a piston on the softened material inside the barrel, a key requirement for the filament to be printed is that the force exerted by the gears in the feeding mechanism, $F_{gears}$, must overcome the force required for extruding the softened material through the nozzle tip, which is dictated by the total pressure drop in the printhead, $P$, and by the cross-sectional area of the filament, $A_f$, according to[43,177]

$$F_{gears} > P \times A_f \tag{3}$$

In the past, the rollers of the feeding mechanism were made of a synthetic rubber such as hypalon or polyurethane. Since the surface of the rollers was smooth, loss of traction could easily occur. Nowadays, rollers are often replaced with wheels. The drive wheel is usually made of metal and the surface is knurled or grooved. This mitigates the risk of slippage and improves the pinching action, but creates small indents in the filament and may cause shear-induced failure.[177] According to the theory developed by Go et al.[177] and further elaborated by Singh et al.,[43] $F_{gears}$ is supplied to the filament via the shear stresses, $\tau_{shear}$, that act on the small area of the filament surface, $A_{shear}$, where the cusps of the drive wheel actually engage the filament, namely

$$F_{gears} = \tau_{shear} \times A_{shear} \tag{4}$$

It must be therefore:

$$F_{gears} = \tau_{shear} \times A_{shear} > P \times A_f \tag{5}$$

The filament will fail if the value of $\tau_{shear}$ exceeds the shear strength of the feedstock material, $\tau^\star$. As a consequence of the viscoelastic behavior of thermoplastic-based materials, $\tau^\star$ depends on the temperature and on the shear rate. However, as a first approximation, $\tau^\star$ can be related to the ultimate tensile strength of the filament, $\sigma^\star$, according to[43,177]

$$\tau^\star = \frac{\sigma^\star}{\sqrt{3}} \tag{6}$$

In Equation (5), the shear contact area, $A_{shear}$, must be evaluated on a case-by-case basis, as it depends on the specific geometry of the teeth of the drive wheel, including their shape, size, depth, and angle.[43,177] Furthermore, Go et al.,[177] observed that an inverse relationship exists between maximum transmittable force and feed rate. This can be attributed to the fact that the depth of engagement of the knurls into the filament, and thus $A_{shear}$, are greater at slower rates. $A_{shear}$ is also affected by the properties of the feedstock material,[43,177] as soft materials are likely to receive larger indents from the teeth of the drive wheel

as compared to harder materials, even if the working conditions are nominally the same.

Agassant et al.[170] recently pointed out that, strictly speaking, the pressure acting on the filament is the sum of two terms, namely the pressure drop in the printhead and the pressure that is generated in the extrudate as a result of the molten polymer being sheared between the print nozzle and the substrate. However, the shear-related pressure at the exit of the nozzle is often neglected under normal printing conditions. Numerous models can be found in the literature to estimate the pressure drop in the printhead, $P$, and some examples are reported in the Appendix. According to the calculations developed by Singh et al.,[43] that follow the model originally proposed by Bellini et al.,[180] $P$ is governed by the geometry of the printhead (that is schematized as comprising three main areas, namely: i) the liquefier; ii) a conical section that transitions from the liquefier to the nozzle; and iii) the nozzle), by the rheological behavior of the molten feedstock, and by the volumetric flow rate of the material being printed, $Q$ (more detail in the Appendix). The volumetric flow rate, $Q$, in turn, depends on the size (cross-sectional area) of the filament, $A_f$, and on the feed rate, $v_f$ (in [m s$^{-1}$]). Further, assuming that the softened material is incompressible, the mass conservation law (applied at the entrance of the liquefier and at the exit of the nozzle tip) leads to the relation

$$Q = A_f \times v_f = A_{out} \times v_{out} \tag{7}$$

where $A_{out}$ and $v_{out}$ are the cross-sectional area of the material flowing out from the nozzle (thus corresponding to the cross-sectional area of the nozzle tip) and the exit velocity, respectively.

To summarize, what happens is that, under a no-slip boundary condition, as the feed rate increases in order to provide a higher throughput, the pressure drop in the printhead, $P$, also increases. The force required to overcome the pressure drop increases accordingly, until it exceeds the limiting force supported by the shear contact area, $A_{shear}$, of the filament and this results in print failure. The previous relations allow the limiting shear force, $F^\star$, to be determined from the results of tensile tests and from an image analysis of the shear contact area, $A_{shear}$, as

$$F^\star = \tau^\star \times A_{shear} = \frac{\sigma^\star \times A_{shear}}{\sqrt{3}} \tag{8}$$

However, in practical cases, as the feed rate increases, slip wall phenomena are likely to occur, and this causes a progressive deviation of the real printing process from the theoretical model. Whereas the theoretical model predicts a monotonic dependence of the force required to overcome the pressure drop on the feed rate, the required force in practice remains lower than the predicted value and then drops to zero when slip phenomena prevail. In spite of this deviation, estimating the limiting shear force is a useful tool to predict the printability of a filament, since print-related issues and failure are expected to occur once this threshold is exceeded.

As discussed by Bellini et al.,[180] when the flow rate is changed while printing, especially in the acceleration (at the beginning) and deceleration (at the end) phases of printing, the system experiences unsteady conditions. The sudden input of new material causes a drop in temperature, which in turn increases the viscosity. Additional pressure $P$ is thus required to maintain the flow out from the nozzle. The force exerted by the feeding gears should increase proportionally, as expressed in Equation (3). However, this causes higher values of the torque being required from the motor that moves the drive wheel, until the maximum motor torque is reached. Beyond this point, the angular velocity remains constants for a certain period of time, until the nominal temperature and the targeted viscosity are re-established owing to the increased heat flow rate from the liquefier to the filament (with the temperature of the liquefier being controlled by a temperature sensor). During this transient, part of the force generated by the feeding mechanism is actually used to overcome the friction force, $F_{fr}$, between the gears and the filament,[180] according to

$$\begin{aligned} F_{fr} &= f_{fr} \times v_{f,g} \\ f_{fr} &= f_0 \times v_{f,g}^{s-1} \end{aligned} \tag{9}$$

where $v_{f,g}$ it the velocity at the feeding gears, and $f_0$ and $s$ are material-related properties.[180]

It has been argued that a more efficient pinching action on the filament would allow the maximum force capacity of FFF mechanisms to be increased and the transient effects to be minimized, which would pave the way for faster and more efficient printing. To this aim, Go and Hart[181] proposed to replace the conventional counter-rotating gears with a co-axial rotating nut to drive a threaded filament. In this way, a linear relationship would be established between feed rate, $v_f$, and angular velocity of the feeding nut, $\dot{\vartheta}$, as

$$v_f = \frac{p}{2\pi}\dot{\vartheta} \tag{10}$$

where $p$ is the thread pitch.[181] However, patents exist on threaded filaments (for example, US10562227B2[182]). Moreover, threading the surface would further increase the price of filaments since more complex extrusion lines would be needed.

### 5.2. From the Feeding Mechanism to the Liquefier Entrance

Venkataram et al.,[183,184] observed that buckling at the liquefier entrance, as exemplified in **Figure 8**, is the most common failure mode in SDS.

According to the model developed by Venkataram et al.,[183,184] since the pressure at the nozzle exit under most printing conditions is nearly atmospheric, the pressure drop, $P$, that builds up through the printhead is the relevant pressure acting on the filament at the liquefier entrance and potentially causing buckling. Buckling is thus predicted to occur if this pressure $P$ exceeds the critical load per unit area (i.e., the critical buckling stress), $\sigma_{cr}$, given by Euler's formula

$$\sigma_{cr} = \frac{\pi^2 E_c}{\left(\frac{L}{R_f}\right)^2} \tag{11}$$

where $E_c$ is the compressive elastic modulus of the feedstock material, $L$ is the unsupported length of the elastic column under compressive stress, which corresponds here to the distance

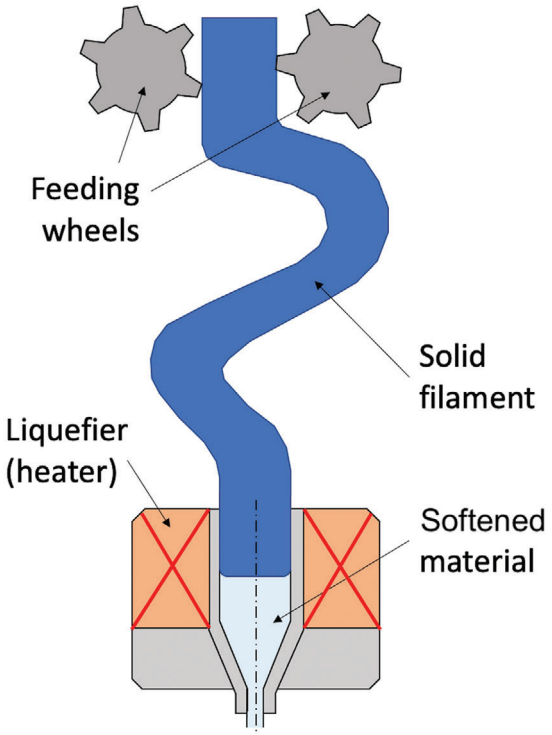


**Figure 8.** If the compressive stiffness-to-viscosity ratio is too low, the filament is predicted to experience buckling at the liquefier entrance. (Note: drawing not in scale.)

between the feeding gears and the liquefier entrance, and $R_f$ is the radius of the filament. The $L/R_f$ term in Equation (11) represents the "slenderness ratio" of the filament. For a given printer, the value of the slenderness ratio is fixed, since it depends on the size (radius or diameter) of the filament, which is dictated by the feeding mechanism, and on the geometry of the printer (distance between wheels and liquefier entrance). However, it is possible to sidestep the effect of the slenderness ratio by introducing a low-friction tube, typically in polytetrafluoroethylene (PTFE, Teflon), to laterally support the filament as it travels from the feeding mechanism to the liquefier.[185] Implementing a support sleeve is obviously indispensable for feeding the filament in Bowden-drive set-ups.[186]

The Euler's buckling criterion can be calculated with different formulas according to different boundary conditions (two fixed ends; one fixed end and one hinged end; two hinged ends). The condition expressed by Equation (11) corresponds to the most conservative scenario, that is, two hinged ends, which leads to the lowest value of the critical buckling stress.[184]

The filament will thus buckle upon printing if

$$P > \sigma_{cr} = \frac{\pi^2 E_c}{4\left(\frac{L}{R_f}\right)^2} \tag{12}$$

On account of the similarity existing between the geometry of the printhead (modeled as a thin tube ending with a conical tip) and the geometry of a capillary rheometer, Venkataram et al.[183,184] formulated the hypothesis that the pressure drop in the printhead, $P$, is proportional to the pressure drop in a capillary rheometer, $P_r$, through a scaling factor $k$

$$P_r = kP \tag{13}$$

The failure under buckling of a filament can thus be related to the flow behavior of the feedstock material through a capillary rheometer, with buckling being predicted to occur if

$$P = \frac{P_r}{k} > \sigma_{cr} = \frac{\pi^2 E_c}{4\left(\frac{L}{R_f}\right)^2} \tag{14}$$

The pressure drop in a capillary rheometer, $P_r$, depends on its geometry (radius, $r$, and length, $l$), on the apparent viscosity of the fluid, $\eta_a$ (with $\eta_a$ being a function of the shear rate at a given temperature), and on the volumetric flow rate, $Q$ (details in Appendix). This leads to the conclusion that buckling will take place if

$$\frac{E_c}{\eta_a} < \frac{8Ql\left(\frac{L}{R_f}\right)^2}{\pi^3 r^4 k} \tag{15}$$

In practical terms, as schematized in **Figure 9**, $E_c$ is the compressive modulus of the filament, $\eta_a$ is the apparent viscosity determined by the capillary rheometer, $Q$ is the volumetric flow rate in the nozzle, $l$ is the length of the liquefier (heating tube), $L$ is the length of the filament between the rollers and the top of the liquefier, $R_f$ is the radius of the filament, and $r$ is the radius of the nozzle.[151,187]

Intuitively, Equation (15) expresses the fundamental concept that the ratio between stiffness and viscosity is key for the

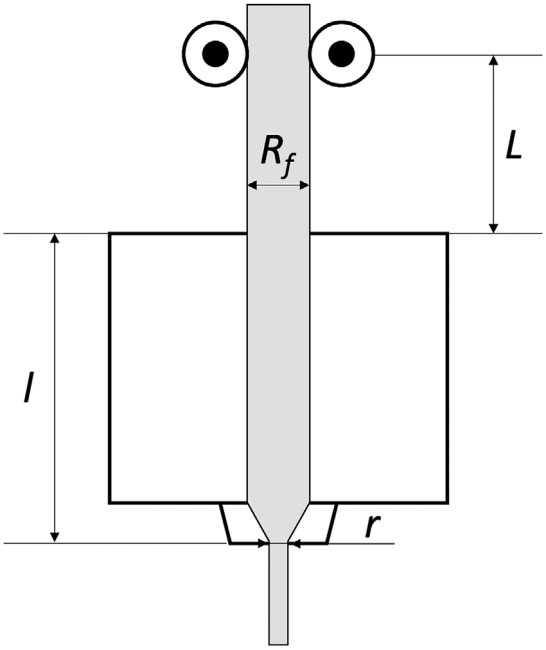


**Figure 9.** Graphical representation of the parameters related to printer hardware that affect the printability of a filament. (Note: drawing not in scale.)

 

filament to be fed without buckling, as the "column strength" of the filament must prevail on the pressure drop that is proportional to the apparent viscosity.[153,187] As for the scaling factor $k$, its exact value should be assessed on a case-by-case basis, as it depends on the printhead geometry and on the volumetric flow rate. However, it does not change with the material[184] and, as a first approximation, it is often assumed $k = 1.1$, a value which also accounts for the difference in the cross-sectional area between the filament and the liquefier (with the barrel diameter of the liquefier being slightly larger than the filament diameter).[183] According to the experimental results, if a 508 µm tip is used for printing (which corresponds to a typical shear rate regime between 100 and 200 $s^{-1}$), buckling will occur if the $E_c/\eta_a$ ratio is lower than a critical value in the range of $3 \times 10^5$ to $5 \times 10^5$ $s^{-1}$. This critical value is predicted to increase with increasing shear rate.

The buckling model proposed by Venkataram et al.[183,184] is frequently cited in the literature regarding the development of new feedstock materials for FFF and, even more so, for SDS. However, some confusion exists about the elastic modulus. Strictly speaking, according to the original model, the elastic modulus, $E_c$ in Equation (15), is the compressive modulus.[187] Buckling of polymers can be treated using Euler's criterion either with the elastic modulus in the case of elastic buckling (linear region of the stress–strain curve) or with the tangent modulus in case of inelastic buckling (nonlinear region of the stress–strain curve). Venkataraman et al.[184] decided to use the elastic modulus instead of the tangent modulus for comparative purposes. In conclusion, the elastic modulus in Equation (15) should be the elastic compressive modulus. As previously mentioned, it is important to remark that, due to the viscoelastic behavior of thermoplastic-based materials, the experimental value of the elastic modulus is affected by the temperature and by the testing speed. Similarly, in order to account for the viscoelastic behavior of thermoplastic-based materials, the apparent viscosity, $\eta_a$, and its dependence on the shear rate should be tested at the same temperature that will be set as the liquefier temperature for printing.[184]

Another important variable in buckling phenomena is the slenderness ratio, which, for a given filament diameter, is defined by the unsupported length of the sample, that is, by the distance of the sample grips in compression tests.[184] In this regard, Janek et al.[188] recently compared the compressive behavior of several filaments as measured under varying test conditions. It was demonstrated that, regardless of the composition of the filament (including two different polyvinyl alcohol (PVA) filaments loaded with 50 wt% of hydroxyapatite and a commercial PLA filament loaded with about 27 wt% of gypsum), the compressive strength drastically decreased when the nominal distance of the sample grips was increased from 16 to 36 mm and then up to 76 mm. With the filament diameter being constant, the increasing gripping distance resulted in a longer unsupported length and, ultimately, in a higher slenderness ratio, which induced a stronger tendency to Euler buckling.[188]

### 5.3. In the Liquefier

As previously mentioned, the filament is assumed to be rigid when it enters the liquefier. Then, as the temperature increases, the material melts, if it is semi-crystalline, or just softens, if it is totally amorphous, and its viscosity progressively becomes lower. Different models have been proposed to describe heating in the liquefier. Whereas the hypothesis of constant heat flux (which is based on the assumption that the temperature remains constant as the material travels along the liquefier) is valid only for low feed rates, according to Go et al.[177] the condition of constant wall temperature is closer to describe the actual functioning of the liquefier, whose temperature is controlled through feedback data from an embedded thermocouple. Moreover, the condition of constant wall temperature accounts for the fact that the filament is actually heated as it moves along the liquefier.[177] However, the accuracy of either model is strictly related to the design of the liquefier.[129]

The viscosity reached in the liquefier plays a key role in FFF, since the pressure drop in the printhead, and hence the force required for printing, consistently increase with increasing values of the viscosity.[10] As they become soft, thermoplastics in FFF usually exhibit a shear-thinning behavior under flow (pseudoplasticity), which means that, at a given temperature, their viscosity decreases with increasing shear rate, and this makes printing easier.[177,189] However, adding a filler is likely to change the rheological behavior, often leading to a significant increase in viscosity.[119]

Another point to consider is that thermoplastics typically have low thermal conductivity, which suggests that significant axial and radial temperature gradients exist across the material in the liquefier. As the filament feed rate increases, the residence time in the liquefier becomes shorter and the temperature reached by the filament core may remain sensibly lower than the targeted value. For example, according to the simulations performed by Go et al.[177] under a quasi-static flow hypothesis, if the wall temperature is set to 260 °C, the temperature of the filament core at a distance of 20 mm from the liquefier inlet drops from around 220 °C to below 100 °C if the filament feed rate is increased from 5 to 15 mm $s^{-1}$. Failure to reach the targeted temperature at the filament core causes abnormal values of viscosity and is expected to result in greater force required for printing.[177]

Whereas conventional models are based on the assumption that the material in the printhead is entirely in the molten state (or softened to a relatively low viscosity for amorphous materials), which justifies the idea of the filament working as a plunger at the liquefier entrance, different theories have been proposed to pinpoint the functioning of an FFF printer under high feed rates, when a certain amount of material may be not melted (or softened). In this regard, Osswald et al.[190] recently argued that conventional "melting and flow" approaches are only valid for low filament velocities, indicatively below 0.25 mm $s^{-1}$, whereas standard filament speeds are close to or even higher than 1 mm $s^{-1}$, above which a limiting maximum flow rate is reached. As the filament velocity (that governs the feed rate) increases, a portion of the filament in the solid state survives within the liquefier and the solid-melt transition zone (which can be interpreted as the solid-to-softened material transition zone for amorphous feedstocks) moves closer and closer to the conical section that connects the liquefier to the nozzle (capillary), as shown in **Figure 10**. For high feed rates, just a thin film of molten (or softened) material can be observed on the surface of the conical section. The pressure applied by the solid filament squeezes the melt (or softened material) toward the centre and out of the nozzle

 

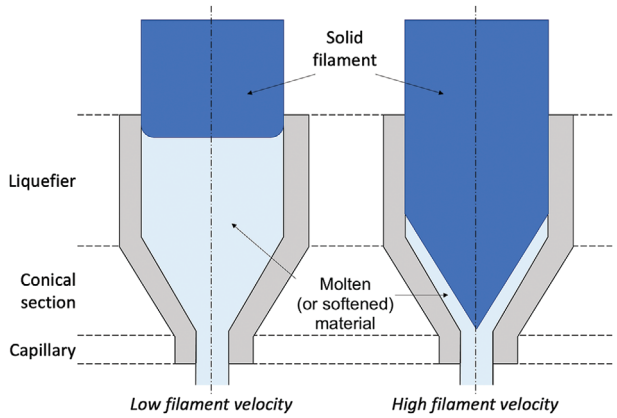


**Figure 10.** Models describing the flow through the hot-end for low and high filament velocities. (Note: drawing not in scale.)

tip, a condition that has been defined as "melting with pressure melt removal".

According to the calculations conducted by Osswald et al.[190] under the hypothesis that the material receives heat from the surface of the conical section, whereas the heat supplied from the vertical sides can be neglected (which, in turn, implies that there is no significant contact between the filament and the vertical sides of the barrel), the thickness of the melt (or softened material) film is inversely proportional to the filament velocity. Moreover, although the trend is not strictly linear, the film thickness decreases monotonically as the filament force is increased, with values that range between 80 to 35 μm for forces between 20 and 100 N, respectively, for a commercial ABS filament. A critical condition is reached when the film thickness approaches zero, which means that the material cannot be completely melted (or softened) in the liquefier and the solid filament touches the conical section of the hot-end. The melting (or softening) rate becomes therefore the rate-limiting factor that controls the print rate.[190] The experimental data collected by Oehlmann et al.[173] for PLA printed at three different temperatures (200, 215, and 230 °C) clearly confirmed that the transition from the "melting and flow" mode to the "melting with pressure melt removal" mode is temperature-dependent. At 230 °C, the transition point was associated to a filament speed of 4.1 mm $s^{-1}$ and a force of 17 N; at 200 °C, the transition point shifted to a filament speed of 4.1 mm $s^{-1}$ (3.95 mm $s^{-1}$ according to the graphs) and a force of 25 N, due to the increased melt viscosity ofat lower temperature.

A wealth of experimental data has been gathered by Serdeczny et al.[185] to precisely correlate the force required for printing (as well as the die swelling coefficient) to the feed rate under different values of the liquefier temperature. At any given printing temperature, it was observed that, at first, the feeding force increases linearly as a function of the feed rate, and this behavior corresponds to the linear extrusion regime. Above a certain critical feeding rate, the feeding force increases swiftly, which represents the transition to the non-linear extrusion regime. If the printing temperature is decreased, the viscosity becomes higher and the thermal driving force for heat transfer becomes lower. As a consequence, the feeding force required to achieve the targeted feed rate increases as the liquefier temperature decreases. Also, the slope of the feeding force-feed rate curve becomes progressively steeper for lower values of the liquefier temperature and the critical feed rate that triggers the transition from the linear to the non-linear regime becomes lower. Serdeczny et al.[185] attributed the shift from linear to non-linear behavior to the limiting condition of the solid filament reaching the conical section of the hot-end, which is coherent with the considerations about the moving transition zone proposed by Osswald et al.[190] The smoother transition observed for ABS than for PLA was explained as a consequence of the different degree of crystallinity of the two materials, with ABS being basically amorphous and thus lacking a sharp melting temperature.

Especially for relatively low values of the liquefier temperature, Serdeczny et al.[185] observed that high feed rates often resulted in melt instabilities, like sharkskin effects and melt fracture (where "melt" also refers to amorphous thermoplastics that have softened due to heating). Ultimately, further increasing the feed rate led to shear failure of the filament between the feeding wheels, as predicted by Go et al.[177] and by Singh et al.[43]

The dependence of the feeding force on the filament velocity is also affected by the hot-end geometry. According to the experimental results provided by Nienhaus et al.,[191] the feeding force reached a minimum for a 56° conical section, but differences in the feeding force were minimal as the conical section was changed from 30° to 118°. The nozzle diameter is influential because it affects the flow rate. If the nozzle diameter is reduced, the mean flow velocity in the capillary must increase accordingly to maintain the same flow rate (mass conservation under the hypothesis of incompressible fluid). This causes higher wall shear rates and hence larger shear stresses, that ultimately call for increased feeding forces, which is coherent with the results of the FE analysis implemented by Ramanath et al.[169] As for the barrel length, the feeding force is almost insensitive to the length of the liquefier at low feed rates, because the polymer has enough time to melt (or to soften) regardless of the length of the flow channel. However, working with a longer barrel may be helpful at high feed rates, because a longer barrel offers a larger surface for heat transfer and a longer residence time for the filament to melt (or to become soft). According to these results, a longer barrel should be chosen for polymers with a high melting point (or that become soft at high temperature), in order to promote complete melting (or softening) in the liquefier. Conversely, as pointed out by Ramanath et al.,[169] a short barrel should be preferred for polymers that melt (or soften) at low temperature, especially if a long stay at high temperature may trigger their heat-induced degradation.

In practical terms, Serdeczny et al.[185] recommended to define the "maximum feed rate," $V_{f,max}$, as the feed rate corresponding to the shift from linear to non-linear regime. Theoretically, it would be possible to print above this threshold, but exceeding $V_{f,max}$ would require very high feeding forces and generate print instabilities. Serdeczny et al.[185] thus estimated the value of $V_{f,max}$ under the key hypothesis that, in order to be successfully printed, the polymer has to be heated to the target temperature $T_t$, which is equal to or greater than the melting temperature for semi-crystalline thermoplastics, before it reaches the end of the liquefier barrel and enters the conical section, which leads to the expression

$$V_{f,max} = \frac{h\Delta T \pi D_L L_L}{\rho_m A_f [\lambda + C_m (T_t - T_f)]} \quad (16)$$

where $\rho_m$ is the density of the melt (or softened material), $h$ is the heat transfer coefficient at the barrel wall (whose value was estimated to be 228 W m$^{-2}$K$^{-1}$ in order to obtain the best fit with the experimental data for a PLA filament printed with an E3D v6 hot-end[185]), $\lambda$ is the heat of fusion (latent heat) of the polymer, $C_m$ is the average specific heat capacity of the melt (or softened material), $A_f$ is the cross-sectional area of the filament, $D_L$ and $L_L$ are the diameter and the length of the liquefier barrel, and $T_f$ is the temperature of the filament as it enters the barrel and, in the first instance, can be assumed to be equal to room temperature. $\Delta T$ is the mean temperature difference between the barrel wall (whose temperature is kept constant at $T_W$) and the melt (or soften material), which is calculated as the mean logarithmic temperature difference

$$\Delta T = \frac{(T_W - T_f) - (T_W - T_t)}{\ln\left(\frac{T_W - T_f}{T_W - T_t}\right)} \tag{17}$$

It is worth noting that the model was validated against PLA and ABS. Whereas PLA is a semi-crystalline material with a melting temperature of around 155 °C, ABS is amorphous, and therefore it does not have a true melting temperature. However, since the printing temperature of ABS is around 20 °C higher than that of PLA, Serdeczny et al.[185] used the "flow temperature" of ABS instead of the melting temperature and defined it as 175 °C.

Clearly, $V_{f,max}$ depends on the thermo-physical properties of the feedstock material, as well as on the geometry of the liquefier barrel and on the temperature field. Although the expression of $V_{f,max}$ as proposed in Equation (16) does not dictate any explicit conditions on the properties of the feedstock material, printing is predicted to be easier for those materials that, owing to their thermo-physical properties (low density, low—or none—heat of fusion, low heat capacity, high thermal conductivity), can be readily heated to the targeted temperature. In particular, Turner et al. remarked the difficulty of processing highly thermally insulating materials.[129] Similarly, Phan et al.[192] commented on the importance of heat transfer and identified it as a major limitation to increasing the manufacturing rate of FFF. Extruders are equipped with one or more rotating screws that push the material forward and simultaneously mix it, thus aiding temperature homogeneity. Conversely, the feeding mechanism of FFF printers moves the material forward, but does not mix it. As a result, the heat transfer for a given thermal driving force is set to only depend on the material properties and a competition is established between how quickly heat is radially conducted through the flowing material compared to the time it takes for the material to egress from the nozzle.[192]

As previously mentioned, the corrective factor 1.1 was introduced in the equations developed by Venkataraman et al.[183,184] in order to account for the difference between filament diameter, $D_f$, and liquefier inlet diameter, $D_L$. The presence of an annular gap between filament and barrel of the liquefier may be conducive to backflow failure, as illustrated in **Figure 11**. Investigating this failure mode was the subject of the contribution by Gilmer et al.[189]

Under the hypotheses that: i) the printer works at steady state in terms of filament feed rate; ii) the flow is axially symmetric (namely, the velocity profile at the solid–liquid transition is circumferentially similar around the annular gap); and iii) the pressure drop, $P$, can be described by a power-law fluid-based momentum balance on the liquefier according to the model developed by Bellini et al.[180] (details in Appendix), Gilmer et al.[189] proposed a dimensionless number called "flow identification number" (FIN) to relate system geometry and material properties to the filament's propensity to backflow according to

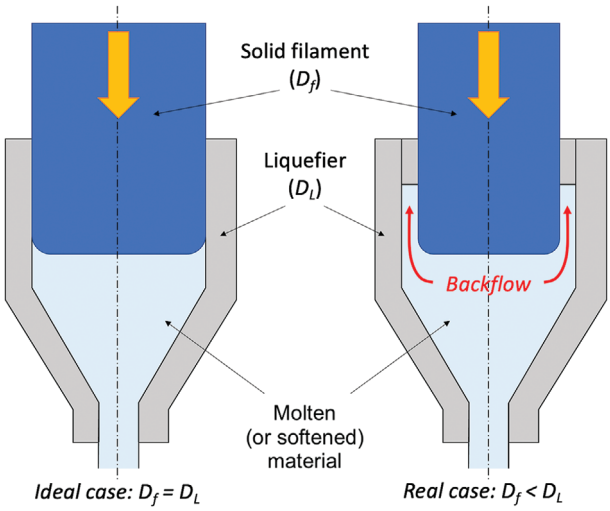


**Figure 11.** Schematic representation of the backflow that may occur through the annular gap between filament (diameter: $D_f$) and liquefier (diameter: $D_L$, with $D_f < D_L$). (Note: drawing not in scale.)

$$\mathrm{FIN} = \frac{P}{L} \times \frac{(D_L^2 - D_f^2)}{\eta_a v_f} \tag{18}$$

where $L$ is the length of the annular region, $v_f$ is the filament feed rate (in m s$^{-1}$) and $\eta_a$ is the apparent viscosity of the melt (or the softened material), as before.

Physically, the FIN indicates if the pressure drop along the length of the annular gap ($P/L$) is sufficient for engendering backflow for given conditions of geometry ($D_L$ and $D_f$), apparent viscosity and feed rate. Under common printing conditions, the filament is expected to print if the FIN is less than 153, provided that the filament does not buckle at the liquefier entrance as predicted by Venkataraman et al.[183,184] Conversely, backflow is expected to occur whenever the FIN exceeds 185. Intermediate values of the FIN identify a transition region, where the filament may be printable, but small changes in the system may be enough to cause substantial backflow and even print failure.[189] Clearly, the FIN is deeply affected by the geometry of the system. Also, the FIN is second order with respect to the filament diameter, which is therefore the governing parameter for a given printing apparatus. Based on the sensitivity analysis conducted by Gilmer et al.,[189] the second most influential factor is the power-law index, $n$, that describes the shear thinning behavior of the melt according to the Ostwald-de Waele power law fluid model, expressed here as

$$\eta_a(\dot{\gamma}) = \varphi \times \dot{\gamma}^{n-1} \tag{19}$$

where $\dot{\gamma}$ is the shear rate, and $\varphi$ is the flow consistency index. Physically, for a given shear rate, a small change in the power

law index, $n$, may cause a substantial change in the apparent viscosity that controls the resistance to flow in the annular region. The degree of shear thinning is thus the main material-related parameter that governs the probability of backflow.

Mackay[186] argued that the equilibrium height reached by the liquid when it is pushed back in the annular region should remain smaller than the barrel length, otherwise the liquid would reach and jam the mechanisms behind the liquefier. At present, no simple models exist to accurately predict the equilibrium height. In addition to the complicated viscoelastic behavior of thermoplastic-based materials, this difficulty in predicting the equilibrium height depends on geometric factors. In particular, Mackay[186] drew attention to the fact that the solid filament progressively softens and disappears as it approaches the liquefier egress, and this translates into a progressive increase of the radial thickness of the annular gap.

### 5.4. Printing Temperature in FFF

Equations (16) and (17) highlight the importance of the melting temperature of the feedstock material (strictly speaking, the flow temperature for amorphous thermoplastics).[185] In principle, the material in the hot-end should be heated to a temperature close to the temperature recommended for injection molding.[177] For amorphous materials, the target temperature should exceed the glass transition temperature; for semicrystalline materials, the temperature should be increased to above the melting temperature. The model detailed by Mackay et al.[193] (for relatively low feed rates) suggests that the minimum temperature required for printing, $T_{min}$, which is the temperature below which the viscosity becomes too high for the material to be successfully fed through the tip of the hot-end, is a material parameter. As a first approximation, this minimum temperature should be around 78 °C higher than the glass transition temperature, $T_g$, for completely amorphous polymers.[193]

$$T_{min} \approx T_g + 78\ ^\circ\mathrm{C} \tag{20}$$

In order to be readily printable, new feedstock materials should have a melting temperature (or a flow temperature, for amorphous materials) compatible with standard printers, which usually work in the 180–260 °C range.[194] Although often neglected in the literature, this requirement is actually crucial. First, the melting point of many materials is too high for printing. Actually, this is one of the main reasons why most metals, although capable of being processed into filaments, cannot be printed by FFF. Just a few low-melting point alloys with a wide semi-solid zone can be melted in the operational range of standard printers (a process known as "thixo-extrusion" or "semi-solid metal extrusion and deposition" or "3D thixo-printing"[195–198]). Research is now emerging in metallic glasses.[199] Similarly, not all thermoplastic materials are suitable for standard printers. For example, high-performance polymers, such as PEEK and PEKK, offer very good mechanical and thermal properties, but require special printing equipment. PEEK, which is a semicrystalline polymer with a melting temperature around 343 °C, must be processed with a nozzle temperature between 360 and 400 °C and with a heated bed at 120 °C.[200–202] PEKK is also a semicrystalline polymer. Although its melting temperature, around 385 °C, is slightly higher than that of PEEK, its crystallization rate is around three orders of magnitude lower, which makes it possible to process PEKK like an amorphous polymer approximately in the same temperature range as PEEK.[15] Nowadays, many industrial printers are available that can routinely reach the nozzle and chamber temperatures needed to process high performance thermoplastics. However, they are more expensive than standard printers, and are not for hobby users. Likewise, high performance thermoplastics are expensive feedstock materials compared to PLA and ABS, so their use is mainly for industrial applications.

Conversely, some polymers may degrade in the temperature range routinely applied for printing, and low-temperature FFF machines are presently less common than high-temperature ones. For example, PCL, a biocompatible polymer with relevant applications in the biomedical sector,[203] has a melting point around 57 °C,[169] which makes it incompatible with most standard printers. Many thermoplastic-matrix composites are also very sensitive to overheating. This may happen due to the presence of vegetable fillers and fibres,[14] which are likely to degrade in the temperature range typically required for printing PLA (190–220 °C), ABS (220–250 °C) and other popular thermoplastic materials for FFF.[15] Since many pharmaceuticals and active principles are thermally labile, the risk of overheating is particularly challenging in the field of 3D pharming.[204–206] Although this is less obvious, thermally-induced damage may also affect composite materials containing inorganic fillers. For example, Electrifi is a copper-based commercial filament specifically formulated for printing electronic devices. Electrifi has been demonstrated to be printable with very low resistance values,[207] but its recommended printing temperature is below 150 °C in order to avoid diffused oxidation of the copper particles that would cause a drop in electrical conduction.

Even if a thermoplastic polymer is not thermally labile, repeated heat processing, especially if coupled with the action of intense shear stresses, may cause scission of the polymer chains. In FFF printing, the feedstock material must be heated at least two times, namely, the first time for producing the filament and the second time for flowing through the hot-end. For this reason, although it is important to heat enough and for enough time in order for the material to become processable, the residence time at high temperature and the working temperature for extruding and printing should be adjusted to minimize heat-induced degradation. However, the effect of repeated processing cannot be generalized, since it is largely affected by the interplay between polymer characteristics (nature and grade) and processing parameters. For example, Hutmacher et al.[208] reported that extruding and printing did not cause any significant changes to the molecular weight of PCL; conversely, Grémare et al.[209] observed that the molecular weight of PLA was reduced by 48% after printing. Moreover, the handling and pre-treatment conditions of polymers may also influence their degradation. Since several mechanisms such as thermal ageing, hydrolysis, oxidation, and shear-induced chain scission may differently contribute to degradation, understanding the degradation mechanisms of the thermoplastic to be processed is crucial to set the appropriate processing conditions to make filaments.[210,211]

 

### 5.5. Flow through the Nozzle Tip

Flowing through the nozzle tip represents the last step of the interaction between the feedstock and the hot-end. The high shear rates acting in the nozzle are known to stretch and orient the polymer molecules.[212] Likewise, FE simulations[213] proved that the shape and length of the nozzle affect the fiber orientation when the feedstock is a composite material. Yang et al.[133] provided experimental evidence that the degree of orientation (expressed as the $A_{zz}$ tensor component) of a short carbon fiber-reinforced filament changed through the nozzle and ultimately increased from the original 0.89 to 0.94 at the exit of the nozzle.

Go et al.[177] remarked that the nozzle diameter, in combination with the layer thickness, the filament feed rate, and the quality of the motion system, governs the printing resolution. Intuitively, a smaller tip enables a higher resolution. However, according to the model developed by Serdeczny et al.,[185] decreasing the nozzle tip in order to enhance the printing accuracy is expected to increase the feeding force required for printing under the same feed rate. Moreover, a smaller tip deposits thinner layers of materials and hence results in longer printing times. Another potential issue with a thin nozzle is the increased risk of clogging, especially if the feedstock is a composite material containing large fillers or aggregates.[214] The addition of abrasive fillers like hard metal and ceramic particles may cause extensive wear of the nozzle, thus vanishing the advantage of working with a thin tip. For example, Gnanasekaran et al.[215] reported that, after processing carbon nanotube (CNT) and graphene-loaded polybutylene terephthalate (PBT) composites, the brass nozzle of their desktop FFF printer had been severely abraded both inside the orifice, as well as on the front surface where the tip touches the printed object. The erosion of the nozzle provokes a progressive loss of printing resolution, which may undermine the aesthetics and the functional properties.[215] The ABS filaments loaded with microdiamond particles investigated by Waheed et al.[107] were so abrasive that they wore out the stainless-steel feeding gears even before entering the liquefier. Replacing the standard components of the printer with bespoke harder ones may thus be necessary for processing abrasive feedstocks and making the part to specification.

### 5.6. Die Swelling at the Nozzle Exit

As already mentioned, essentially, printing by FFF is an extrusion process and, as such, is affected by the die swelling effect. When the material leaves the nozzle, the elastic deformation is recovered and the diameter of the extrudate becomes larger than the nominal size of the tip.[129] Several theories have been put forward to describe the die swelling effect, however, their applicability to FFF is not obvious due to some peculiarities of FFF printers, especially the relatively short capillary (that may cause incomplete development of the velocity profile) and the close proximity between the nozzle tip and the base platform/previously printed layers (that may physically interrupt die swelling).[186] Gaining a deeper understanding of this phenomenon would be very important, since minimizing the die swelling effect is imperative for keeping the real diameter of the extrudate as close as possible to the nominal value. Also, die swelling interferes with the preferential orientation of polymer chains and elongated fillers in the extrudate. Heller et al.[213] simulated the flow of an ABS-short carbon fiber composite feedstock through the nozzle of a standard FFF printer and, under the simplifying assumption of incompressible Newtonian fluid, observed that the fiber orientation increased to nearly 100% while travelling through the conical section of the nozzle, and then sensibly decreased in the die swell due to the expansion flow in the radial direction. The reduced fiber orientation was proven to negatively affect the modulus of elasticity of the extrudate.[213]

According to Serdeczny et al.,[185] the die swelling ratio depends on the feed rate and on the temperature. Qualitatively, the trend is the same for the die swelling ratio and for the feeding force (described above), since both of them increase with increasing values of the feed rate and decrease with increasing values of the liquefier temperature. For PLA filaments, the transition from linear to non-linear regime occurs at the same feed rate both for the die swelling ratio and for the feeding force, suggesting the two phenomena are correlated.[185]

Conceivably, besides the printing parameters, also the nature of the feedstock material has an effect on die swelling. Serdeczny et al.[185] tracked down the die swelling ratio of PLA under a wide range of printing conditions and observed that, oftentimes, the die swelling ratio was higher than it would be expected for creeping Newtonian fluids (typically around 1.13), which was considered a characteristic feature of the viscoelastic behavior of polymer melts. However, as previously mentioned for the filament extrusion process, die swelling can be sensibly reduced with the addition of fillers that constrain the polymer chain mobility and hinder the elastic recovery, as often stated in the literature.[14,24,133,139,213,216,217] The stabilizing effect of inorganic fillers is emphasized in SDS owing to the extremely high filler loading.[218] However, as discussed in the following sections, the addition of fillers may interfere with the polymer chain diffusion mechanism across the raster–raster interface (termed "healing" hereafter) that is responsible for the consolidation of the printed part, as remarked by Mackay.[186]

### 5.7. Flow Instabilities at the Nozzle Exit

Like conventional extrusion, printing by FFF may result in sharkskin effects when the flow rate is high enough. Due to exit instabilities, at high flow rates the extrudate surface becomes very rough and scaly immediately after leaving the nozzle tip. If the flow rate is increased further, the flow is distorted and affected by gross melt fracture. At present, the effect of sharkskin instabilities in FFF has not been elucidated yet. However, according to Mackay,[186] it is expected that the surface roughness will limit the adhesive strength between neighbouring rasters of material in the printed part. Agassant et al.[219] advised that the occurrence of the sharkskin effect can be mitigated by the proper revision of the exit geometry or by the incorporation of additives in the feedstock material. Also, Mackay[186] remarked that the sharkskin effect is governed by the shear stress acting on the softened polymer, with critical values of the shear stress being in the order of 0.1 MPa. Conversely, it is generally observed that there is not a critical shear rate. For this reason, in principle the processing rate can be increased without incurring in sharkskin effects

 

leveraging the viscous (shear-thinning) behavior of the softened polymer, since the shear stress is proportional to the shear rate with the proportionality function being the viscosity, which is dependent on shear rate, temperature, and pressure.

### 5.8. Rheological Properties and Flowability

How exactly the polymer flows through the hot-end of an FFF printer is still the subject of debate in the literature. However, all models provided so far demonstrate that the rheological behavior of the feedstock plays a key role for successful printing.[24,129,131,186] As expressed in Equation (19) and Equation (A3), softened thermoplastics are non-Newtonian fluids, and their viscosity depends both on the temperature and on the shear rate. Generally speaking, increasing the printing temperature enhances the polymer chain mobility, thus reducing the viscosity. In terms of shear rate, as previously mentioned fluids with a shear-thinning behavior are favored in FFF, because this helps the material flow through the nozzle and then regain structure and shape after printing.[189,220] Spoerk et al.[221] conducted various experiments on a rotational rheometer and estimated that, at a shear rate of 100 rad $s^{-1}$ (which corresponds to the high shear rates frequently observed at the nozzle wall under standard printing conditions), the temperature should be high enough to keep the melt viscosity of PLA below 200 Pa s in order to print the material smoothly and achieve a strong inter-raster adhesion, which is a prerequisite for good mechanical properties (further detail below).

On account of the importance of viscosity, accurate rheological tests should be performed when selecting new candidate materials for FFF. Capillary rheometers are usually preferred to rotational rheometers at high shear rates, which are representative of the material behavior in the hot-end.[24] However, in spite of the increasing attention paid in the literature to rheological tests, at present no indicator or acceptable viscosity range can be provided to exactly predict the success of printing a new material by FFF.[19,220]

A pragmatic, but sensible, approach consists in comparing the viscosity of the new material to a benchmark (for example, a commercial filament) that can be easily 3D printed by FFF. Although this does not automatically imply that the new material is printable, it is useful to verify that the two viscosity profiles are similar at the operating shear rate.[220] A simplified check can be performed using the melt flow index (MFI, sometimes also known as melt flow rate) instead of the viscosity profile. The MFI is a single-point measurement that estimates the ability of a fluid (in FFF, a heated thermoplastic polymer or composite) to flow under standard testing conditions (namely, under a fixed load at a certain temperature) that are specific to each material.[222] Granules of the testing material are heated to the targeted temperature (with the flowability of being higher at increasing temperature) and then extruded through a short cylindrical die using a plunger actuated by a weight. The weight (in grams) of the material extruded in 10 min is the MFI.[223,224] Alternatively, if the density of the polymer is known, the MFI can be calculated from the volume rate that is measured by the piston displacement.[224] As a term of comparison, the MFI of ABS, grade P430, measured as per ASTM D1238 has been found to be 2.411 g per 10 min.[225]

As stressed by Rahim et al.,[19] estimating the MFI is less informative than running comprehensive rheological measurements. Moreover, as previously mentioned, the viscosity alone does guarantee printability in an FFF machine, since the mechanical properties of the filament are also crucial. Further, different materials can have comparable MFI or viscosity behavior, and different printability. However, this approach based on the MFI is very practical, as the test can be completed in a few minutes and requires relatively simple and affordable equipment. The MFI can thus be considered as a convenient tool for screening new feedstock materials, especially when composite materials are being developed and several filler loadings should be compared. In this regard, particular attention should be paid to account for the so-called "gravitational factor," namely, the influence of the increased density and hence of the stronger gravitational force that typically acts on a composite material as compared to the neat polymer upon testing.[226]

Adding a filler always modifies the viscosity of the thermoplastic matrix. Quite often, inorganic fillers increase the viscosity, as they act as rigid inclusions that hinder the polymer chain mobility.[119] Moreover, above a critical filler loading known as the rheological percolation threshold, the filler forms an interconnected network that can significantly increase the resistance to flow.[10] If needed, plasticizers and surfactants can be introduced to reduce the viscosity of highly loaded systems.[110] However, the change in viscosity depends on a number of factors including the size, concentration, orientation, dispersion, distribution, and shear deformation mode of the filler.[10] Ultimately, the real effect is not obvious. For example, it has been demonstrated that the presence of 2 wt% of talc has negligible effects on the viscosity of PLA, whereas introducing 5 wt% of short carbon fibers can reduce the melt viscosity of PLA in a shear flow due to the repulsive forces between carbon fibers and PLA and due to the progressive alignment of the reinforcement.[227]

## 6. Part's Build-Up

### 6.1. Part's Consolidation Mechanisms

In FFF, the build-up of a 3D object relies on the deposition of neighboring rasters of material layer upon layer. However, the simple placing of additional material does not automatically result in a solid part. In order for consolidation to occur, it is necessary that the freshly deposited raster "fuses" with the pre-existing rasters. As remarked by Costa et al.,[228] there exists some confusion in the literature regarding the terminology to describe this "fusion" occurring between neighboring rasters, since different terms have been used, including sintering, coalescence, and bonding. According to Sun et al.,[229] the term sintering describes the neck growth phenomenon, while healing refers to the molecular diffusion at the interface between neighboring rasters. Similarly, Mackay et al.[186] described the "fusion" between neighboring rasters as a two-step process, since the rasters wet each other and the interface disappears through molecular diffusion.

The bonding process is schematically shown in **Figure 12**. At first, the hot extrudate touches the previously printed raster, which is already cold, and heats it to an interface temperature that is the average of the two ("surface contact"). Then, sintering occurs between the two rasters through "neck formation" and

 

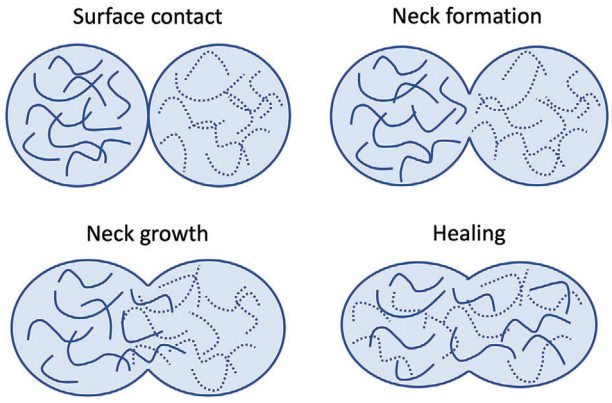


**Figure 12.** Schematic representation of the fusion occurring between neighboring rasters via surface contact, neck formation and growth, and randomization of molecular chains.

"growth." This is typically a viscous-flow sintering phenomenon, where capillary forces work to minimize the free surface energy of the system and surface tension is thus the driving force of the process.[230] Owing to the acquired molecular chain mobility, the interface disappears through molecular diffusion and randomization across the neck ("healing").

Bellehumeur et al.[231] applied a Newtonian polymer sintering model to describe the neck growth occurring over time in FFF. Using the symbols in **Figure 13**, it is possible to correlate the radius of the particles, $a = a(t)$, and the corresponding neck growth as a function of time, $y = y(t)$, as[232,233]

$$\frac{d\psi}{dt} = \frac{\Gamma}{a_0 \eta} \times \frac{2^{-\frac{5}{3}} \cos\psi \sin\psi (2 - \cos\psi)^{\frac{1}{3}}}{(1 - \cos\psi)(1 + \cos\psi)^{\frac{1}{3}}}$$

$$\sin\psi = \frac{y}{a} \tag{21}$$

where $a_0$, $\eta$, and $\Gamma$ represent the initial particle radius, the viscosity, and the surface tension of the molten (or softened) polymer, respectively. Although the model strictly applies to the sintering of two spherical particles, Bellehumeur et al.[231] observed a good agreement with experimental results obtained from two cylindrical particles produced by cutting short segments (length: 0.33 mm, diameter: 0.47 mm) of material extruded from the print nozzle. However, the experiments were conducted under isothermal conditions. Conversely, printing by FFF is strongly non-isothermal, as the cooling rate is typically very high. For example, Seppala and Migler[234] provided evidence that the temperature at the interface between ABS rasters drops below the glass transition temperature within 2 s of egress from the nozzle tip.

The establishment of intimate contact through neck formation and growth is a pre-requisite for healing to occur. The reptation theory, which describes the motion of a linear polymer chain in an amorphous bulk, is often applied to explain polymer healing between touching surfaces. However, the original reptation theory is only valid under isothermal conditions and, as such, is unable to faithfully represent polymer healing in FFF. Starting from the original reptation theory, Yang and Pitchumani[235] developed a model for the healing process between two polymer layers under non-isothermal conditions that is more suitable for describing polymer healing in FFF, as it accounts for the dependence of the bond strength on the temperature history. According to Yang and Pitchumani,[235] the degree of healing between two polymer layers, $D_h$, is a function of time, $t$, according to

$$D_h(t) = \left[\int_0^t \frac{1}{t_W(T)}\, dt\right]^{\frac{1}{4}} \tag{22}$$

where $t_W(T)$ is the welding time, which is the time required for reaching the maximum bond strength at a certain temperature $T$. The dependence of the welding time on temperature should be experimentally evaluated for each material.[235] Although originally formulated for polymer layers, this approach has been successfully extended to predict the degree of healing between adjacent rasters in FFF parts. Accordingly, Costa et al.[236] applied Equation (22) as the adhesion criterion in a MAtLAb code for predicting if neighboring rasters in FFF parts will adhere adequately to each other before the system cools down and polymer chain mobility is frozen.

The cooling rate of the freshly printed raster is critical for the advancement of healing. Once the glass transition temperature is reached, molecular diffusion is halted.[186] In other terms, raster healing in FFF is a thermally-driven diffusive process, where interdiffusion is hindered as the material rapidly cools down below the glass transition temperature.[237] On the one hand, slow cooling and, hence, slow solidification would be desirable for ensuring satisfactory inter-raster bonding, which is necessary for achieving good mechanical properties. On the other hand, quick cooling would be necessary for retaining a high viscosity and "freezing" the targeted geometry, thus avoiding deformation due to raster spreading (as discussed below) and due to the weight of the subsequent layers. This means that mechanical strength and dimensional accuracy are conflicting goals in FFF.[228,236]

Exactly predicting the cooling rate of the freshly printed material is difficult, because this is the outcome of several concurrent phenomena. Heat exchange mainly occurs through convection with the environment, conduction and radiation between adjacent rasters, and conduction with the base platform (mainly for the first layer).[228,238] As a consequence, heat exchange depends on many processing parameters such as the printing temperature, the temperature of the base platform and the temperature of the environment (or the temperature of the enclosed build chamber, if applicable), the size of the raster (which, in turn, is governed by the diameter of the nozzle tip and by its vertical position), the layer thickness, the raster pattern, and the printing speed (feed rate during printing).[228,229,231]

In terms of material properties, a low heat transfer coefficient with air (responsible for convection) would be useful for retarding cooling as the extrudate travels from the nozzle tip to the previous layer (or to the base platform). Meanwhile, a high thermal conductivity (responsible for conduction) would be favorable for receiving heat from the liquefier. As pointed out by Turner et al.,[129] this leads to the apparently puzzling conclusion that the greater the thermal conductivity, the slower the raster will cool down, since a higher thermal conductivity helps the transfer of heat from the liquefier to the new raster. Also, as previously mentioned in Section 5.3, materials having a high thermal conductivity can be readily heated to the targeted temperature in the liquefier.

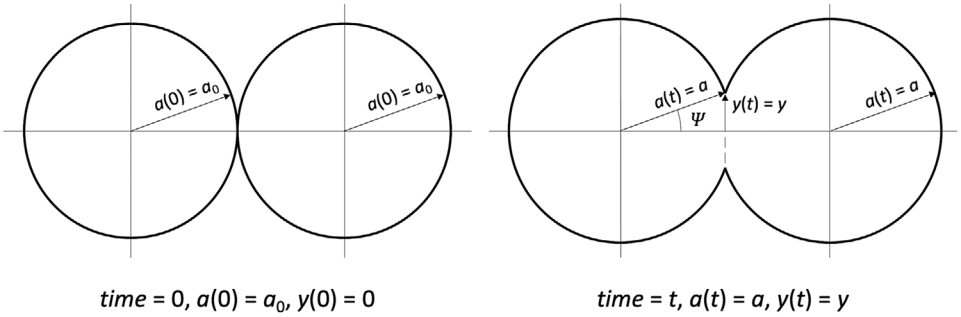


**Figure 13.** Evolution of the particles' radius and neck growth over time under the driving force of surface tension (Newtonian viscous flow under isothermal conditions).

The achievement of consolidated parts is thus determined by the establishment of a large neck (sintering) and by the promptness of molecular interdiffusion (healing) before the newly deposited raster freezes below the glass transition temperature. In practical terms, it has been reported that faster interdiffusion occurs when the molecular weight and the viscosity are low,[239] since the motion of larger molecules (namely, higher molecular weights) is typically slower especially at relatively low temperature.[240] According to Coogan et al.,[241] the interfacial bond strength in ABS parts is governed by molecular interdiffusion mechanisms, which are slow due to the long relaxation time of ABS; conversely, the interfacial bond strength in high-impact polystyrene (HIPS) parts is constrained by the poor interface contact, since the shorter relaxation time of HIPS enables a faster molecular interdiffusion as compared to ABS.

Recent investigations have substantiated the hypothesis that the heat transfer-driven molecular interdiffusion model can be successfully extended to multi-material FFF, even if neighboring rasters belong to different materials. For multi-material systems, the Flory–Huggins interaction parameter becomes critical, as it dictates the solubility of the two polymers which, in turn, influences the degree of mixing and therefore the advancement of healing through molecular interdiffusion.[242]

### 6.2. Raster Spreading

Quite often, sintering in FFF is described on the ground of the Frenkel–Eshelby model. However, this model originally described the rate of sintering driven by Newtonian viscous flow, whereas several authors have pointed out that various mechanisms other than Newtonian flow may come into play.[239] For example, as previously mentioned, the Frenkel–Eshelby model describes a two-body (particle–particle) interaction and does not consider the adhesion force between the particles and the substrate.[239] Conversely, a new raster in FFF generally establishes multiple interactions, as it interacts with the neighboring raster(s) on the same layer, and, simultaneously, with the rasters that form the layer underneath (or with the base platform).

Another point to consider is that, originally, Frenkel's model applied to identical spherical particles, and this condition is only met in the early stages of sintering, when the particles' radius remains relatively constant.[239] Most of all, FFF does not entail sintering of discrete spherical particles. On the contrary, rasters

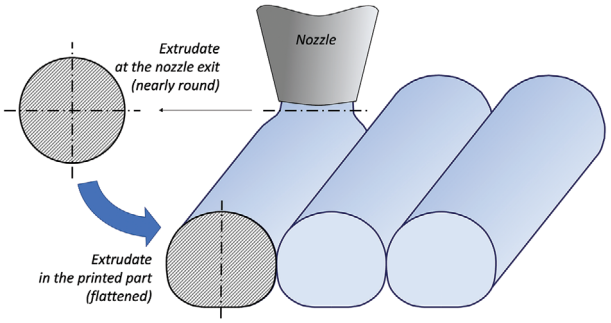


**Figure 14.** Although the extrudate is a round cylinder when it leaves the nozzle tip, the shape becomes slightly flattened on the base platform (or the previous layers) due to raster spreading.

in FFF are extremely long (typically, several centimetres) and slightly flattened cylinders, as shown in **Figure 14**. Gurrala and Regalla[243] modified the Frenkel's equation to describe the neck growth between two adjacent round cylinders. However, additional corrections are required to account for the real shape of the rasters in FFF, whose cross section is not perfectly round. In fact, the extrudate does receive the shape of a nearly round cylinder from the nozzle tip (whose standard cross-section is circular, although the literature describes some attempts at using different geometries, such as square or rectangular nozzles, to reduce the inter-raster void channels[244,245]); nonetheless, the raster comes to be flattened as a result of the tendency of the polymer whilst it is still hot to spread on the previous layer (or on the base platform at the beginning of printing). As a rule of thumb, the width of the raster in FFF is around 1.2–1.5 times the diameter of the nozzle tip.[178] However, Valerga et al.[162] recorded a strong dependence of spreading on the printing temperature, since the raster width of PLA increased linearly from around 0.71 mm at 180 °C to around 0.76 mm at 240 °C. Correspondingly, the raster thickness (layer height) decreased linearly from almost 0.76 mm at 180 °C to around 0.70 mm at 240 °C.[162] Also, the computational fluid dynamics (CFD) simulations of the deposition flow on a moving substrate conducted by Comminal et al.[246] (based on the simplifying assumptions of a Newtonian fluid in isothermal condition) suggest a strong dependence of the raster's cross section on the distance between the nozzle and the substrate, and on the ratio of the velocity of the moving substrate to the average velocity of the flow inside the nozzle.

In terms of materials properties, whereas several models have been proposed in the literature to describe the spreading of a liquid droplet on a surface,[247,248] raster spreading in FFF has some peculiarities. As commonly observed in the spreading of liquids, the spreading rate and the final shape in FFF depend on the viscosity of the extrudate, and on the relative surface energies of the extrudate and the substrate on which it is printed. However, the freshly printed raster in FFF cools down and solidifies very quickly, and this stops the spreading process before the equilibrium is reached. Also, the raster shrinks upon cooling, which changes its cross sectional area.[129] Meanwhile, the molten (softened) polymer experiences the combined action of the pressure exerted by the nozzle tip, which pushes the material against the previous layer (or the base platform), and of the force of gravity. As recently discussed by Agassant et al.,[170] the spreading mechanisms are governed by the distance between the print nozzle and the substrate. If this gap is greater than the nozzle diameter, the extrudate flows under a free surface condition and spreading is governed by surface tension; otherwise, if the gap is smaller than the nozzle diameter, spreading is governed by shear and pressure. According to the results of these computational and analytical models, the flow pressure at the nozzle exit increases with decreasing values of the gap between the nozzle tip and the substrate, as well as with decreasing values of the printhead velocity. Similarly, Coogan and Kazmer[241] recently observed that the exit pressure can push the printed layers together more effectively and more rapidly than spontaneous wetting phenomena, since a smaller layer thickness leads to a higher exit pressure, which is responsible for forcing the new layer into intimate contact with the previous layer.[241] However, as critically discussed by Tao et al.,[233] if the layer thickness becomes too small, the high cooling rate will rapidly reduce the polymer chain mobility, and this will prematurely stop the neck formation and inter-raster healing processes. As a consequence, the advantage of having a larger contact area will be outbalanced by the disadvantage of having a poorer interface healing. Moreover, working with thinner layers produces more heating–cooling cycles to complete the part, which may be responsible for sharp thermal gradients and ultimately for stronger thermal stresses. This is coherent with the experimental results reported by Aliheidari et al.[249] for ABS parts printed with three different values of the layer thickness (0.1, 0.2, or 0.3 mm). The highest fracture resistance corresponded to a layer thickness of 0.2 mm, with lower values being observed both at 0.1 mm (poor inter-layer adhesion; strong thermal stresses) and at 0.3 mm (limited contact area).

As explained in **Figure 15**, the contact area between neighboring rasters is deeply affected by this spreading effect. Additionally, the contact area also depends on several printing parameters such as the flow rate (flow multiplier value) and the distance between infill lines (infill line distance). Having a large contact area is beneficial not just for promoting the sintering and healing processes, but also for reducing the voids that may survive at the junction between neighboring rasters. As shown in Figure 15, these voids resemble empty channels in case the infill pattern is rectilinear. Increasing the inter-raster contact area and simultaneously reducing the presence of inter-raster voids typically results in high mechanical properties, with values of the Young's modulus that may approach those of the bulk material.[250] However, increasing the infill degree in order to augment the overlap

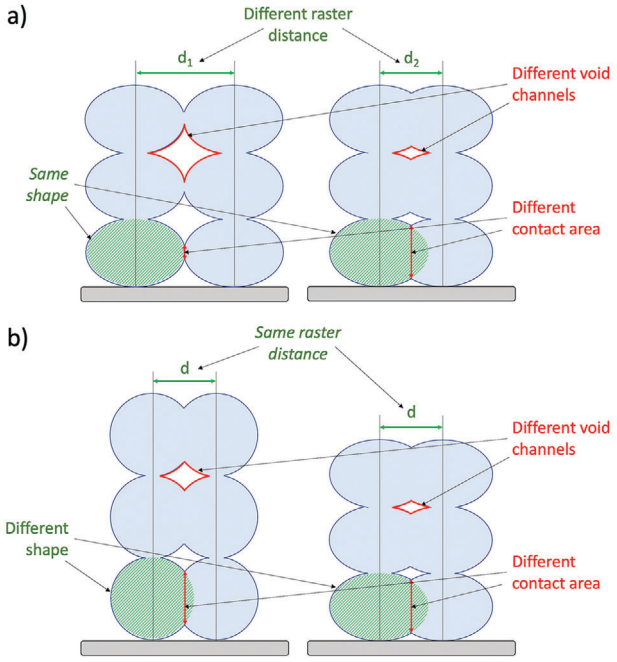


**Figure 15.** The contact area and the void channels between neighboring rasters are governed by the interplay between a) raster distance and b) polymer spreading. The cross section of the rasters is approximated to an ellipse for simplicity. The drawings also neglect wetting and sticking to the base platform.

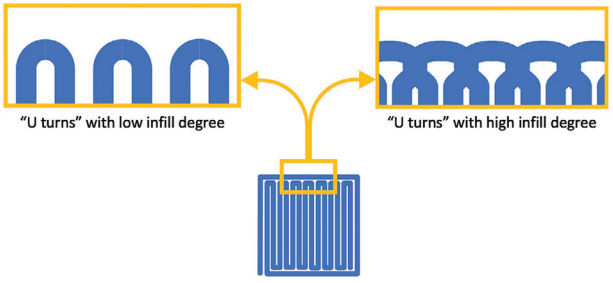


**Figure 16.** Increasing the infill degree (i.e., reducing the raster gap) may cause defects where the toolpath trajectory follows sharp directional changes, such as the "U turns" at the ends of each raster.

and thus the contact area between neighboring rasters comes to the cost of the part's weight and dimensional stability, since a high infill degree is often conducive to strong thermal stresses and eventually to warpage.[251]

Although less obvious, adopting a high infill degree may also worsen the voids and printing defects that typically occur when the toolpath trajectory follows a "U turn" at the end of each raster, sometimes referred to as "sub-perimeter voids".[233] As shown in **Figure 16**, decreasing the distance between neighboring rasters reduces the raster gap; however, this also reduces the curvature radius and, depending on its flexural properties, the feedstock material may be too stiff to accommodate this sharp directional change. This issue is particularly serious when the polymer matrix is reinforced with continuous fibers, since the increased flexural stiffness may severely limit the accomplishable return radius.[92,252–255]

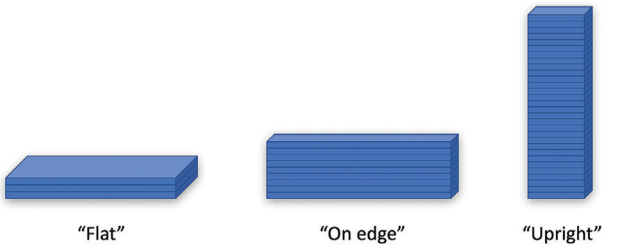


**Figure 17.** Different inter-layer interfaces generated in the same part when printed "flat" or "on edge" or "upright" on the base platform.

### 6.3. Molecular Orientation and Anisotropy

As previously mentioned, it has been observed that polymer chain orientation in FFF is possible because the conical section in the nozzle causes the molten (softened) material to experience an elongational flow.[192] However, orientation is thought to be partly disrupted by the die swelling effect[213] and by the curved trajectory that the extrudate follows when it leaves the nozzle tip and lays horizontal on the base platform or on the pre-existing layers.[212] Conversely, the portion of the raster that has already cooled down and fused to the underlying material may exert a drawing effect on the fresh extrudate, thus promoting orientation.[186] Owing to the interplay between these opposing phenomena, the extent of molecular orientation surviving in any FFF part is unknown,[192] and this should be measured case-by-case (for example, by neutron scattering) and related to the processing conditions and to the rheological properties.[186]

Notwithstanding this uncertainty, FFF parts are always imbued with some degree of molecular orientation, which increases the longitudinal strength of the rasters.[192] Molecular orientation is thus one of the main causes of the anisotropic behavior of FFF parts.[256,257] Even if molecular orientation may be leveraged to maximize the part's directional strength under given loading conditions, it has been postulated that a high degree of molecular orientation would be disadvantageous to polymer sintering and thus to the part's consolidation, as it would cause a strongly directional disentanglement of the polymer chains and contrast molecular interdiffusion at the raster interface.[212,251] Vice versa, annealing the printed part would promote polymer sintering and increase the inter-raster bond strength, but it would also impair molecular orientation and thus diminish the longitudinal strength of the rasters. No universal rule exists for balancing these contrasting factors.[186]

Alongside molecular orientation, the existence of void channels and the presence of inter-raster and inter-layer interfaces are other important reasons for the anisotropic behavior of FFF parts.[256] As shown in **Figure 17**, the part's orientation upon printing governs the inter-layer surfaces.

Whereas the mechanical properties (e.g., tensile stiffness and strength) are often similar for parts printed "flat" or "on edge" (namely, for parts having the major dimension parallel to the base platform), the "upright" position (whereby the major dimension is parallel to the growth direction) is regarded as the worst one due to the highest number of inter-layer interfaces.[19,24,257] According to literature data,[257,258] tensile samples can be up to 50% weaker if printed in the upright orientation. In order to outline

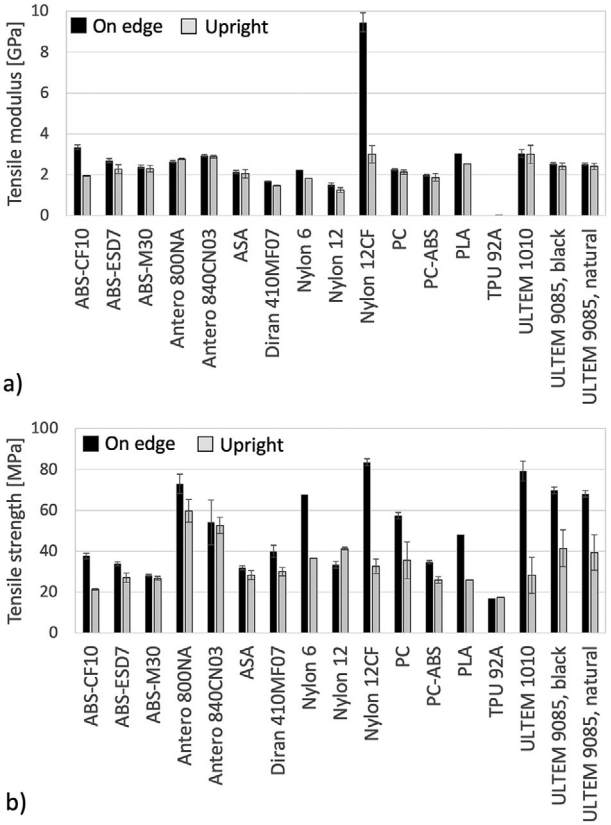


**Figure 18.** a) Stiffness (tensile modulus) and b) strength of tensile samples printed on edge and upright starting from commercial filaments (values reported in material data sheets[73]).

the effect of printing the same part under different orientations, the charts in **Figure 18** compare the stiffness (Figure 18a) and the strength (Figure 18b) values of tensile samples printed on edge and upright as reported in the material data sheets of commercial filaments.[73] Similarly, the anisotropy of FFF parts also impacts the fatigue performance (with the growth direction often being reported as the most problematic one[259,260]), and key functional properties,[261] such as thermal conductivity[262] and electrical conductivity.[263]

In addition to the printing orientation, the raster angle (shown in Figure 2) also has a strong effect on the tensile properties of FFF parts. As the raster angle increases from 0° to 45° to 90°, the tensile strength decreases because the inter-raster interfaces receive an increasing fraction of the applied load. However, the role of the raster angle can be less severe in FFF parts printed with a symmetrically balanced stacking sequence, for example, ±45°.[258]

Although this may seem counterintuitive, reducing the layer thickness is useful for improving the performance in the growth direction.[264] In fact, adopting a higher resolution (i.e., a smaller layer thickness) has been proven to reduce the inter-layer porosity thanks to the relatively short time interval occurring between the deposition of subsequent layers. The advantage of having a stronger inter-layer bonding prevails on the potential disadvantage of having more inter-layer surfaces. Moreover, thinner layers produce a smoother outer surface[265] and minimize the

 

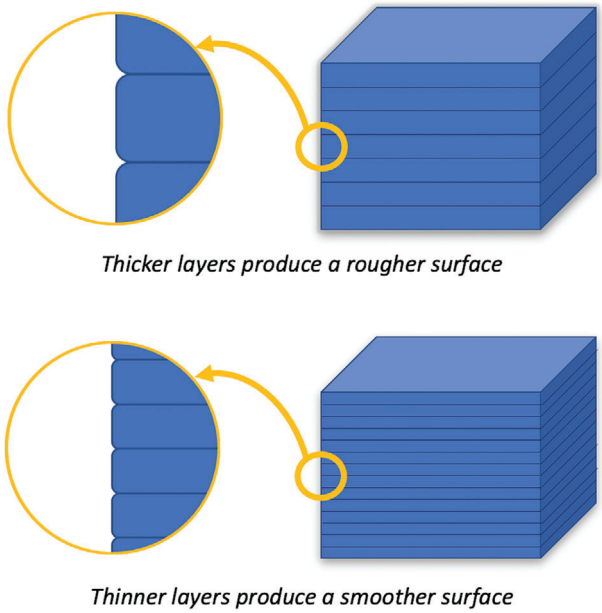


**Figure 19.** Printing with thinner layers produces a smoother surface, with smaller grooves between adjacent layers. (Note: drawing not in scale.)

notch-like effect that may be caused by the groove between adjacent layers, as shown in **Figure 19**. In addition to the surface finish, this may be relevant to the strength and mechanical reliability of the printed part. Although the correlation existing between surface quality and mechanical properties is more commonly investigated in metal AM than in polymer AM,[266] it is reasonable to expect that a lower surface roughness would be associated with a higher strength,[267] as the inter-layer indents, like surface defects, may trigger premature failure.

Two different parameters can be defined in order to quantify the anisotropy of FFF parts, namely the orientation-induced degree of anisotropy, $D_{a,O}$, and the raster-induced degree of anisotropy, $D_{a,R}$[258]

$$D_{a,O} = \frac{UTS_{flat} - UTS_{upright}}{UTS_{flat}} \quad (23)$$

$$D_{a,R} = \frac{UTS_{0°} - UTS_{90°}}{UTS_{0°}} \quad (24)$$

where UTS is the ultimate tensile strength of samples printed under different orientations (flat vs upright) or under different raster angles (0° vs 90°).

As reviewed by Gao et al.,[258] all FFF parts have positive values of the degree of anisotropy (both orientation-induced and raster-induced). However, the extent of the anisotropic behavior largely depends on the printing parameters.[256] Although this point is sometimes overlooked in the literature, the nature and the properties of the feedstock material are also very important. According to the data surveyed by Gao et al.,[258] the tensile properties become progressively more isotropic down the sequence (ABS) → (PLA) → (TPU and PEEK) → (PA, PE, and PP). This may result from several factors, such as the different propensity of different polymer chains (e.g., linear vs branched) to become preferentially orientated while flowing through the print nozzle or the different molecular mobility that is responsible for neck growth and inter-raster healing upon printing. Also, as reviewed by Gao et al.,[258] the achievement of isotropic properties depends on the interlayer bond strength, which is favored by a low viscosity. For example, whilst the viscosity of amorphous materials like ABS, especially if grafted, is relatively high,[268] polymers with a high degree of crystallinity like polyolefins typically have a very low viscosity once melted.[14]

Complicated effects on anisotropy have been reported when printing composite materials for FFF.[258] Adding a filler may have contrasting results depending on its geometry. The presence of strongly elongated fibers may accentuate the anisotropic behavior,[217] because fibers and particles having a high aspect ratio are likely to orient themselves along the printing direction.[133] As for short fibers and particles, the governing parameter is the viscosity of the polymer matrix. The greatest part of fillers (for instance, graphene nanoplatelets[132]) increase the viscosity of the neat polymer matrix, and this typically lowers the inter-layer adhesion and thus worsen anisotropy. However, some fillers (for instance, talc[227]), as well as several additives (for instance, low molecular weight additives, LMWs,[269] and poly-ethylene glycol, PEG, above the critical entanglement molecular weight[270]), lower the viscosity of the polymer matrix and the increased propensity to flow produces a more homogeneous microstructure, where the role of inter-raster and inter-layer surfaces is substantially reduced and anisotropy is mitigated.[227,271]

Additional evidence of the effect of the feedstock material on the anisotropic behavior of FFF parts comes from the printable furan-maleimide Diels–Alder (fmDA) reversible thermosets (DARTs) developed by Yang et al.[272] The fmDA linkages are reversible, meaning that they can be de-crosslinked during printing in order to enable melt processing between 90 and 150 °C, and then re-crosslinked to their entropically favored state at lower temperatures. Parts printed with these first-generation DARTs had nearly-isotropic properties, with less than 4% reduction in toughness when tested along the build (growth) direction,[272] which was attributed to the establishment of strong crosslinked bonds that mitigated the anisotropic effects. Similarly, Chen et al.[273] observed the nearly isotropic behavior of thermoset parts printed by FFF starting from a mixture of bisphenol A-based epoxy (DGEBA) resin and benzoxazine. The mixture was formulated in such a way as to feature a thermoplastic behavior at low temperature and a thermoset behavior at high temperature. This allowed the material to be extruded, 3D printed by FFF, and subsequently post-cured into a covalently crosslinked systems. CNTs were also added to improve the mechanical properties and modify the rheology, especially to prevent shape deformation during post-curing.[273]

### 6.4. Spider Web

In FFF, every time a layer or an isolated area within a layer are finished, the nozzle is moved upward, the filament is retracted to slightly pull back the extrudate, and the nozzle is moved to the new starting point for printing. Sometimes, it may happen that the extrudate does not break up neatly and a very thin polymer fiber is drawn along with the nozzle tip and falls on the

pre-existing layers. This effect, which is known as "spider web" (with other common names being "stringing" and "ozing"[274]), should be avoided because it seriously impairs the visual quality of the object. Mackay et al.[186] extensively reviewed the literature to reveal the main causes of the spider web effect and, wherever possible, to identify potential countermeasures. The final outcome was that the available knowledge is contradictory in this regard, since research in fiber spinning suggests that breakup should be governed by the elasticity of the softened polymer, whereas research in fluid dispensing leads to the opposite result that breakup should be dictated by the viscosity of the softened polymer. Additional efforts are thus required to understand how the spider web effect can be mitigated through materials properties. Meanwhile, some printer-related reasons have been identified, since the spider-web effect is often observed as a consequence of high temperatures or high printing speeds or misconfiguration in retraction settings.[274]

### 6.5. Surface Finish

As far as surface finish is concerned, PLA is often acknowledged as the FFF material providing the best surface quality.[275–277] Even if few contributions in the literature deal with a systematic comparison of the surface roughness of different materials in FFF, the better surface quality of PLA parts as compared to other feedstock materials such as ABS may be due to the ease of printing at a relatively low temperature. For example, Alsoufi and Elsayed[276] observed that the surface quality and dimensional accuracy of PLA parts were superior to those of ABS counterparts and this difference was attributed to the fact that all samples were printed at the same temperature of 220 °C, which was the maximum printing temperature for PLA and the minimum printing temperature for ABS.

However, regardless of the feedstock material in use, the roughness of FFF parts is often too high for precision manufacturing, where tight tolerances are required. According to Valerga et al.,[162] the average surface roughness, $R_a$, of transparent PLA is around 17 μm with a printing temperature of 180 °C and increases to nearly 25 μm with a printing temperature of 240 °C. Under the same printing parameters, the surface roughness was affected by the presence of pigments and dyes that modified the printability of neat PLA, mainly due to the different rheology of the melt and to the different crystallization.[162]

Many surface treatments are currently available to improve the smoothness and surface appearance of FFF parts.[278] Whilst polishing and machining are based on the mechanical removal of material from the surface where it is not needed, other finishing methods target the peculiar nature of thermoplastic materials that can be reprocessed upon heating[279] or chemically dissolved by selected solvents or by solvent vapors.[280–282] Materials that can be readily machined, thermally processed, or chemically dissolved are thus relatively simple to post-process, which explains why, for example, surface finishing is reportedly easier for PLA than for TPU.[74,75]

Even though the addition of fillers and especially of natural fibers may worsen the surface quality of FFF parts (as observed, for example, by Stoof et al.[283]), the available knowledge regarding the surface finish and the effect of surface treatments on composite parts is still limited and certainly deserves further attention.[284–288]

### 6.6. Warpage

Warpage is a common issue with FFF. Quite often, printed parts are bent or twisted out of shape and, if not controlled, warping may cause the part to break off from the base platform. Warpage is caused by the thermal gradients that are likely to build up across the part.[289] Depending on their coefficient of thermal expansion, thermoplastic polymers shrink upon cooling. Even if the feedstock material is isotropic in bulk form, the coefficient of thermal expansion becomes anisotropic after extruding and printing as a consequence of molecular orientation. Layers printed under different raster angles naturally tend to shrink along different directions, but subsequent layers are mutually constrained, and this engenders thermal stresses that progressively increase as the temperature is decreased from the glass transition temperature of the polymer to room temperature. The thermal behavior is made even more complicated by the presence of inter-raster and inter-layer interfaces, whose properties are locally different from those of the material inside the raster.[290]

Several factors influence the development of thermal stresses, and hence the entity of warpage. First, the part's geometry and printing orientation are known to affect the temperature distribution and thus the thermal gradients.[139,291] For example, Valerga et al.[162] compared the printability of different PLA objects without using any adhesive on the build platform. Whereas 3 cm wide cubes could be successfully printed, 12 cm × 2 cm single-layer parts delaminated from the base platform due to excessive warpage. Cooling rates are locally controlled by the printing conditions, such as the temperature of the liquefier, of the base platform, and of the environment/build chamber, and by the properties of the feedstock material, especially by its thermal conductivity and by its heat exchange coefficients.[129]

In terms of printing hardware, warpage can be mitigated by the adoption of a heated base platform, which reduces the thermal gradient between the bottom layers and the top ones and helps the printed part cool down more evenly.[19] Since the stickiness (and hence the adhesion) of certain polymers such as PP[61,125,139] and PE[292] to the surface of standard base platforms can be very poor, another aid against warpage and delamination consists in applying an adhesive tape or coating on the base platform.[19] Several options are available, including kapton tape, thermoplastic elastomer (styrene-ethylene-butylene-styrene or SEBS, Kraton), hard paper, phenolic cotton laminated plastics, printed circuit board, blue painter's tape, masking tape, washable glue stick, and even hair spray.[19,293–295] However, the adhesion to the base platform must not be so strong that the part cannot be removed after printing.[129,139,292,294,296]

The properties of the feedstock material are fundamental. Warpage may be affected by several parameters, including coefficient of thermal expansion, thermal conductivity, heat capacity, and Young's modulus. However, the FE simulations conducted by Fitzharris et al.[297] suggest that the coefficient of thermal expansion has the strongest effect, so that decreasing the coefficient of thermal expansion leads to decreasing the warpage by the same factor. A popular strategy to reducing warpage and making

 

it more isotropic consists in adding a filler having a low aspect ratio. Particles, if evenly distributed, tend to reduce the molecular mobility of the matrix, and hence alleviate shrinkage and warpage.[125,290] In this regard, the effectiveness of the constraining effect is governed by the achievement of a strong adhesion at the interface between the polymer matrix and the filler.[290] Moreover, smaller particles have been reported to exert a stronger effect because of their larger specific surface area at the matrix-filler interface.[290] The improved geometric stability may be particularly advantageous if large objects are to be produced[132,298–304] or if polyolefins are to be processed.[14,139,305] Even if this may seem counterintuitive, even elongated fillers may be helpful for reducing warpage. As discussed by Spoerk et al.,[139] reinforcing fibres, which are typically stiffer than the polymer matrix, hinder the entropically driven contraction movement of polymer chains and stabilize the part's geometry. Moreover, if carbon fibers are used, the high thermal conductivity helps to locally redistribute heat and makes the temperature field more homogenous.

Lastly, warpage is severely aggravated by the change in specific volume associated with the growth of crystalline phases in semicrystalline polymers, which is one of the main hindrances to the wider uptake of polyolefins as feedstock materials in FFF.[61,139,292,293] For semicrystalline polymers, a high crystallization temperature would be advantageous, since the surrounding amorphous matrix at high temperature is still soft and hence able to accommodate the volumetric change associated to crystallization.[290] The propensity to crystallize can be reduced by modifying the molecular structure of semicrystalline polymers, or by blending them with other thermoplastics.[139] The addition of fillers may also be beneficial, because the reduced polymer chain mobility may hinder the arrangement of molecular chains into ordered crystalline regions.[306] However, many fillers are known to promote heterogenous nucleation of semicrystalline polymers such as PLA,[307] PEEK,[308] and polyolefins.[221,309] Since the balance between nucleating effect and restraining effect is different for each system and may also depend on the filler loading,[310] it is not possible to generalize the effect of adding a filler on the crystallinity and hence on the thermal behavior as well as on the thermodilatometric properties of the polymer matrix. Each case must be thoroughly assessed individually in order to adjust the processing conditions and, wherever possible, mitigate the side effects of crystallization.

Some polymers may also experience a very slow crystallization over time or a secondary crystallization. This is the case, for example, with PHA bioplastics, which are very promising materials for 3D printing biocompatible and bioresorbable prostheses.[311] For example, if not processed or modified properly, polyhydroxybutirate (PHB) may have a very high crystallinity of around 60–70% due to the growth of very large spherulites. Moreover, the crystallinity can increase over time due to secondary crystallization. This causes a progressive embrittlement of the polymer, and a loss of geometric stability. Since the crystallization rate is very slow, PHAs are unable to crystallize during the first cooling/second reheating cycle of standard thermal analysis and, for this reason, the entity and consequence of crystallization have often been underestimated.[312]

Although the literature is currently limited in this regard, it is worth noting that the development of thermal stresses, and hence the occurrence of warpage or fracture may be worsened in multi-material FFF if the coefficients of thermal expansion of the two feedstock materials are sensibly different.[242]

## 7. Environmental Footprint and Safety Issues

### 7.1. Eco-Sustainability of 3D Printing by FFF

Common perception is that all AM methods including FFF are "green" technologies, with a reduced environmental footprint as compared to conventional processing. However, Cerdas et al.[313] demonstrated that distributed manufacturing by 3D printing has no absolute advantage in greenhouse gas emissions with respect to injection molding, and that the modified transportation of materials and goods does not provide a decisive contribution to energy saving in 3D printing. As argued by Ma et al.,[314] the shift from centralized manufacturing by injection molding to decentralized manufacturing by 3D printing does not avoid transportation, but changes from transportation of raw materials (polymer granules) and finished products to transportation of raw materials (polymer granules) and intermediate products (filaments).

Assessing the eco-sustainability of FFF products is extremely challenging, because the same object, with the same shape and geometry, can be fabricated with different printing parameters. As a result, the same object will feature different functional properties. At the same time, the life cycle and the environmental impact of the FFF part will also be different.[314] Ma et al.[314] proved that the infill density is the most critical parameter that affects the energy consumption in FFF, followed by layer thickness, printing temperature and printing speed. The energy consumption increases with increasing values of the infill density and of the printing temperature, and decreases with increasing values of the layer height and of the printing speed. Increasing the infill density is particularly impactful because a higher infill density requires longer printing times, consumes more energy and increases the weight of the finished part. Since more material is necessary for printing the same object with a higher infill density, the cost and energy required for the transportation of the raw materials and of the filaments increase accordingly.[314] Typically, maximizing the mechanical strength and maximizing the surface finish are the main goals of most users of FFF printers. However, increasing the mechanical strength often requires increasing the infill density; likewise, improving the surface finish requires reducing the layer thickness. In both cases, raising the quality (namely, the mechanical strength and/or the surface finish) of the printed part increases the time and energy for printing. Accordingly, the environmental impact of FFF becomes considerably worse. For this reason, as recommended by Ma et al.,[314] the properties of FFF parts should be commensurate with the intended usage, rather than "maximized", since overperformance brings about unnecessary environmental loads. Whereas the contribution by Ma et al.[314] clearly analyzes the role of different printing parameters on the sustainability of FFF, it would be interesting to understand if printing different feedstock materials may similarly have an effect on the environmental footprint of FFF. According to the results presented by Ma et al.,[314] the electric heating system (including liquefier and heated base platform) is the largest energy-consuming component of an FFF printer. Feedstock materials having a higher printing temperature are thus expected to induce higher energy consumption. However,

different materials may have different service life, and this requires a case-by-case life cycle assessment (LCA) to simultaneously account for energy consumption and life span.

### 7.2. Recycling and Waste Disposal

The nature of the feedstock material has a deep impact on the eco-sustainability of the AM process itself.[315] In this regard, FFF offers a key advantage over other AM techniques (for example, VPP methods that work with thermoset resins), as it is based on thermoplastic materials that can be processed repeatedly. The adoption of recycled plastics is expected to reduce the cost and the environmental impact of the feedstock for FFF.[315] Besides thermoplastic waste from conventional recycling bins,[316] waste printing materials can also be collected and re-extruded into printed filaments, so that a "closed-loop" strategy can be established.[317] As pointed by Mikula et al.[318] in their comprehensive review, the ability to re-manufacture 3D printed materials is critical, since AM is still frequently employed as a rapid prototyping tool, which results in a large volume of single-use objects. Moreover, on-site recycling of 3D printing materials into filaments that can be used again for printing (distributed recycling) would mitigate pollution from transportation to centralized collection points.[319,320] Meanwhile, a wide range of recycled materials, from rice husk[321] to turbine blade-derived fiberglass,[322] have been explored as fillers and reinforcements in FFF parts.

In spite of the prospective advantages in terms of decreasing material waste, recycling poses some technical and regulatory issues. Firstly, mechanical recycling is still considered the most straightforward and affordable avenue to re-processing. However, the combined action of heat and mechanical shear upon re-processing causes the polymer to degrade, and this progressively lowers its mechanical performance.[323] For example, it has been reported that the yield strength of as-extruded PA6 ranges between 35 and 186 MPa, but it drops to 56–87 MPa after mechanical recycling.[324] Similarly, closed-loop recycling of ABS is feasible for two cycles, although this decreases the impact strength by about 14%.[325] The tensile strength of 3D printed PLA decreased by 10.9% after crushing, re-extruding, and re-printing, while the tensile modulus remained almost unchanged.[326] Lanzotti et al.[327] reported that the short-beam (three point bending) strength of virgin PLA parts slightly decreased from 119.1 ± 6.6 to 106.8 ± 9.0 MPa after the first crushing, re-extruding, and re-printing cycle. Then, it remained almost unchanged at 108.5 ± 9.9 MPa after the second re-processing cycle, but drastically dropped to 75.0 ± 16.2 MPa after the third cycle. Thermal properties (melting temperature, crystallization, etc.) and physical attributes (surface properties, color, etc.) are also affected by thermal-mechanical degradation.[323] Even the time required for composting PLA becomes shorter after mechanical recycling due to the reduced molecular weight.[328] In addition to the processing-induced degradation, all thermoplastics are subject to gradual degradation during lifetime as a consequence of heat, oxygen, light, radiation, moisture, and mechanical stress.[323] To some extent, the molecular changes caused by this environmental degradation are similar to those caused by processing-induced thermal–mechanical degradation. Nonetheless, the additional exposure to oxygen is also responsible for photo-oxidative processes.[329] Various stabilizers (often inspired from the polyvinyl chloride [PVC] industry) are available to mitigate the degradative processes.[330] However, they may have side effects on the polymer, like changing its viscosity, and this may also alter the printability. Moreover, most stabilizers have historically been based on metallic salts (often barium, cadmium, lead, or zinc salts), or on organometallic compounds (mainly containing tin), which may be dangerous to the environment and to human beings. For this reason, over the last 30 years much effort has been spent in the development of less impactful non-metallic organic stabilizers. Nowadays, natural compounds such as Vitamin E are taken into consideration for their stabilizing and anti-oxidant action.[331] Alternatively, similar to the masterbatch technique previously described in Section 4.1, virgin PLA can be added to the recycled PLA filament in order to improve and stabilze the viscosity upon processing, and ultimately to increase the mechanical and thermal properties.[32]

Different approaches other than mechanical recycling are feasible.[324] Emerging routes like chemolysis, gasification, pyrolysis, fluid-catalyzed cracking, and hydrocracking aim to revert plastic waste to valuable products such as monomers or petrochemical feedstocks, and, wherever possible, to recover energy.[323] For example, PLA can be recycled back to lactic acid (LA, its monomer) by hydrolysis or alcoholysis.[332] However, chemical routes are generally complicated, and potentially impactful on the environment.[333] On the other hand, PLA is biodegradable and compostable. Although this may seem counterintuitive, the LCA conducted by Cosate de Andrade et al.[334] considering the categories of climate change, human toxicity, and fossil depletion, proved that mechanical recycling resulted in the lowest environmental impact, followed by chemical recycling and composting. Electricity consumption determined the higher impact of chemical recycling over mechanical recycling. As for composting, the results can be explained by the fact that mechanical and thermal recycling lead to recycled polymer as an output, which can be used again, sometimes repeatedly, while composting does not. However, when recycling is not possible (for example, when the properties of the recycled polymer have become too poor for further use), composting is a good alternative.

Special recycling procedures are needed to account for the presence of fillers and reinforcements in composite parts, because fillers, especially inorganic ones, should be treated differently from the thermoplastic matrix.[335,336] A pathway to developing more sustainable composite feedstocks for FFF consists in adopting vegetable fillers.[337] The design of "fully green" composites, that combine both matrix and filler from renewable resources,[338] is thus the ultimate trend of research in sustainable AM.[339]

Continuous fiber-reinforced polymers may be very challenging, because most conventional recycling methods break down the fibers, and this downgrades the original mechanical properties of the composite.[340] In principle, the problem of preserving the original length of the fibers affects both inorganic reinforcements (e.g., carbon and glass fibers), and organic ones (e.g. hemp fibers). New strategies are thus urgently needed. In this regard, Tian et al.[341] have recently demonstrated that 3D printed continuous carbon fiber-reinforced PLA-matrix composites can be recycled and remanufactured without impairing their original performance by means of a local remelting process. A hot air gun was

 

slowly moved along the reverse path of the printing process in order to melt the PLA matrix point-by-point. Meanwhile, the carbon fiber was gently pulled out from the melt. The fiber remained unaffected, while the molten PLA matrix adhered to it, thus forming a polymer-impregnated fiber-reinforced filament which, after smoothing the surface, could be spooled or directly used for remanufacturing by FFF.[341]

Another possible concern comes from the additives that may be added for improving the printability. Whereas their exact nature and concentration in commercial filaments are often unknown for confidentiality reasons, their presence may interfere with reprocessing, recycling, and disposal methods, and also pose safety concerns. For example, plasticizers and other harmful additives may be added to the base polymer to improve its processability. Presently, plasticizers are the most common polymer additives world-wide. However, traditional petroleum-based plasticizers, including phthalates, trimellitates, and dicarboxylates, are toxic to human beings and to the environment, and their dangerousness (especially in children's toys, biomedical devices, and food packaging) is worsened by their ease of leaching from the polymer matrix. Bio-based plasticizers such as starch derivatives, epoxidized linseed and soybean vegetable oils, citrate derivatives and levulinic acid, may represent safer and greener alternatives.[342,343]

In conclusion, it appears that shear stress, temperature, and oxygen degrade polymers. The degradative effects have been observed not only in polymers sensitive to these factors, such as PLA, but also in polymers that are relatively resistant, such as polyolefins.[318] However, new strategies are emerging to reduce the side effects of re-processing. Whilst it is not possible to rank FFF materials based on their recyclability, it is clear that, in order to reduce the environmental footprint, there is an increasing interest toward biodegradable plastics, both bio-based (like PLA and PHA plastics) and also petroleum-based ones (PVA, polyethylene terephthalate (PET), and HIPS).[344,345] Similarly, inorganic reinforcements like carbon fibers and glass fibers may be replaced with greener options, like sawdust, cellulose fibres, or other natural fibres.[346]

Secondly, standard guidelines have not been issued yet for directing the correct management of FFF waste. Whilst some attempts have been done to develop recycling codes (for example, by Hunt et al.[347]), bespoke parts, especially if printed at the hobbyist level, presently do not receive any labeling for the identification of the safe disposal and recycling procedures. This may impair the recycling of 3D printed materials at an early stage. According to the general recycling procedure outlined by Mikula et al.,[318] in the first step, materials should be separated and washed. With very few exceptions,[91,272,273] all feedstock materials for FFF are thermoplastic-based. Nonetheless, individual plastics should be sorted apart based on their composition and color for a successful recycling.[348] At an industrial level, density can be leveraged for separating different plastics. PLA, whose density is around 1.25 g $cm^{-3}$, is denser than other polymers commonly used in FFF, including ABS (whose density is around 1.04 g $cm^{-3}$). The difference is even greater with polyolefins, whose density is around or even lower than 1 g $cm^{-3}$. Thus, the relatively high density of PLA turns out to be an advantage for recycling, since PLA objects can be easily separated from ordinary thermoplastic waste based on their specific weight.[349,350] Similarly, industrial optic systems allow for the separation of different colors. However, the management of plastic waste from consumer 3D printers is still an open challenge.

### 7.3. Emissions and Potential Health Hazards

FFF can be defined as a "safe" AM technique, as long as it does not entail the usage of loose powders and solvents. As previously mentioned, this, together with its "cleanliness" (no sticky resins), is one of the main reasons for the success of FFF with hobbyists and amateurs. Nonetheless, recent reports in the scientific literature clearly point out that ultra-fine particles (UFPs) and volatile and semi-volatile substances (volatile organic compounds, VOCs) are released upon printing due to thermal degradation. The emissions are different depending on the filament's composition. For example, the study by Azimi et al.[351] identified caprolactam as the most abundant VOC emitted from nylon-based and imitation wood and brick filaments, styrene from ABS and HIPS filaments, and lactide from PLA filaments.

It is generally acknowledged that, unlike other thermoplastics such as ABS, PLA is odorless when heated up for printing.[80] Further, the emission of particles and other by-products is lower because the printing temperature of PLA is lower than that of ABS and other feedstock materials.[34,352–354] For these reasons, the usage of PLA has been regarded as being potentially less harmful for human health.[353,355] However, Tang and Seeger[356] have recently pointed out that it is not possible to establish a meaningful ranking of emissions based on the polymer type alone. Besides the polymer type, the addition of fillers, dyes, and other additives (stabilizers and plasticizers, for example), as well as the presence of unknown impurities may also change the thermal stability of the polymer matrix, and thus influence the emission of particles.[357,358] In other terms, the emissions are governed by the "filament product" as a whole, rather than by the polymer type.[356] For example, Potter et al.[359,360] demonstrated that not all VOCs can be attributed to the degradation of the polymer backbone, which suggests that some emissions are rather caused by the volatilization or degradation of polymer additives such as plasticizers and stabilizers. Amongst other VOCs (mainly lactide and acetaldehyde), the plasticizer bis(2-ethylhexyl) phthalate, which is considered a probable carcinogen, was emitted by metal-filled PLA filaments, although it was not disclosed in the filament composition.[360] Preliminary investigations suggest that pigments have a minor, but not negligible effect on the emissions.[35,353,358,361–363] Both metal fillers[357,364,365] and wood fillers[364] were reported to increase the emissions of PLA filaments. Metal fillers may also promote the emission of smaller particles, which have a higher deposition rate in alveoli.[354] However, also opposite trends have been observed. For example, the research conducted by Vance et al.[366] showed that the average aerosol emission rate of copper-infused PLA was higher than that of PLA, whereas that of wood-infused PLA was lower. In this regard, it is important to note that most papers in the literature aim to provide a sensible estimate of the emissions that may occur under real-use conditions, when printing in business offices, public libraries, university laboratories and classrooms, and even at home.[353] For this reason, they use commercially available filaments, whose exact composition may be unknown except for the

base polymer type and the primary filler.[365] For example, they may be produced with different polymer grades, or may contain "proprietary additivation" (as noted by Stabile et al.[364]) or even "non-advertized additives" (as pointed out by Potter et al.,[359,360]) and all these compositional variables interfere with the effect of the primary filler on the emissions.

It should also be mentioned that a sound comparison across the literature is impaired by the variability of the printing conditions. According to Tang and Seeger,[356] the emissions depend on the printer model (different hardware and software), and on the specific printer settings, with the printing temperature being particularly important.[356] Stabile et al.[364] observed that the same PLA filament did not cause any particle emissions when printed below 220 °C, whereas the emission rates became sensible at 220 °C ($6.78 \times 10^9$ particles $min^{-1}$) and increased by more than one order of magnitude when the temperature was increased up to 240 °C. Yi et al.[353] argued that, as the difference between the printing temperature and the melting temperature increases, more vapor can be generated and condense to form ultrafine particles by gas-to-particle conversion via nucleation and/or condensation processes. Accordingly, for safety reasons operators should not exceed the recommended printing temperature.[354]

Lastly, Tang and Seeger[356] have recently drawn attention to the lack of international standards for the measurement of emissions in FFF. Historically, several measurement techniques have been applied, as critically discussed by Zhang et al.[354] in their comprehensive review. In order to measure particle and chemical emissions from 3D printers, ANSI/CAN/UL 2904[367] proposes to print a cube with a fixed printing time of 4 h regardless of the printer model and the filament type. The particle emission is then normalized by either the mass of filament used or the printing time. However, according to Tang and Seeger,[356] this adjustment is still ineffective, because it does not take into account that filaments may largely vary by density (for example, due to the presence of metal fillers) and by printing time. Another point to consider it that the particle emission is quantified over a relatively long time interval, whereas emissions are known to commonly reach a maximum within few (5–10) minutes of printing.[366] In order to mitigate these issues, Tang and Seeger[356] outlined a standardized test procedure based on printing a fixed length (i.e., a fixed volume of material for a given filament diameter) of a filament as a strand without building a 3D object. Whilst this approach neglects the progressive addition of layers required for building up 3D objects, it makes it possible to emphasize the effect of the heat stress that is the main reason for emissions. The total number of emitted particles (TP) during a print job was identified as the key evaluation parameter, and all measurements were conducted in 1 $m^3$ emission test chamber, according to ISO 16000-9:2006.[368] Tang and Seeger[356] tested the new procedure against 44 commercial filaments (standard length used: 800 mm) and the results confirmed the strong effect of fillers and additives on the emissions of filaments nominally produced with the same polymer type. Whereas TP values were either not quantifiable or below $10^{10}$ for PLA (low emitter), average values for two copper-filled PLA filaments exceed $10^{11}$ (high emitters). The variability was even larger for ABS-based filaments, as the range in TP values spanned over three orders of magnitude between the lowest and the highest emitter. Interestingly, the TP of the one PVA filament under examination was below the lower level of quantification, and also the PP filament was ranked as low emitter.

Whilst the standard protocol described by Tang and Seeger[356] paves the way for a more consistent measurement of emissions, additional research is still needed to ascertain the safety of FFF printing, not just in professional settings like laboratories and scientific hubs, but also in homes and schools.[365] Presently, many papers in the literature systematically compare the effect of different fillers, or different filler loadings, or additives, on the mechanical performance of FFF parts produced starting from custom-made filaments that are extruded on purpose under controlled conditions (typically, starting from neat polymer pellets and adding increasing amounts of fillers or additives). In future, it would be interesting to apply a similar approach in order to systematically evaluate the effect of individual fillers and additives on the emissions in FFF.

## 8. Critical Considerations Regarding SDS

A key requirement in SDS is that a high filler loading, typically between 50 and 65 vol%, is needed to mitigate shrinkage and the risk of slumping upon sintering. Hasib et al.[102] observed that the sintering-induced shrinkage was inversely proportional to the initial volumetric content of inorganic filler in the green part. However, working with high filler loadings may cause poor printing quality or even failure due to the high viscosity in the liquefier.[43] Raising the printing temperature may help reduce the viscosity, but overheating above the degradation temperature of the polymer matrix should be avoided.[43]

As summarized by Singh et al.,[43] the best particles for metal injection molding are spherical with a diameter smaller than 45 µm, because they flow easily and possess good filling properties, which is helpful for achieving a high packing density in the green part while keeping the viscosity low. For the same reason, spherical particles are also recommended in SDS, although irregular particles having a higher specific surface area may favor interlocking and promote sintering.[37,102]

Working with fine powders boosts the driving force for sintering, since they have higher specific surface area, stronger sintering stress, and shorter diffusion distances than large particles.[369] Provided they do not form large agglomerates, smaller particles may also be advantageous in order to limit the risk of clogging the nozzle upon printing and to achieve parts with minute details. As a pre-requisite, particles should be smaller than the nozzle diameter, whose standard size is 400 µm, but can range between 100 µm and 1 mm.[177] This requirement is relatively easy to meet for primary particles, but can be challenging for larger aggregates, which calls for the preferential usage of small and de-aggregated powders.[370] The choice of the particle size should also account for the part's geometry, as particles should not exceed 1/10 of the smallest detail to produce.[218] However, an important downside with working with fine powders is their effect on the viscosity, because smaller particles cause stronger inter-particle friction and hence increase the viscosity as compared to larger particles.[43] Singh et al.[43] observed that the maximum feed rate attainable when printing filaments produced with a coarse Ti-6Al-4V powder (median particle size: 30 µm; filler loading: 59 vol%) was twice as much as that

 

achievable with fine powder counterparts (median particle size: 13 μm; filler loading: 59 vol%). Although the limiting force as defined by Equation (8) was the same for both kinds of filaments, the presence of the coarse powder resulted in a lower viscosity and thus enabled printing at higher feed rates. Similarly, Kukla et al.[371] observed that the apparent shear viscosity of feedstock materials containing 55 vol% of 316L stainless steel particles substantially decreased when the average particle size was increased from 5.5 to 8.6 μm. However, the secant modulus and the strain at break of the filaments also decreased. As a result, the feedstock with smaller particles could be printed, whilst the feedstock with larger particles could not.[371] This suggests that printability is the result of a delicate balance between filler properties and binder composition.

In SDS, the polymer matrix mainly works as a sacrificial binder that "glues" the filler particles together while printing. Quite often, debinding is accomplished in two separate steps. In the first step, also called "primary debinding," a fraction of the binder is selectively removed by means of thermal, chemical, or catalytic routes, and then the remaining polymer backbone is thermally decomposed just before sintering in a second step called "secondary debinding."[40] The two-stage approach is also feasible in straight thermal debinding, since the binder is a multicomponent formulation including a thermally labile fraction that can be removed at lower temperature and a more thermally stable backbone that is debound at higher temperature.[372] Primary debinding is necessary to create a network of interconnected pore channels that, later on, will enable the safe release of the decomposed gas molecules of the backbone to the ambient atmosphere. Otherwise, off-gases would remain entrapped inside the part and the pressure build-up would ultimately cause cracks and blisters.[373] Moreover, the interconnected pore channels produced during the primary debinding stage accelerate the transport of matter as compared to diffusion phenomena and increase the debinding rate.[372] The polymer backbone, meanwhile, is unaffected and holds the inorganic filler in place until diffusion bonds are established between the particles.

The appropriate formulation of a binder for SDS is extremely challenging and, for this reason, details are not always disclosed in the literature.[40,370] As a general guideline, the binder in SDS is made of three components[40,374–376]

i) The main binder component, which is removed during the first debinding stage and accounts for 50–90 vol% of the whole binder system;
ii) The backbone, which survives through the first debinding stage and is thermally removed just prior to sintering. The backbone may account for up to 50 vol% of the whole binder system;
iii) Additives like dispersant agents, compatibilizers, plasticizers, and stabilizers, which are introduced to enhance the filler distribution, prevent agglomeration, and phase separation, impart flexibility to the filament, and adjust the mechanical and rheological properties. Additives may include waxes, to adjust the viscosity,[377] and tackifiers (e.g., hydrocarbon resin), that increase the inter-layer adhesion.[40] Additives may account for up to 10 vol% of the whole binder system.

In addition to "glueing" the filler particles together, the binder should provide the filament with appropriate rheological and mechanical properties. In spite of the high viscosity that is frequently observed as a consequence of the high filler loading, the filaments should not buckle at the entrance of the liquefier, as already discussed in Section 5.2. To this aim, a high compressive modulus may be necessary. At the same time, the filament should preserve some flexibility for spooling and feeding into the printer. This can be accomplished either by using polymers that are intrinsically flexible, like elastomers or amorphous polyolefins, or by modifying stiffer polymers, like semi-crystalline polyolefins, with plasticizers. Common plasticizers can be low-molecular weight polyolefins.[40]

The exact formulation of the binder should be adjusted to the intended de-binding strategy. The polymer matrix for thermal debinding should not contain solvents and should not generate an acidic atmosphere or produce any other side products that may contaminate the inorganic filler.[378] The basic requirement in chemical debinding is that the main binder component can be selectively removed in a solvent (either in an organic solvent, or in water) that does not affect the backbone. This is the case, for example, of cyclohexane in conjunction with PE as the backbone.[296] Catalytic debinding, which was first introduced by BASF in powder injection molding (Catamold system), is based on polyacetal binders. When the temperature is above 100 °C, the polyacetal binder unzips through the action of a catalyst (quite often, $HNO_3$) and vaporizes as formaldehyde gas. The debinding temperature is preferably chosen around 120 °C to not exceed the softening point of the binder (150–160 °C), because this would cause thermally-induced warping and sagging. Most polyacetals are shear-sensitive and crystalline, and thus unsuitable for powder injection molding and also for SDS, as they would experience chain degradation upon processing, and substantial shrinkage upon cooling. However, new polyacetal-based formulations, whose main ingredient is polyoxymethylene (POM, also known as polyformaldehyde), are compatible with normal processing conditions and enable a fast catalytic debinding.[379]

The binder formulation should also account for the specific composition and properties of the filler. For example, Agarwala et al.[380,381] reported that the base binder composition named "RU1" (containing 35 wt% of polymer as the backbone, 30 wt% of wax to adjust the viscosity, 20 wt% of elastomer to provide flexibility, and 15 wt% of tackifier to promote adhesion) was tested for the production of filaments for SDS containing different kinds of powders, including $Si_3N_4$, $SiO_2$, lead zirconium titanate (PZT), WC-Co, and stainless steel. However, PZT and WC-Co also required the addition of 1 wt% of oleyl alcohol as a dispersant to reduce the viscosity to values permissible in FFF. All the preliminary filaments, extruded with a capillary rheometer, were not flexible and hence broke down to straight and stiff pieces, which had to be manually fed into the printer. In order to obtain single screw extruded filaments featuring the flexibility required for spooling, the binder formulation for $Si_3N_4$ had to be changed to contain 19 wt% of polymer, 20 wt% of wax, 26 wt% of elastomer, and 35 wt% of tackifier, with the addition of 3 wt% of oleyl alcohol. However, Agarwala et al.[380,381] reached the conclusion that different adjustments to the base binder formulation would be required to achieve spoolable filaments with different powders. As a matter of fact, in a later contribution a different binder was proposed for

 

PZT, which contained polyolefin-based binder, hydrocarbon resin tackifier, PE wax, and polybutylene plasticizer in a 100:20:15:5 ratio, with the addition of stearic acid as the most suitable surfactant (with the other options being oleyl alcohol, stearyl alcohol, oleic acid).[382] As remarked by Cano et al.,[296] the adhesion to fillers having a polar surface can be improved by using binders grafted with polar reactive groups.

Besides the appropriate formulation of the binder, coating the filler with a surfactant may enhance the powder dispersion.[383] Even if stearic acid is often used to prevent particle agglomeration,[375] surfactants may be different for different powders. As already mentioned for binders grafted with polar groups, surfactants containing polar molecules tend to bond with the surface of polar particles, whilst non-polar molecules tend to bond with the surface of non-polar particles. Some long-chain alcohols or fatty acids may contain a polar group at one end of the chain, and a non-polar group at the other end, which allows them to adsorb onto both non-polar and polar surfaces.[383] A strong adhesion to the particle surface is crucial to avoid incorporating the molecules of the surfactant into the polymer phase, as this would change the mechanical, thermal, and rheological properties of the binder.[140]

To conclude, it is possible to appreciate the complexity of achieving a proper binder formulation, due to the numerous requirements and variables in play, which should be assessed on a case-by-case basis. Some examples of this variability are summarized in **Table 1**.[119,138,188,218,296,370,371,374,378,382,384–408]

## 9. Summary

Some key considerations emerged from this survey of the literature regarding materials requirements in FFF:

i) Although printability is a pre-requisite, the successful development of new feedstock materials for FFF should take into account the whole life cycle, and not just the printing step. In order to assist materials developers in this challenging task, **Table 2** provides a roadmap to the main materials requirements in FFF. The most important materials properties are reported for each step of the process, from the synthesis of the feedstock material to the disposal of end-of-life printed parts. Wherever possible, precise bounds are placed on acceptable feedstock properties. For completeness, Table 2 also lists the corresponding sections of this review paper where additional information can be retrieved, as well as specific references from the literature.
ii) Feedstock materials for FFF must meet several processing requirements at the same time, sometimes following mutually conflicting trends. For example, mechanical strength relies on the establishment of inter-raster bonds in the printed part, which would be favored by a large processing window above the glass transition temperature (or melting temperature) and by slow cooling down, whereas dimensional accuracy relies on the retention of the printed shape, which would be favored by a narrow processing window and by fast cooling.
iii) The formulation of new composite materials for FFF is particularly demanding, because adding a filler drastically changes the thermo-mechanical and rheological properties and hence the printability of the thermoplastic matrix. Whereas increasing the filler loading is often necessary to reach the targeted functionality (for example, exceeding the percolation threshold for electrical conductivity), this will likely make printing more difficult. These processing issues are emphasized in the production of fully inorganic parts, since the filler loading should exceed 50 vol% for sintering.
iv) A general recommendation that emerges from research articles is that existing commercial filaments for 3D printing should be carefully characterized in order to provide a benchmark, since new materials should have similar thermo-mechanical and rheological properties in order to be printable with standard FFF hardware. However, this is a very pragmatic approach, that contributes to identifying what is printable and what is not, but does not explain *why*.
v) No international standard exists for testing feedstock materials and printed parts, and this may cause inconsistencies in the published data and thus hamper the ability of researchers to compare different materials and draw far-reaching conclusions from them.
vi) Some fundamental features of a typical FFF process are still largely unknown. For example, there is not a single theoretical framework describing the behavior and flow of the polymer through the liquefier, as the available studies are often based on different model geometries and simplifying assumptions. The governing parameters for some phenomena, such as the spider web effect, are unresolved. In this regard, research is still needed to improve current-day understanding of the processing science and enable a holistic approach to the development of new advanced materials for FFF.

## Appendix

### A Predictive Models of the Pressure Drop

#### *A.1 Model Followed by Venkataraman et al.*

As shown in **Figure** A1, the basic assumption of the model developed by Venkataraman et al.[183,184] is that, owing to the similar geometries, the pressure drop in the nozzle, $P$, can be related to the pressure drop in a capillary rheometer, $P_r$, through a scaling factor $k$, as seen in Equation (13).

The pressure drop in a capillary rheometer, in its turn, depends on the geometry of the rheometer (where $l$ is the length, and $r$ is the radius of the capillary), on the apparent viscosity of the fluid, $\eta_a$, and on the volumetric flow rate, $Q$, according to

$$P_r = \frac{8\eta_a Ql}{\pi r^4} \tag{A1}$$

and hence

$$P = \frac{8\eta_a Ql}{\pi r^4 k} \tag{A2}$$

#### *A.2 Model Followed by Singh et al.*

Although this assumption has been questioned in the literature,[185,409] the rheological behavior of the polymer melt is

 

**Table 1.** Examples of binder formulations for SDS as reported in the literature.

| Reference | Disclosed binder components | Filler | Debinding strategy |
|---|---|---|---|
| Abe et al., 2021 [384] | Polyoxymethylene, polypropylene, paraffin wax | 17-4PH | Thermal |
| Abel et al., 2019 [385] | Thermoplastic elastomer compound, functionalized polyolefin, stearic acid | Tetragonal zirconia (yttria stabilized), or 17-4PH | Chemical (solvent debinding) |
| Arnesano et al., 2020 [386] | Low-density polyethylene, polylactic acid, paraffinic wax, polyethylene grafted maleic anhydride | Alumina | Chemical (dewaxing) |
| Boschetto et al., 2022 [387] | Polyoxymethylene | SS 316L | Catalytic |
| Cano et al., 2019 [296] | Acrylic acid-grafted high-density polyethylene, stearic acid, soluble fraction (either amorphous polyolefin or styrene-ethylene/butylene-styrene copolymer, used neat, mixed with paraffin wax, or mixed with paraffinic extender oil) | Tetragonal zirconia (yttria stabilized) | Chemical (solvent debinding) |
| Cano et al., 2020 [119] | Thermoplastic elastomer compound, polyolefin grafted with a polar component | Tetragonal zirconia (yttria stabilized) | Chemical (solvent debinding) |
| Damon et al., 2019 [370] | Polyacetal binder system | SS 316L | Catalytic |
| Ebrahimi and Ju, 2018 [388] | Poly(lactic acid) | Copper | Thermal |
| Egorov et al., 2021 [389] | Organosilicon polymers, additives (various) | Alumina, or SiC, or BN, or zirconia | – |
| Esslinger et al., 2021 [390] | Poly(lactic acid), poly(ethylene glycole) | $\beta$-tricalcium phosphate | Thermal |
| Godec et al., 2020 [391] | Thermoplastic elastomer, grafted polyolefin | 17-4PH | – |
| Gong et al., 2019 [392] | Polymer | SS 316L | Catalytic |
| Gonzalez-Gutierrez et al., 2017 [393] | Thermoplastic elastomer, grafted polyolefin | Strontium ferrite ($SrFe_{12}O_{19}$) | – |
| Gonzalez-Gutierrez et al., 2019 [394] | Grafted polyolefin, thermoplastic elastomer | 17-4PH | Chemical (solvent debinding) |
| Gorjan et al., 2019 [395] | Polymethylsiloxane resin ($SiO_2$ source), ethylene vinyl acetate | $\gamma$-alumina | Thermal |
| Gorjan et al., 2020 [396] | Ethylene vinyl acetate, stearic acid | Alumina | Thermal |
| Iyer et al., 2008 [397] | Investment casting wax | $Si_3N_4$ (coated with oleyl alcohol) | Thermal |
| Janek et al., 2020 [188] | Polyvinyl alcohol | Hydroxyapatite | – |
| Kukla et al., 2017 [371] | Thermoplastic elastomer, grafted polyolefin | SS 316L | – |
| Kukla et al., 2017 [138] | Thermoplastic elastomer, grafted polyolefin, dispersant/compatibilizing agents | SS 316L, or Ti-6Al-4V, or NdFeB, or strontium ferrite ($SrFe_{12}O_{19}$), or ziconia | Chemical (solvent debinding) |
| Kukla et al., 2019 [398] | Thermoplastic elastomer compound, polyolefin grafted with a polar component, stearic acid | Tetragonal zirconia (yttria stabilized) | Chemical (solvent debinding) |
| Kurose et al., 2020 [399] | Polyoxymethylene, paraffin wax | SS 316L | Thermal |
| Liu et al., 2020 [400] | Poly-formaldehyde, additives (polypropylene, dioctyl phthalate, dibutyl phthalate, zinc oxide) | SS 316L | Catalytic |
| Marsh et al., 2021 [401] | Elastomer, polyolefin, fatty acids (stearic acid) | Silver-modified 58S bioactive glass | Thermal |
| McNulty et al., 1998 [382] | Polyolefin base binder, hydrocarbon resin tackifier, polyethylene wax, polybutylene plasticizer | Lead zirconate titanate, PZT (coated with stearic acid as surfactant), or hydroxyapatite (coated with stearic acid as surfactant) | – |
| Nötzel et al., 2018 [218] | Low density polyethylene, paraffin, stearic acid as surfactant, release agents | Alumina | Chemical (dewaxing) |
| Pekin et al., 1998 [374] | Ethylene vinyl acetate copolymers, microcrystalline wax | Alumina | Thermal |
| Pellegrini et al., 2022 [402] | Polyoxymethylene, polypropylene, additives (dioctyl phthalate, dibutyl phthalate, zinc oxide) | SS 316L | Catalytic |
| Pistor, 2001 [403] | Aluminum oxide, ethylene vinyl acetate, ethylene ethyl acrylate, heavy mineral oil, methoxypolyethylene glycol | $Si_3N_4$ | Thermal (burn-out) |
| Prathumwan and Subannajui, 2020 [404] | Poly(lactic acid) | Aluminum | Thermal (controlled oxidation) |
| Riecker et al., 2016 [378] | Polyamide, organic additives (plasticizer, dispersing agent) | SS 316L | Thermal |
| Schumacher and Moritzer, 2021 [405] | Polyoxymethylene | SS 316L | – |
| Thomson et al., 2019 [406] | Thermoplastic elastomer compound, grafted polyolefin | SS 316L | Chemical (solvent debinding) |
| Thomson et al., 2021 [407] | Styrene-based thermoplastic elastomer, grafted polyolefin, additives | Commercially pure titanium | Chemical (solvent debinding) |
| Zhang et al., 2020 [408] | Polyolefin-thermoplastic system | Ti-6Al-4V | Chemical (solvent debinding) + thermal |

**Table 2.** Roadmap to materials requirements in FFF.

| Materials requirements | | |
|---|---|---|
| Step | Requirement | Reference |
| Feedstock synthesis | Affordability and scalability | Section 4.1 |
| Filament production | Extrudability (or drawability) | Section 4.2 |
| | Viscosity between 5000 Pa s and 10000 Pa s | Section 4.3, Ref. [124] |
| Filament spooling | Minimum strain at yield of 5% under tensile load | Section 4.4, Ref. [139] |
| | Maximum filler loading: 30 vol% in PLA, 50 vol% in PLA + plasticizer | Section 4.4, Ref. [142] |
| Feeding mechanism | High shear strength to overcome pressure drop | Section 5.1, Refs. [43, 177] |
| Liquefier entrance | $E_c/\eta_a$ higher than a critical value in the range $3 \times 10^5$ to $5 \times 10^5$ $s^{-1}$ to avoid buckling | Section 5.2, Refs. [183, 184] |
| Flow through the liquefier | Polymer having shear thinning behavior | Section 5.3 |
| | Polymer having high heat transfer coefficient for fast melting/softening | Section 5.3, Ref. [185] |
| | Molten/softened polymer having high apparent viscosity to avoid backflow | Section 5.3, Ref. [189] |
| | Processing temperature in the 180–260 °C range for standard printers | Section 5.4 |
| General printability | Molten/softened polymer having apparent viscosity around 200 Pa s for good printability and inter-raster bonding | Section 5.8, Ref. [221] |
| Part's build-up | Low heat transfer coefficient with air for slow cooling and strong bonding (but worse print accuracy) | Section 6.1, Ref. [129] |
| | High thermal conductivity for slow cooling and strong bonding (but worse print accuracy) | Section 6.1, Ref. [129] |
| | Low molecular weight for fast inter-diffusion | Section 6.1, Ref. [239] |
| | Low viscosity for fast inter-diffusion | Section 6.1, Ref. [239] |
| Spider web | Unknown | Section 6.4 |
| Surface finish | Ease of melting/softening or chemical dissolution | Section 6.5 |
| Shrinkage and warpage | Low coefficient of thermal expansion | Section 6.6, Ref. [297] |
| | Limited crystallization | Section 6.6 |
| | High crystallization temperature (if any) | Section 6.6, Ref. [290] |
| Sustainability | Recyclability/Biodegradability | Section 7.2 |
| Health and safety | No harmful additives/fillers | Section 7.3 |
| Shaping, debinding, and sintering | Filler loading higher than 50 vol% for reducing shrinkage | Section 8, Ref. [40, 376] |
| | Spherical particles smaller than 45 µm for sintering | Section 8, Ref. [43] |
| | Particles smaller than 1/10 of smallest detail | Section 8, Ref. [218] |
| | Two-stage debinding | Section 8, Ref. [372] |

often described according to the power law of Ostwald-de Waele for non-Newtonian fluids formulated as

$$\dot{\gamma} = \Phi \times \tau^m \tag{A3}$$

where $\dot{\gamma}$ is the shear rate, $\tau$ is the shear stress, $\Phi$ is the material fluidity, and $m$ is a parameter describing the flow characteristics, mainly the deviation from a pure Newtonian flow (with $m$ typically ranging between 2 and 4 for non-Newtonian fluids in the shear rate range of $10^0$–$10^4$ $s^{-1}$).[43]

A comparison between Equation (19) and Equation (A3) leads to the equivalences[410]

$$\phi = \Phi^{-\frac{1}{m}} \tag{A4}$$

and

$$n = \frac{1}{m} \tag{A5}$$

The model described by Singh et al.[43] is based on the equations originally formulated to describe the flow through an extrusion die by Michaeli and adapted for an FFF nozzle by Bellini et al.[180] Taking into account the geometry of the liquefier-nozzle system schematized in **Figure** A2, the total pressure drop, $P$, is the sum of three contributions, $P_1$, $P_2$, and $P_3$:

$$P = P_1 + P_2 + P_3 \tag{A6}$$

Under the hypotheses that:

i) the melt is incompressible and isothermal;
ii) there is a no-slip boundary condition at the wall; and
iii) the flow is fully developed, steady-state, and laminar.

The momentum balance performed on the three sections of the liquefier-nozzle system leads to the following equations

$$P_1 = 2L_1\left[\frac{Q(m+3)}{\pi\Phi\left(\frac{D_1}{2}\right)^{m+3}}\right]^{\frac{1}{m}} \tag{A7}$$

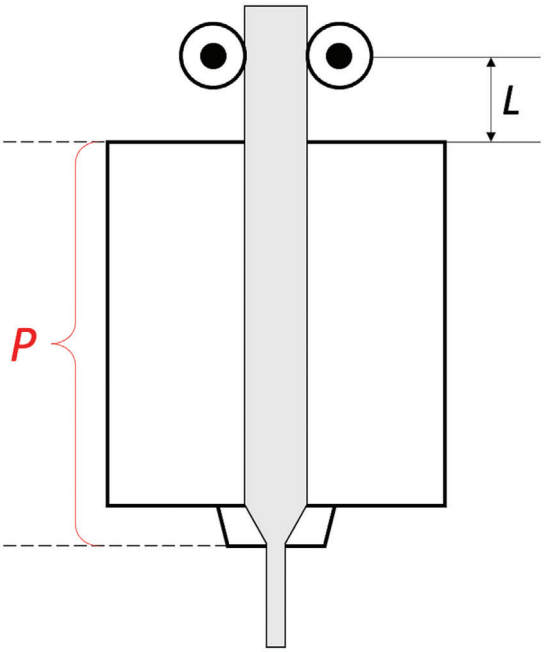


**Figure A1.** Schematic representation of the geometry of the liquefier-nozzle system and corresponding value of the pressure drop according to the model developed by Venkataraman et al.[183,184]

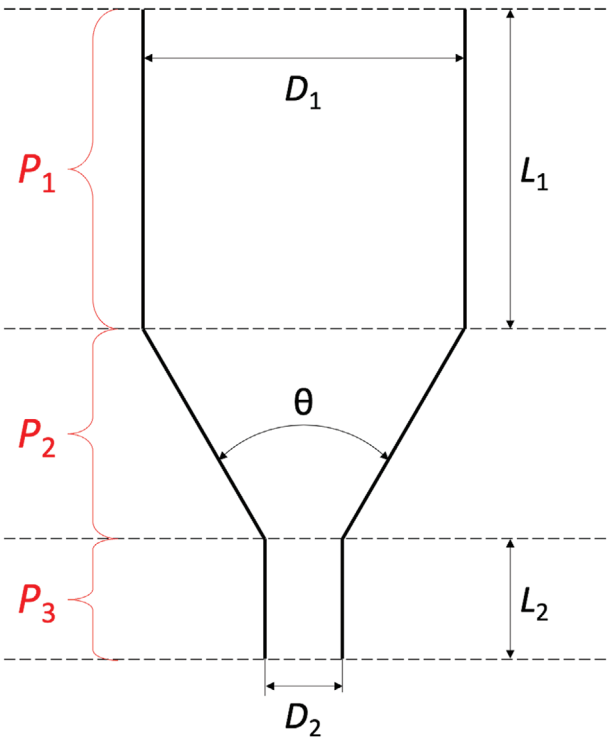


**Figure A2.** Schematic representation of the geometry of the liquefier-nozzle system and corresponding values of the pressure drop according to the model developed by Singh et al.[43]

$$P_2 = \frac{m}{3\tan\frac{\theta}{2}} \times \left(\frac{1}{D_2^{\frac{3}{m}}} - \frac{1}{D_1^{\frac{3}{m}}}\right) \times \left[\frac{Q}{\pi\Phi}(m+3)2^{m+3}\right]^{\frac{1}{m}} \quad \text{(A8)}$$

$$P_3 = 2L_2\left[\frac{Q(m+3)}{\pi\Phi\left(\frac{D_2}{2}\right)^{m+3}}\right]^{\frac{1}{m}} \quad \text{(A9)}$$

where $Q$ is the volumetric flow rate as defined in the main text. $D_1$ corresponds to the diameter of the liquefier barrel, which is $D_L$ in the main text, $L_1$ corresponds to $L_L$, and $D_2$ to the diameter of the nozzle tip, which would be $D_{out}$ according to the definition of $A_{out}$ in the main text.

## Acknowledgements

A.S. is grateful to the Commonwealth Scientific and Industrial Research Organisation (CSIRO) Research Office for the support through the "Science Leader in Active Materials" platform.

## Conflict of Interest

The author declares no conflict of interest.

## Keywords

additive manufacturing, composite material, fused filament fabrication, printability, thermoplastic

Received: March 19, 2022
Revised: August 8, 2022
Published online: September 1, 2022

[1] A. Melocchi, M. Uboldi, A. Maroni, A. Foppoli, L. Palugan, L. Zema, A. Gazzaniga, *Int. J. Pharm.* **2020**, *579*, 119155.
[2] *ISO/ASTM 52900:2021*, Additive Manufacturing—General Principles—Fundamentals and Vocabulary, International Organization for Standardization, Geneva **2021**.
[3] A. Al Rashid, S. A. Khan, S. G. Al-Ghamdi, M. Koç, *J. Mater. Res. Technol.* **2021**, *14*, 910.
[4] M. Ahmadifar, K. Benfriha, M. Shirinbayan, A. Tcharkhtchi, *Appl. Compos. Mater.* **2021**, *28*, 1335.
[5] P. Awasthi, S. S. Banerjee, *Addit. Manuf.* **2021**, *46*, 102177.
[6] S. S. Dewada, A. Telang, *Mater. Res. Express* **2021**, *8*, 122001.
[7] A. Dey, I. N. Roan Eagle, N. Yodo, *J. Manuf. Mater. Process.* **2021**, *5*, 69.
[8] R. Dua, Z. Rashad, J. Spears, G. Dunn, M. Maxwell, *Polymers* **2021**, *13*, 4046.
[9] G. Ehrmann, A. Ehrmann, *J. Appl. Polym. Sci.* **2021**, *138*, 50847.
[10] J. J. Fallon, S. H. McKnight, M. J. Bortner, *Addit. Manuf.* **2019**, *30*, 100810.
[11] D. Fico, D. Rizzo, R. Casciaro, C. E. Corcione, *Polymers* **2022**, *14*, 465.
[12] M. Handwerker, J. Wellnitz, H. Marzbani, *Prog. Addit. Manuf.* **2021**, *6*, 663.
[13] S. F. Kabir, K. Mathur, A.-F. M. Seyam, *Compos. Struct.* **2020**, *232*, 111476.

 

[14] V. Mazzanti, L. Malagutti, F. Mollica, *Polymers* **2019**, *11*, 1094.
[15] S. Park, K. K. Fu, *Compos. Sci. Technol.* **2021**, *213*, 108876.
[16] C. Parulski, O. Jennotte, A. Lechanteur, B. Evrard, *Adv. Drug Delivery Rev.* **2021**, *175*, 113810.
[17] P. K. Penumakala, J. Santo, A. Thomas, *Composites, Part B* **2020**, *201*, 108336.
[18] J. Pratama, S. I. Cahyono, S. Suyitno, M. A. Muflikhun, U. A. Salim, M. Mahardika, B. Arifvianto, *Polymers* **2021**, *13*, 4022.
[19] T. N. A. T. Rahim, A. M. Abdullah, H. Md Akil, *Polym. Rev.* **2019**, *59*, 589.
[20] V. Shanmugam, M. V. Pavan, K. Babu, B. Karnan, *Polym. Compos.* **2021**, *42*, 5656.
[21] S. Wasti, S. Adhikari, *Front. Chem.* **2020**, *8*, 315.
[22] P. Zhang, Z. Wang, J. Li, X. Li, L. Cheng, *Nanotechnol. Rev.* **2020**, *9*, 1594.
[23] C. Duty, C. Ajinjeru, V. Kishore, B. Compton, N. Hmeidat, X. Chen, P. Liu, A. A. Hassen, J. Lindahl, V. Kunc, *J. Manuf. Processes* **2018**, *35*, 526.
[24] A. Das, E. L. Gilmer, S. Biria, M. J. Bortner, *ACS Appl. Polym. Mater.* **2021**, *3*, 1218.
[25] F. M. Mwema, E. T. Akinlabi, in *Fused Deposition Modeling: Strategies for Quality Enhancement*, (Eds: F. M. Mwema, E. T. Akinlabi), Springer International Publishing, Cham, Switzerland **2020**, pp. 1–15.
[26] D. Pramanik, N. Roy, A. S. Kuar, in *Reference Module in Materials Science and Materials Engineering* (Ed: M. S. J. Hashmi), Elsevier, Oxford **2021**. https://www.sciencedirect.com/science/article/pii/B9780128203521001255.
[27] All3DP, https://all3dp.com/2/cartesian-3d-printer-delta-scara-belt-corexy-polar/ (accessed: September 2021).
[28] R. Chen, H. Yin, I. S. Cole, S. Shen, X. Zhou, Y. Wang, S. Tang, *Chemosphere* **2020**, *259*, 127452.
[29] M. Sousa, P. Arezes, F. Silva, *J. Phys.: Conf. Ser.* **2019**, *1323*, 012013.
[30] L. Bergonzi, M. Vettori, *Mater. Des. Process. Commun.* **2021**, *3*, e250.
[31] K. DePalma, M. R. Walluk, A. Murtaugh, J. Hilton, S. McConky, B. Hilton, *J. Cleaner Prod.* **2020**, *264*, 121567.
[32] P. Zhao, C. Rao, F. Gu, N. Sharmin, J. Fu, *J. Cleaner Prod.* **2018**, *197*, 1046.
[33] G. A. Roth, C. L. Geraci, A. Stefaniak, V. Murashov, J. Howard, *J. Occup. Environ. Hyg.* **2019**, *16*, 321.
[34] A. Manoj, M. Bhuyan, S. R. Banik, M. R. Sankar, *Mater. Today: Proc.* **2021**, *44*, 1375.
[35] A. B. Stefaniak, R. F. LeBouf, J. Yi, J. Ham, T. Nurkewicz, D. E. Schwegler-Berry, B. T. Chen, J. R. Wells, M. G. Duling, R. B. Lawrence, S. B. Martin Jr, A. R. Johnson, M. A. Virji, *J. Occup. Environ. Hyg.* **2017**, *14*, 540.
[36] S. H. Masood, in *Comprehensive Materials Processing*, (Eds: S. Hashmi, G. F. Batalha, C. J. Van Tyne, B. Yilbas), Elsevier, Oxford **2014**, pp. 69–91.
[37] K. Rane, M. Strano, *Adv. Manuf.* **2019**, *7*, 155.
[38] L. Ammosova, S. C. Cano, S. Schuschnigg, C. Kukla, K. Mönkkönen, M. Suvanto, J. Gonzalez-Gutierrez, *Precis. Eng.* **2021**, *72*, 604.
[39] J. Gonzalez-Gutierrez, Y. Thompson, D. Handl, S. Cano, S. Schuschnigg, P. Felfer, C. Kukla, C. Holzer, C. Burkhardt, *Mater. Lett.* **2021**, *283*, 128909.
[40] J. Gonzalez-Gutierrez, S. Cano, S. Schuschnigg, C. Kukla, J. Sapkota, C. Holzer, *Materials* **2018**, *11*, 840.
[41] G. Mitteramskogler, R. Gmeiner, R. Felzmann, S. Gruber, C. Hofstetter, J. Stampfl, J. Ebert, W. Wachter, J. Laubersheimer, *Addit. Manuf.* **2014**, *1*, 110.
[42] M. Ziaee, N. B. Crane, *Addit. Manuf.* **2019**, *28*, 781.
[43] P. Singh, V. K. Balla, A. Tofangchi, S. V. Atre, K. H. Kate, *Int. J. Refract. Met. Hard Mater.* **2020**, *91*, 105249.
[44] Y. Thompson, K. Zissel, A. Förner, J. Gonzalez-Gutierrez, C. Kukla, S. Neumeier, P. Felfer, *J. Mater. Sci.* **2022**, *57*, 9541.
[45] M. Rafiee, R. D. Farahani, D. Therriault, *Adv. Sci.* **2020**, *7*, 1902307.
[46] R. Singh, R. Kumar, I. Farina, F. Colangelo, L. Feo, F. Fraternali, *Polymers* **2019**, *11*, 62.
[47] M. H. Ali, N. Mir-Nasiri, W. L. Ko, *Int. J. Adv. Manuf. Technol.* **2016**, *86*, 999.
[48] M. Boulaala, D. Elmessaoudi, I. Buj-Corral, J. El Mesbahi, O. Ezbakhe, A. Astito, M. El Mrabet, A. El Mesbahi, *Int. J. Adv. Manuf. Technol.* **2020**, *110*, 45.
[49] S. Tibbits, *Archit. Des.* **2014**, *84*, 116.
[50] M. Bodaghi, R. Noroozi, A. Zolfagharian, M. Fotouhi, S. Norouzi, *Materials* **2019**, *12*, 8.
[51] X. Kuang, D. J. Roach, J. Wu, C. M. Hamel, Z. Ding, T. Wang, M. L. Dunn, H. J. Qi, *Adv. Funct. Mater.* **2019**, *29*, 1805290.
[52] C. De Maria, I. Chiesa, D. Morselli, M. R. Ceccarini, S. Bittolo Bon, M. Degli Esposti, P. Fabbri, A. Morabito, T. Beccari, L. Valentini, *Adv. Funct. Mater.* **2021**, *31*, 2105665.
[53] A. Le Duigou, M. Castro, R. Bevan, N. Martin, *Mater. Des.* **2016**, *96*, 106.
[54] K. S. Prakash, T. Nancharaih, V. S. Rao, *Mater. Today: Proc.* **2018**, *5*, 3873.
[55] B. Gapiński, M. Wieczorowski, A. Bak, A. P. Domínguez, T. Mathia, *AIP Conf. Proc.* **2018**, *1960*, 140009.
[56] H. I. Medellin-Castillo, J. Zaragoza-Siqueiros, *Chin. J. Mech. Eng.* **2019**, *32*, 53.
[57] S. Brischetto, C. G. Ferro, R. Torre, P. Maggiore, *Curved Layered Struct.* **2018**, *5*, 80.
[58] M. Filippi, G. Born, M. Chaaban, A. Scherberich, *Front. Bioeng. Biotechnol.* **2020**, *8*, 474.
[59] G. L. Koons, M. Diba, A. G. Mikos, *Nat. Rev. Mater.* **2020**, *5*, 584.
[60] J. E. Trachtenberg, F. K. Kasper, A. G. Mikos, in *Principles of Tissue Engineering* (Eds: R. Lanza, R. Langer, J. Vacanti), 4th ed., Academic Press, Elsevier, Boston **2014**, pp. 423–440.
[61] O. S. Carneiro, A. F. Silva, R. Gomes, *Mater. Des.* **2015**, *83*, 768.
[62] K. Gunasekaran, V. Aravinth, C. M. Kumaran, K. Madhankumar, S. P. Kumar, *Mater. Today: Proc.* **2021**, *45*, 1849.
[63] S. Fafenrot, N. Grimmelsmann, M. Wortmann, A. Ehrmann, *Materials* **2017**, *10*, 1199.
[64] J. Gonzalez-Gutierrez, S. Cano, J. V. Ecker, M. Kitzmantel, F. Arbeiter, C. Kukla, C. Holzer, *Appl. Sci.* **2021**, *11*, 7262.
[65] T. T. P. Phan, T. Q. Phan, A. S. El-Gizawy, *Addit. Manuf.* **2019**, *30*, 100832.
[66] X. Xiao, B.-M. Roh, F. Zhu, *Appl. Sci.* **2021**, *11*, 6100.
[67] G. Gómez Ciriza, T. Gómez Cía, J. A. Rivas González, M. d. l. N. Velasco Forte, I. Valverde, *Front. Cardiovasc. Med.* **2021**, *8*, 498.
[68] N. G. Tanikella, B. Wittbrodt, J. M. Pearce, *Addit. Manuf.* **2017**, *15*, 40.
[69] B. M. Tymrak, M. Kreiger, J. M. Pearce, *Mater. Des.* **2014**, *58*, 242.
[70] B. Wittbrodt, J. M. Pearce, *Addit. Manuf.* **2015**, *8*, 110.
[71] U. M. Dilberoglu, B. Gharehpapagh, U. Yaman, M. Dolen, *Proc. Manuf.* **2017**, *11*, 545.
[72] T. J. Word, A. Guerrero, D. A. Roberson, *MRS Commun.* **2021**, *11*, 129.
[73] Stratasys, https://www.stratasys.com/materials/search (accessed: February 2022).
[74] 3D Matter, https://www.3dhubs.com/knowledge-base/fdm-3d-printing-materials-compared/ (accessed: February 2022).
[75] Simplify3d, https://www.simplify3d.com/support/materials-guide/properties-table/ (accessed: February 2022)
[76] Treatstock, https://www.treatstock.co.uk/guide/article/118-express-guide-of-fdm-3d-printing-materials (accessed: February 2022)

 

[77] F. Calignano, D. Manfredi, E. P. Ambrosio, S. Biamino, M. Lombardi, E. Atzeni, A. Salmi, P. Minetola, L. Iuliano, P. Fino, *Proc. IEEE* **2017**, *105*, 593.
[78] A. M. Peterson, *Addit. Manuf.* **2019**, *27*, 363.
[79] Z. Liu, Y. Wang, B. Wu, C. Cui, Y. Guo, C. Yan, *Int. J. Adv. Manuf. Technol.* **2019**, *102*, 2877.
[80] E. H. Tümer, H. Y. Erbil, *Coatings* **2021**, *11*, 390.
[81] Y. Joo, I. Shin, G. Ham, S. M. Abuzar, S.-M. Hyun, S.-J. Hwang, *J. Pharm. Invest.* **2020**, *50*, 131.
[82] W. J. Chong, S. Shen, Y. Li, A. Trinchi, D. Pejak, I. L. Kyratzis, A. Sola, C. Wen, *Mater. Sci. Technol.* **2022**, *11*, 120.
[83] M. Forni, C. Bernardini, F. Zamparini, A. Zannoni, R. Salaroli, D. Ventrella, G. Parchi, M. Degli Esposti, A. Polimeni, P. Fabbri, et al., *Nanomaterials* **2020**, *10*, 243.
[84] T. Distler, N. Fournier, A. Grünewald, C. Polley, H. Seitz, R. Detsch, A. R. Boccaccini, *Front. Bioeng. Biotechnol.* **2020**, *8*, 552.
[85] D. Drummer, S. Cifuentes-Cuéllar, D. Rietzel, *Rapid Prototyping J.* **2012**, *18*, 500.
[86] I. Gendviliene, E. Simoliunas, S. Rekstyte, M. Malinauskas, L. Zaleckas, D. Jegelevicius, V. Bukelskiene, V. Rutkunas, *J. Mech. Behav. Biomed. Mater.* **2020**, *104*, 103616.
[87] J. Pellegrino, T. Makila, S. McQueen, E. Taylor, *NIST Adv. Manuf. Ser.* **2016**, *100*, 57.
[88] D. Roberson, C. M. Shemelya, E. MacDonald, R. Wicker, *Rapid Prototyping J.* **2015**, *21*, 137.
[89] S. A. Tofail, E. P. Koumoulos, A. Bandyopadhyay, S. Bose, L. O'Donoghue, C. Charitidis, *Mater. Today* **2018**, *21*, 22.
[90] T. Wohlers, T. Gornet, *Wohlers Rep.* **2014**, *24*, 118.
[91] Z. Jiang, B. Diggle, M. L. Tan, J. Viktorova, C. W. Bennett, L. A. Connal, *Adv. Sci.* **2020**, *7*, 2001379.
[92] M. Heidari-Rarani, M. Rafiee-Afarani, A. Zahedi, *Composites, Part B* **2019**, *175*, 107147.
[93] H. Zhang, T. Huang, Q. Jiang, L. He, A. Bismarck, Q. Hu, *J. Mater. Sci.* **2021**, *56*, 12999.
[94] H. Abdali, A. Ajji, in *Graphene Functionalization Strategies: From Synthesis to Applications* (Eds: A. Khan, M. Jawaid, B. Neppolian, A. M. Asiri), Springer, Singapore **2019**, pp. 127–156.
[95] M. Silva, I. S. Pinho, J. A. Covas, N. M. Alves, M. C. Paiva, *Funct. Compos. Mater.* **2021**, *2*, 8.
[96] Y. Y. Huang, E. M. Terentjev, *Polymers* **2012**, *4*, 275.
[97] U. Siemann, in *Scattering Methods and the Properties of Polymer Materials* (Eds: N. Stribeck, B. Smarsly), vol. *130*, Springer, Berlin, Heidelberg **2005**, pp. 1–14.
[98] Z. Brounstein, C. M. Yeager, A. Labouriau, *Polymers* **2021**, *13*, 580.
[99] T. Villmow, P. Pötschke, S. Pegel, L. Häussler, B. Kretzschmar, *Polymer* **2008**, *49*, 3500.
[100] M. Mičušík, M. Omastová, I. Krupa, J. Prokeš, P. Pissis, E. Logakis, C. Pandis, P. Pötschke, J. Pionteck, *J. Appl. Polym. Sci.* **2009**, *113*, 2536.
[101] H. Patil, R. V. Tiwari, M. A. Repka, *AAPS PharmSciTech* **2016**, *17*, 20.
[102] A. G. Hasib, S. Niauzorau, W. Xu, S. Niverty, N. Kublik, J. Williams, N. Chawla, K. Song, B. Azeredo, *Addit. Manuf.* **2021**, *41*, 101967.
[103] F. Delogu, G. Gorrasi, A. Sorrentino, *Prog. Mater. Sci.* **2017**, *86*, 75.
[104] X. Yang, H. Ren, C. Wu, Y. Xiong, Q. Ge, in *2021 27th Int. Conf. on Mechatronics and Machine Vision in Practice (M2VIP)*, IEEE, Piscataway, NJ **2021**, pp. 546–551.
[105] J. L. White, K. Min, in *Comprehensive Polymer Science and Supplements* (Eds: G. Allen, J. C. Bevington), Pergamon, Amsterdam, The Netherland **1989**, pp. 285–302.
[106] B. Lecouvet, J. Gutierrez, M. Sclavons, C. Bailly, *Polym. Degrad. Stab.* **2011**, *96*, 226.
[107] S. Waheed, J. M. Cabot, P. Smejkal, S. Farajikhah, S. Sayyar, P. C. Innis, S. Beirne, G. Barnsley, T. W. Lewis, M. C. Breadmore, B. Paull, *ACS Appl. Mater. Interfaces* **2019**, *11*, 4353.
[108] W. J. Chong, S. Shen, Y. Li, A. Trinchi, D. P. Simunec, I. L. Kyratzis, A. Sola, C. Wen, *Smart Mater. Manuf.* **2022**, 100004, https://doi.org/10.1016/j.smmf.2022.100004.
[109] M. Cavillon, P. Dragic, B. Faugas, T. W. Hawkins, J. Ballato, *Materials* **2019**, *12*, 2898.
[110] K. S. Boparai, R. Singh, H. Singh, *Prog. Addit. Manuf.* **2016**, *1*, 115.
[111] T. A. Osswald, *Understanding Polymer Processing*, 2nd ed., Hanser Publications, Munich **2017**.
[112] A. Shrivastava, *Introduction to Plastics Engineering*, William Andrew Publishing, Norwich, NY **2018**.
[113] R. Thakkar, R. Thakkar, A. Pillai, E. A. Ashour, M. A. Repka, *Int. J. Pharm.* **2020**, *576*, 118989.
[114] J. Vlachopoulos, N. Polychronopoulos, M. Kontopoulou, in *Applied Polymer Rheology: Polymeric Fluids with Industrial Applications* (Ed: M. Kontopoulou), 1st ed., Wiley, Hoboken, NJ **2011**, pp. 1–27.
[115] J. Yang, J.-Z. Liang, F.-J. Li, *J. Macromol. Sci., Part B: Phys.* **2012**, *51*, 1715.
[116] J. Frakland, Plastics Technology, https://www.ptonline.com/articles/what-about-melt-strength (accessed: August 2022).
[117] M. Hernández-Alamilla, A. Valadez-Gonzalez, *J. Polym. Eng.* **2016**, *36*, 31.
[118] J. P. Greene, in *Automotive Plastics and Composites* (Ed: J. P. Greene), William Andrew Publishing, Norwich, NY **2021**, pp. 57–69.
[119] S. Cano, T. Lube, P. Huber, A. Gallego, J. A. Naranjo, C. Berges, S. Schuschnigg, G. Herranz, C. Kukla, C. Holzer, J. Gonzalez-Gutierrez, *Materials* **2020**, *13*, 3158.
[120] E. Sykacek, M. Hrabalova, H. Frech, N. Mundigler, *Composites, Part A* **2009**, *40*, 1272.
[121] W. Ahmed, F. Alnajjar, E. Zaneldin, A. H. Al-Marzouqi, M. Gochoo, S. Khalid, *Materials* **2020**, *13*, 4065.
[122] I. Bayraktar, D. Doganay, S. Coskun, C. Kaynak, G. Akca, H. E. Unalan, *Composites, Part B* **2019**, *172*, 671.
[123] E. Verdejo de Toro, J. Coello Sobrino, A. Martínez Martínez, V. Miguel Eguía, J. Ayllón Pérez, *Materials* **2020**, *13*, 672.
[124] F. Zavřel, M. Novák, J. Kroupová, C. Beveridge, F. Štěpánek, G. Ruphuy, *Adv. Eng. Mater.* **2021**, *24*, 2100820.
[125] M. Bertolino, D. Battegazzore, R. Arrigo, A. Frache, *Addit. Manuf.* **2021**, *40*, 101944.
[126] H. Ponsar, R. Wiedey, J. Quodbach, *Pharmaceutics* **2020**, *12*, 511.
[127] S. Bandari, D. Nyavanandi, N. Dumpa, M. A. Repka, *Adv. Drug Delivery Rev.* **2021**, *172*, 52.
[128] E. Gkartzou, E. P. Koumoulos, C. A. Charitidis, *Manuf. Rev.* **2017**, *4*, 1.
[129] B. N. Turner, R. Strong, S. A. Gold, *Rapid Prototyping J.* **2014**, *20*, 192.
[130] J. C. Miller, *Polym. Eng. Sci.* **1963**, *3*, 134.
[131] J. Aho, J. P. Boetker, S. Baldursdottir, J. Rantanen, *Int. J. Pharm.* **2015**, *494*, 623.
[132] S. Dul, L. Fambri, A. Pegoretti, *Composites, Part A* **2016**, *85*, 181.
[133] D. Yang, H. Zhang, J. Wu, E. D. McCarthy, *Addit. Manuf.* **2021**, *37*, 101686.
[134] J. Z. Liang, *Polym. Test.* **2008**, *27*, 936.
[135] M. Cloitre, R. T. Bonnecaze, *Rheol. Acta* **2017**, *56*, 283.
[136] S. Bhagia, R. R. Lowden, D. Erdman III, M. Rodriguez Jr, B. A. Haga, I. R. M. Solano, N. C. Gallego, Y. Pu, W. Muchero, V. Kunc, A. J. Ragauskas, *Appl. Mater. Today* **2020**, *21*, 100832.
[137] S. Farah, D. G. Anderson, R. Langer, *Adv. Drug Delivery Rev.* **2016**, *107*, 367.
[138] C. Kukla, J. Gonzalez-Gutierrez, S. Cano-Cano, S. Hampel, C. Burkhardt, T. Moritz, C. Holzer, presented at *VI Congreso Nacional de Pulvimetalurgia y I Congreso Iberoamericano de Pulvimetalurgia*, Ciudad Real, Spain, June **2017**.
[139] M. Spoerk, C. Holzer, J. Gonzalez-Gutierrez, *J. Appl. Polym. Sci.* **2020**, *137*, 48545.

 

[140] T. F. McNulty, D. J. Shanefield, S. C. Danforth, A. Safari, *J. Am. Ceram. Soc.* **1999**, *82*, 1757.
[141] A. Rosato, K. J. Strandburg, F. Prinz, R. H. Swendsen, *Phys. Rev. Lett.* **1987**, *58*, 1038.
[142] A. Maurel, S. Grugeon, B. Fleutot, M. Courty, K. Prashantha, H. Tortajada, M. Armand, S. Panier, L. Dupont, *Sci. Rep.* **2019**, *9*, 18031.
[143] Y. Wu, D. Isakov, P. S. Grant, *Materials* **2017**, *10*, 1218.
[144] G. F. Acosta-Vélez, B. M. Wu, *Polym. Sci.* **2016**, *2*, 3.
[145] A. A. Konta, M. García-Piña, D. R. Serrano, *Bioengineering* **2017**, *4*, 79.
[146] A. Melocchi, F. Parietti, A. Maroni, A. Foppoli, A. Gazzaniga, L. Zema, *Int. J. Pharm.* **2016**, *509*, 255.
[147] J. M. Nasereddin, N. Wellner, M. Alhijjaj, P. Belton, S. Qi, *Pharm. Res.* **2018**, *35*, 151.
[148] P. Xu, J. Li, A. Meda, F. Osei-Yeboah, M. L. Peterson, M. Repka, X. Zhan, *Int. J. Pharm.* **2020**, *588*, 119760.
[149] J. Zhang, X. Feng, H. Patil, R. V. Tiwari, M. A. Repka, *Int. J. Pharm.* **2017**, *519*, 186.
[150] J. Zhang, P. Xu, A. Q. Vo, S. Bandari, F. Yang, T. Durig, M. A. Repka, *J. Drug Delivery Sci. Technol.* **2019**, *52*, 292.
[151] J. Leng, J. Wu, J. Zhang, *Ind. Eng. Chem. Res.* **2019**, *58*, 21476.
[152] V. Kishore, C. Ajinjeru, P. Liu, J. Lindahl, A. Hassen, V. Kunc, C. Duty, *Solid Freeform Fabr. Proc.* **2017**, *2017*, 1696.
[153] S. Rangarajan, G. Qi, N. Venkataraman, A. Safari, S. C. Danforth, *J. Am. Ceram. Soc.* **2000**, *83*, 1663.
[154] C. Hu, Q.-H. Qin, *Curr. Opin. Solid State Mater. Sci.* **2020**, *24*, 100867.
[155] M. Chapiro, *Reinf. Plast.* **2016**, *60*, 372.
[156] J. Adeniyi, E. Kolawole, *Eur. Polym. J.* **1984**, *20*, 43.
[157] B. Palacios-Ibáñez, J. J. Relinque, D. Moreno-Sánchez, A. S. de León, F. J. Delgado, R. Escobar-Galindo, S. I. Molina, *Polymers* **2022**, *14*, 496.
[158] M. Broudin, V. Le Saux, P.-Y. Le Gac, C. Champy, G. Robert, P. Charrier, Y. Marco, *Polym. Test.* **2015**, *43*, 10.
[159] G. Gorrasi, R. Pantani, in *Synthesis, Structure and Properties of Poly(lactic acid)* (Eds: M. L. Di Lorenzo, R. Androsch), vol. *279*, Springer International Publishing, Cham, Switzerland **2018**, pp. 119–151.
[160] Y. Huang, C. Zhang, Y. Pan, Y. Zhou, L. Jiang, Y. Dan, *Polym. Degrad. Stab.* **2013**, *98*, 943.
[161] L. Monson, M. Braunwarth, C. W. Extrand, *J. Appl. Polym. Sci.* **2008**, *107*, 355.
[162] A. P. Valerga, M. Batista, J. Salguero, F. Girot, *Materials* **2018**, *11*, 1322.
[163] H. D. Vora, S. Sanyal, *Prog. Addit. Manuf.* **2020**, *5*, 319.
[164] A. Célino, S. Fréour, F. Jacquemin, P. Casari, *Front. Chem.* **2014**, *1*, 43.
[165] N. Nakayama, T. Hayashi, *Polym. Degrad. Stab.* **2007**, *92*, 1255.
[166] S. Therias, J.-F. Larché, P.-O. Bussiere, J.-L. Gardette, M. Murariu, P. Dubois, *Biomacromolecules* **2012**, *13*, 3283.
[167] D. Damato, Computer Aided Technology, https://www.cati.com/blog/2016/07/polyjet-and-fdm-material-expirations-and-shelf-life/ (accessed: February 2022).
[168] A. Maurel, M. Courty, B. Fleutot, H. Tortajada, K. Prashantha, M. Armand, S. Grugeon, S. Panier, L. Dupont, *Chem. Mater.* **2018**, *30*, 7484.
[169] H. S. Ramanath, C. K. Chua, K. F. Leong, K. D. Shah, *J. Mater. Sci.: Mater. Med.* **2008**, *19*, 2541.
[170] J.-F. Agassant, F. Pigeonneau, L. Sardo, M. Vincent, *Addit. Manuf.* **2019**, *29*, 100794.
[171] A. A. Rashid, M. Koç, *Polymers* **2021**, *13*, 3534.
[172] M. Elbadawi, T. Gustaffson, S. Gaisford, A. W. Basit, *Int. J. Pharm.* **2020**, *590*, 119868.
[173] P. Oehlmann, P. Osswald, J. C. Blanco, M. Friedrich, D. Rietzel, G. Witt, *Prod. Eng.* **2021**, *15*, 467.
[174] Y. Tlegenov, G. S. Hong, W. F. Lu, *Rob. Comp. Integr. Manuf.* **2018**, *54*, 45.
[175] H. K. Dave, S. T. Patel, in *Fused Deposition Modeling Based 3D Printing* (Eds: H. K. Dave, J. P. Davim), Springer International Publishing, Cham, Switzerland **2021**, pp. 1–21.
[176] M. Mohammadizadeh, H. Lu, I. Fidan, K. Tantawi, A. Gupta, S. Hasanov, Z. Zhang, F. Alifui-Segbaya, A. Rennie, *Inventions* **2020**, *5*, 44.
[177] J. Go, S. N. Schiffres, A. G. Stevens, A. J. Hart, *Addit. Manuf.* **2017**, *16*, 1.
[178] M. K. Agarwala, V. R. Jamalabad, N. A. Langrana, A. Safari, P. J. Whalen, S. C. Danforth, *Rapid Prototyping J.* **1996**, *2*, 4.
[179] C. Korte, J. Quodbach, *Pharm. Dev. Technol.* **2018**, *23*, 1117.
[180] A. Bellini, S. Güçeri, M. Bertoldi, *J. Manuf. Sci. Eng.* **2004**, *126*, 237.
[181] J. Go, A. J. Hart, *Addit. Manuf.* **2017**, *18*, 276.
[182] J. Go, A. J. Hart, *US10 562 227B2*, **2020**.
[183] N. Venkataraman, S. Rangarajan, M. J. Matthewson, A. Safari, S. C. Danforth, A. Yardimci, S. I. Guceri, in *Proc. 1999 Int. Solid Freeform Fabrication Symp.*, University of Texas at Austin, Austin, TX **1999**, pp. 351–360.
[184] N. Venkataraman, S. Rangarajan, M. J. Matthewson, B. Harper, A. Safari, S. C. Danforth, G. Wu, N. Langrana, S. Guceri, A. Yardimci, *Rapid Prototyping J.* **2000**, *6*, 244.
[185] M. P. Serdeczny, R. Comminal, D. B. Pedersen, J. Spangenberg, *Addit. Manuf.* **2020**, *32*, 100997.
[186] M. E. Mackay, *J. Rheol.* **2018**, *62*, 1549.
[187] J. Wu, N. Chen, F. Bai, Q. Wang, *Polym. Compos.* **2018**, *39*, E508.
[188] M. Janek, V. Žilinská, V. Kovár, Z. Hajdúchová, K. Tomanová, P. Peciar, P. Veteška, T. Gabošová, R. Fialka, J. Feranc, L. Omaníkováa, R. Plavec, L. Baca, *J. Eur. Ceram. Soc.* **2020**, *40*, 4932.
[189] E. L. Gilmer, D. Miller, C. A. Chatham, C. Zawaski, J. J. Fallon, A. Pekkanen, T. E. Long, C. B. Williams, M. J. Bortner, *Polymer* **2018**, *152*, 51.
[190] T. A. Osswald, J. Puentes, J. Kattinger, *Addit. Manuf.* **2018**, *22*, 51.
[191] V. Nienhaus, K. Smith, D. Spiehl, E. Dörsam, *Addit. Manuf.* **2019**, *28*, 711.
[192] D. D. Phan, Z. R. Swain, M. E. Mackay, *J. Rheol.* **2018**, *62*, 1097.
[193] M. E. Mackay, Z. R. Swain, C. R. Banbury, D. D. Phan, D. A. Edwards, *J. Rheol.* **2017**, *61*, 229.
[194] R. B. Kristiawan, F. Imaduddin, D. Ariawan, Z. Arifin Ubaidillah, *Open Eng.* **2021**, *11*, 639.
[195] A. Jabbari, K. Abrinia, *J. Manuf. Processes* **2018**, *35*, 664.
[196] A. Jabbari, K. Abrinia, *Int. J. Adv. Manuf. Technol.* **2018**, *94*, 3819.
[197] D. D. Lima, K. N. Campo, S. T. Button, R. Caram, *Mater. Des.* **2020**, *196*, 109161.
[198] J. Mireles, D. Espalin, D. Roberson, B. Zinniel, F. Medina, R. Wicker, in *Proc. 2012 Int. Solid Freeform Fabrication Symp.*, University of Texas at Austin, Austin, TX **2012**.
[199] M. A. Gibson, N. M. Mykulowycz, J. Shim, R. Fontana, P. Schmitt, A. Roberts, J. Ketkaew, L. Shao, W. Chen, P. Bordeenithikasem, J. S. Myerberg, R. Fulop, M. D. Verminski, E. M. Sachs, Y.-M. Chiang, C. A.Schuh, A. J. Hart, J. Schroers, *Mater. Today* **2018**, *21*, 697.
[200] A. Haleem, M. Javaid, *Clin. Epidemiol. Global Health* **2019**, *7*, 654.
[201] G. Liu, Y. He, P. Liu, Z. Chen, X. Chen, L. Wan, Y. Li, J. Lu, *Engineering* **2020**, *6*, 1232.
[202] A. R. Zanjanijam, I. Major, J. G. Lyons, U. Lafont, D. M. Devine, *Polymers* **2020**, *12*, 1665.
[203] E. Malikmammadov, T. E. Tanir, A. Kiziltay, V. Hasirci, N. Hasirci, *J. Biomater. Sci., Polym. Ed.* **2018**, *29*, 863.
[204] G. Kollamaram, D. M. Croker, G. M. Walker, A. Goyanes, A. W. Basit, S. Gaisford, *Int. J. Pharm.* **2018**, *545*, 144.
[205] T. C. Okwuosa, D. Stefaniak, B. Arafat, A. Isreb, K.-W. Wan, M. A. Alhnan, *Pharm. Res.* **2016**, *33*, 2704.

 

[206] M. Sadia, A. Sośnicka, B. Arafat, A. Isreb, W. Ahmed, A. Kelarakis, M. A. Alhnan, *Int. J. Pharm.* **2016**, *513*, 659.
[207] P. F. Flowers, C. Reyes, S. Ye, M. J. Kim, B. J. Wiley, *Addit. Manuf.* **2017**, *18*, 156.
[208] D. W. Hutmacher, T. Schantz, I. Zein, K. W. Ng, S. H. Teoh, K. C. Tan, *J. Biomed. Mater. Res.* **2001**, *55*, 203.
[209] A. Grémare, V. Guduric, R. Bareille, V. Heroguez, S. Latour, N. L'heureux, J.-C. Fricain, S. Catros, D. Le Nihouannen, *J. Biomed. Mater. Res., Part A* **2018**, *106*, 887.
[210] A. Farahanchi, M. J. Sobkowicz, *Polym. Degrad. Stab.* **2017**, *138*, 40.
[211] C. Loyer, P. Ferreira, J. B. Marijon, V. Michel, G. Régnier, J. Vera, V. Duval, E. Richaud, *Polym. Degrad. Stab.* **2022**, *196*, 109843.
[212] C. McIlroy, P. D. Olmsted, *J. Rheol.* **2017**, *61*, 379.
[213] B. P. Heller, D. E. Smith, D. A. Jack, *Addit. Manuf.* **2016**, *12*, 252.
[214] H. Zhang, L. Zhang, H. Zhang, J. Wu, X. An, D. Yang, *Int. J. Adv. Manuf. Technol.* **2021**, *117*, 3549.
[215] K. Gnanasekaran, T. Heijmans, S. Van Bennekom, H. Woldhuis, S. Wijnia, G. De With, H. Friedrich, *Appl. Mater. Today* **2017**, *9*, 21.
[216] L. G. Blok, M. L. Longana, H. Yu, B. K. S. Woods, *Addit. Manuf.* **2018**, *22*, 176.
[217] H. L. Tekinalp, V. Kunc, G. M. Velez-Garcia, C. E. Duty, L. J. Love, A. K. Naskar, C. A. Blue, S. Ozcan, *Compos. Sci. Technol.* **2014**, *105*, 144.
[218] D. Nötzel, R. Eickhoff, T. Hanemann, *Materials* **2018**, *11*, 1463.
[219] J.-F. Agassant, D. R. Arda, C. Combeaud, A. Merten, H. Munstedt, M. R. Mackley, L. Robert, B. Vergnes, *Int. Polym. Process.* **2006**, *21*, 239.
[220] M. A. Azad, D. Olawuni, G. Kimbell, A. Z. M. Badruddoza, M. Hossain, T. Sultana, *Pharmaceutics* **2020**, *12*, 124.
[221] M. Spoerk, F. Arbeiter, H. Cajner, J. Sapkota, C. Holzer, *J. Appl. Polym. Sci.* **2017**, *134*, 45401.
[222] T. Osswald, N. Rudolph, *Rheometry*, Carl Hanser Verlag, Munich, Germany **2014**, Ch. 6, pp. 187–220.
[223] ASTM D1238-20, Standard test method for melt flow rates of thermoplastics by extrusion plastometer, ASTM International, West Conshohocken, PA **2020**.
[224] ISO 1133-1:2011, Plastics – Determination of the melt mass-flow rate (MFR) and melt volume-flow rate (MVR) of thermoplastics – Part 1: Standard method, International Organization for Standardization, Geneva **2011**.
[225] H. Garg, R. Singh, *Rapid Prototyping J.* **2016**, *22*, 338.
[226] P. Olesik, M. Godzierz, M. Kozioł, *Materials* **2019**, *12*, 2520.
[227] X. Gao, D. Zhang, S. Qi, X. Wen, Y. Su, *J. Appl. Polym. Sci.* **2019**, *136*, 47824.
[228] A. E. Costa, A. F. da Silva, O. S. Carneiro, *Rapid Prototyping J.* **2018**, *25*, 555.
[229] Q. Sun, G. M. Rizvi, C. T. Bellehumeur, P. Gu, *Rapid Prototyping J.* **2008**, *14*, 72.
[230] C. Balemans, M. A. Hulsen, P. D. Anderson, *Appl. Sci.* **2017**, *7*, 516.
[231] C. Bellehumeur, L. Li, Q. Sun, P. Gu, *J. Manuf. Processes* **2004**, *6*, 170.
[232] O. Pokluda, C. T. Bellehumeur, J. Vlachopoulos, *AIChE J.* **1997**, *43*, 3253.
[233] Y. Tao, F. Kong, Z. Li, J. Zhang, X. Zhao, Q. Yin, D. Xing, P. Li, *J. Mater. Res. Technol.* **2021**, *15*, 4860.
[234] J. E. Seppala, K. D. Migler, *Addit. Manuf.* **2016**, *12*, 71.
[235] F. Yang, R. Pitchumani, *Macromolecules* **2002**, *35*, 3213.
[236] S. F. Costa, F. M. Duarte, J. A. Covas, *J. Mater. Process. Technol.J. Mater. Process. Technol.* **2017**, *245*, 167.
[237] C. McIlroy, P. D. Olmsted, *Polymer* **2017**, *123*, 376.
[238] S. F. Costa, F. M. Duarte, J. A. Covas, *Virtual Phys. Prototyping* **2015**, *10*, 35.
[239] C. T. Bellehumeur, M. K. Bisaria, J. Vlachopoulos, *Polym. Eng. Sci.* **1996**, *36*, 2198.
[240] H. Zhang, K. Lamnawar, A. Maazouz, *Rheol. Acta* **2012**, *51*, 691.
[241] T. J. Coogan, D. O. Kazmer, *J. Rheol.* **2019**, *63*, 655.
[242] J. Yin, C. Lu, J. Fu, Y. Huang, Y. Zheng, *Mater. Des.* **2018**, *150*, 104.
[243] P. K. Gurrala, S. P. Regalla, *Virtual Phys. Prototyping* **2014**, *9*, 141.
[244] B. Gharehpapagh, M. Dolen, U. Yaman, *Proc. Manuf.* **2019**, *38*, 52.
[245] E. A. Papon, A. Haque, M. A. R. Sharif, *Rapid Prototyping J.* **2021**, *27*, 518.
[246] R. Comminal, M. P. Serdeczny, D. B. Pedersen, J. Spangenberg, *Addit. Manuf.* **2018**, *20*, 68.
[247] O. Arjmandi-Tash, N. M. Kovalchuk, A. Trybala, I. V. Kuchin, V. Starov, *Langmuir* **2017**, *33*, 4367.
[248] G. Reiter, in *Handbook of Adhesion Technology* (Eds: L. F. M. da Silva, A. Oechsner, R. D. Adams), 2nd ed., Springer, Cham, Switzerland **2017**, pp. 1–13.
[249] N. Aliheidari, J. Christ, R. Tripuraneni, S. Nadimpalli, A. Ameli, *Mater. Des.* **2018**, *156*, 351.
[250] E. Cuan-Urquizo, E. Barocio, V. Tejada-Ortigoza, R. B. Pipes, C. A. Rodriguez, A. Roman-Flores, *Materials* **2019**, *12*, 895.
[251] A. K. Sood, R. K. Ohdar, S. S. Mahapatra, *J. Adv. Res.* **2012**, *3*, 81.
[252] X. Bi, H. Tan, Z. Li, Y. Li, T. Liu, *IOP Conf. Ser.: Mater. Sci. Eng.* **2020**, *772*, 012084.
[253] Q. He, H. Wang, K. Fu, L. Ye, *Compos. Sci. Technol.* **2020**, *191*, 108077.
[254] A. Le Duigou, A. Barbé, E. Guillou, M. Castro, *Mater. Des.* **2019**, *180*, 107884.
[255] R. Matsuzaki, T. Nakamura, K. Sugiyama, M. Ueda, A. Todoroki, Y. Hirano, Y. Yamagata, *Addit. Manuf.* **2018**, *24*, 93.
[256] S.-H. Ahn, M. Montero, D. Odell, S. Roundy, P. K. Wright, *Rapid Prototyping J.* **2002**, *8*, 248.
[257] T. J. Gordelier, P. R. Thies, L. Turner, L. Johanning, *Rapid Prototyping J.* **2019**, *25*, 953.
[258] X. Gao, S. Qi, X. Kuang, Y. Su, J. Li, D. Wang, *Addit. Manuf.* **2021**, *37*, 101658.
[259] V. Shanmugam, O. Das, K. Babu, U. Marimuthu, A. Veerasimman, D. J. Johnson, R. E. Neisiany, M. S. Hedenqvist, S. Ramakrishna, F. Berto, *Int. J. Fatigue* **2021**, *143*, 106007.
[260] V. Shanmugam, D. J. J. Rajendran, K. Babu, S. Rajendran, A. Veerasimman, U. Marimuthu, S. Singh, O. Das, R. E. Neisiany, M. S. Hedenqvist, F. Berto, S. Ramakrishna, *Polym. Test.* **2021**, *93*, 106925.
[261] N. Zohdi, R. C. Yang, *Polymers* **2021**, *13*, 3368.
[262] H. Prajapati, D. Ravoori, R. L. Woods, A. Jain, *Addit. Manuf.* **2018**, *21*, 84.
[263] A. Dijkshoorn, M. Schouten, S. Stramigioli, G. Krijnen, *Sensors* **2021**, *21*, 3710.
[264] S. Wickramasinghe, T. Do, P. Tran, *Polymers* **2020**, *12*, 1529.
[265] R. Anitha, S. Arunachalam, P. Radhakrishnan, *J. Mater. Process. Technol.* **2001**, *118*, 385.
[266] M. R. Khosravani, F. Berto, M. R. Ayatollahi, T. Reinicke, *Theor. Appl. Fract. Mech.* **2020**, *109*, 102763.
[267] M. Altan, M. Eryildiz, B. Gumus, Y. Kahraman, *Mater. Test.* **2018**, *60*, 471.
[268] H. Kubota, *J. Appl. Polym. Sci.* **1975**, *19*, 2299.
[269] N. P. Levenhagen, M. D. Dadmun, *Polymer* **2017**, *122*, 232.
[270] X. Gao, S. Qi, D. Zhang, Y. Su, D. Wang, *Addit. Manuf.* **2020**, *35*, 101414.
[271] A. R. Torrado, C. M. Shemelya, J. D. English, Y. Lin, R. B. Wicker, D. A. Roberson, *Addit. Manuf.* **2015**, *6*, 16.
[272] K. Yang, J. C. Grant, P. Lamey, A. Joshi-Imre, B. R. Lund, R. A. Smaldone, W. Voit, *Adv. Funct. Mater.* **2017**, *27*, 1700318.
[273] Q. Chen, L. Han, J. Ren, L. Rong, P. Cao, R. C. Advincula, *ACS Appl. Mater. Interfaces* **2020**, *12*, 50052.
[274] K. Paraskevoudis, P. Karayannis, E. P. Koumoulos, *Processes* **2020**, *8*, 1464.
[275] C. Abeykoon, P. Sri-Amphorn, A. Fernando, *Int. J. Lightweight Mater. Manuf.* **2020**, *3*, 284.

 

[276] M. S. Alsoufi, A. E. Elsayed, *Mater. Sci. Appl.* **2018**, *9*, 11.
[277] F. R. Ramli, M. S. M. Faudzie, M. A. Nazan, M. R. Alkahari, M. N. Sudin, S. Mat, S. N. Khalil, *APR J. Eng. Appl. Sci.* **2018**, *13*, 1139.
[278] M. Harris, J. Potgieter, R. Archer, K. M. Arif, *Materials* **2019**, *12*, 1664.
[279] M. Adel, O. Abdelaal, A. Gad, A. B. Nasr, A. Khalil, *J. Mater. Process. Technol.* **2018**, *251*, 73.
[280] L. M. Galantucci, F. Lavecchia, G. Percoco, *CIRP Ann.* **2009**, *58*, 189.
[281] Y. Jin, Y. Wan, B. Zhang, Z. Liu, *J. Mater. Process. Technol.* **2017**, *240*, 233.
[282] R. Singh, S. Singh, I. P. Singh, F. Fabbrocino, F. Fraternali, *Composites, Part B* **2017**, *111*, 228.
[283] D. Stoof, K. Pickering, Y. Zhang, *J. Compos. Sci.* **2017**, *1*, 8.
[284] L. Chen, X. Zhang, Y. Wang, T. A. Osswald, *Polym. Compos.* **2020**, *41*, 1356.
[285] D. Mohan, A. N. Bakir, M. S. Sajab, S. B. Bakarudin, N. N. Mansor, R. Roslan, H. Kaco, *Polym. Compos.* **2021**, *42*, 2408.
[286] J. Nagendra, M. K. Srinath, S. Sujeeth, K. S. Naresh, M. S. Ganesha Prasad, *Mater. Today: Proc.* **2021**, *44*, 674.
[287] P. Parandoush, P. Fernando, H. Zhang, C. Ye, J. Xiao, M. Zhang, D. Lin, *Rapid Prototyping J.* **2021**, *27*, 754.
[288] P. Yadav, A. Sahai, R. S. Sharma, *J. Inst. Eng. (India): Ser. C* **2021**, *102*, 921.
[289] A. El Moumen, M. Tarfaoui, K. Lafdi, *Int. J. Adv. Manuf. Technol.* **2019**, *104*, 1661.
[290] M. Spoerk, J. Sapkota, G. Weingrill, T. Fischinger, F. Arbeiter, C. Holzer, *Macromol. Mater. Eng.* **2017**, *302*, 1700143.
[291] H.-C. Wu, T.-C. T. Chen, *Rapid Prototyping J.* **2018**, *24*, 607.
[292] M. Nabipour, B. Akhoundi, A. Bagheri Saed, *J. Appl. Polym. Sci.* **2020**, *137*, 48717.
[293] C. G. Schirmeister, T. Hees, E. H. Licht, R. Muelhaupt, *Addit. Manuf.* **2019**, *28*, 152.
[294] M. Spoerk, J. Gonzalez-Gutierrez, J. Sapkota, S. Stephan, C. Holzer, *Plast., Rubber Compos.* **2018**, *47*, 17.
[295] J. J. Tully, G. N. Meloni, *Anal. Chem.* **2020**, *92*, 14853.
[296] S. Cano, J. Gonzalez-Gutierrez, J. Sapkota, M. Spoerk, F. Arbeiter, S. Schuschnigg, C. Holzer, C. Kukla, *Addit. Manuf.* **2019**, *26*, 117.
[297] E. R. Fitzharris, N. Watanabe, D. W. Rosen, M. L. Shofner, *IInt. J. Adv. Manuf. Technol.* **2018**, *95*, 2059.
[298] S. Hwang, E. I. Reyes, N. S. Kim, K. S. Moon, R. C. Rumpf, in (Ed: F. Zheng), *Biotechnology, Agriculture, Environment and Energy - Proceedings of the 2014 International Conference on Biotechnology, Agriculture, Environment and Energy (ICBAEE 2014)*, CRC Press, Boca Raton **2014**, pp. 347–352.
[299] S. Hwang, E. I. Reyes, K.-s. Moon, R. C. Rumpf, N. S. Kim, *J. Electron. Mater.* **2015**, *44*, 771.
[300] L. J. Love, V. Kunc, O. Rios, C. E. Duty, A. M. Elliott, B. K. Post, R. J. Smith, C. A. Blue, *J. Mater. Res.* **2014**, *29*, 1893.
[301] S. H. Masood, W. Q. Song, *Mater. Des.* **2004**, *25*, 587.
[302] S. H. Masood, W. Q. Song, *Assem. Autom.* **2005**, *25*, 309.
[303] M. Nikzad, S. H. Masood, I. Sbarski, *Mater. Des.* **2011**, *32*, 3448.
[304] Z. Weng, J. Wang, T. Senthil, L. Wu, *Mater. Des.* **2016**, *102*, 276.
[305] N. E. Zander, J. H. Park, Z. R. Boelter, M. A. Gillan, *ACS Omega* **2019**, *4*, 13879.
[306] L. Li, C. Y. Li, C. Ni, L. Rong, B. Hsiao, *Polymer* **2007**, *48*, 3452.
[307] X. Gao, S. Qi, B. Yang, Y. Su, J. Li, D. Wang, *Polymer* **2021**, *215*, 123426.
[308] S. Berretta, R. Davies, Y. Shyng, Y. Wang, O. Ghita, *Polym. Test.* **2017**, *63*, 251.
[309] M. Spoerk, C. Savandaiah, F. Arbeiter, J. Sapkota, C. Holzer, *Polym. Compos.* **2019**, *40*, 638.
[310] A. Buzarovska, A. Grozdanov, *J. Appl. Polym. Sci.* **2012**, *123*, 2187.
[311] M. Degli Esposti, D. Morselli, F. Fava, L. Bertin, F. Cavani, D. Viaggi, P. Fabbri, *FEBS Open Bio* **2021**, *11*, 967.
[312] S. Pratt, L.-J. Vandi, D. Gapes, A. Werker, A. Oehmen, B. Laycock, in *Biorefinery: Integrated Sustainable Processes for Biomass Conversion to Biomaterials, Biofuels, and Fertilizers* (Eds: J.-R. Bastidas-Oyanedel, J. E. Schmidt), Springer International Publishing, Cham, Switzerland **2019**, pp. 615–638.
[313] F. Cerdas, M. Juraschek, S. Thiede, C. Herrmann, *J. Ind. Ecol.* **2017**, *21*, S80.
[314] H. Ma, Y. Zhang, Z. Jiao, W. Yang, X. He, G. Xie, H. Li, *J. Inst. Eng. (India): Ser. C* **2021**, *102*, 59.
[315] E. Sanchez-Rexach, T. G. Johnston, C. Jehanno, H. Sardon, A. Nelson, *Chem. Mater.* **2020**, *32*, 7105.
[316] A. B. Stefaniak, L. N. Bowers, G. Cottrell, E. Erdem, A. K. Knepp, S. B. Martin Jr, J. Pretty, M. G. Duling, E. D. Arnold, Z. Wilson, B. Krider, A. R. Fortner, R. F. LeBouf, M. A. Virji, A. Sirinterlikci, *Resour., Conserv. Recycl.* **2022**, *176*, 105911.
[317] C. Correia, T. E. P. Gomes, I. Gonçalves, V. Neto, *J. Manuf. Mater. Process.* **2022**, *6*, 26.
[318] K. Mikula, D. Skrzypczak, G. Izydorczyk, J. Warchoł, K. Moustakas, K. Chojnacka, A. Witek-Krowiak, *Environ. Sci. Pollut. Res.* **2021**, *28*, 12321.
[319] M. A. Kreiger, M. Mulder, A. G. Glover, J. M. Pearce, *J. Cleaner Prod.* **2014**, *70*, 90.
[320] S. Zhong, J. M. Pearce, *Resour., Conserv. Recycl.* **2018**, *128*, 48.
[321] M.-J. Le Guen, S. Hill, D. Smith, B. Theobald, E. Gaugler, A. Barakat, C. Mayer-Laigle, *Front. Chem.* **2019**, *7*, 735.
[322] A. Rahimizadeh, J. Kalman, K. Fayazbakhsh, L. Lessard, *Composites, Part B* **2019**, *175*, 107101.
[323] K. Ragaert, L. Delva, K. Van Geem, *Waste Manage.* **2017**, *69*, 24.
[324] J. P. Rett, Y. L. Traore, E. A. Ho, *Adv. Eng. Mater.* **2021**, *23*, 2001472.
[325] P. Dal Fabbro, A. La Gala, W. Van De Steene, D. R. D'hooge, G. Lucchetta, L. Cardon, R. Fiorio, *Rapid Prototyping J.* **2021**, *27*, 268.
[326] I. Anderson, *3D Print. Addit. Manuf.* **2017**, *4*, 110.
[327] A. Lanzotti, M. Martorelli, S. Maietta, S. Gerbino, F. Penta, A. Gloria, *Proc. CIRP* **2019**, *79*, 143.
[328] F. R. Beltrán, M. P. Arrieta, E. Moreno, G. Gaspar, L. M. Muneta, R. Carrasco-Gallego, S. Yáñez, D. Hidalgo-Carvajal, M. U. de la Orden, J. Martínez Urreaga, *Polymers* **2021**, *13*, 1247.
[329] F. P. La Mantia, in *Recycling of PVC and Mixed PLASTIC Waste* (Ed: F. P. La Mantia), Chem Tec Publishing, Toronto **1996**, pp. 63–76.
[330] S. Ulutan, *J. Appl. Polym. Sci.* **2003**, *90*, 3994.
[331] V. Ambrogi, C. Carfagna, P. Cerruti, V. Marturano, in *Modification of Polymer Properties* (Eds: C. F. Jasso-Gastinel, J. M. Kenny), 1st ed., William Andrew, Norwich, NY **2017**, pp. 87–108.
[332] P. McKeown, M. D. Jones, *Sustainable Chem.* **2020**, *1*, 1.
[333] V. Piemonte, S. Sabatini, F. Gironi, *J. Polym. Environ.* **2013**, *21*, 640.
[334] M. F. Cosate de Andrade, P. Souza, O. Cavalett, A. R. Morales, *J. Polym. Environ.* **2016**, *24*, 372.
[335] R. Bernatas, S. Dagréou, A. Despax-Ferreres, A. Barasinski, *Cleaner Eng. Technol.* **2021**, *5*, 100272.
[336] A. E. Krauklis, C. W. Karl, A. I. Gagani, J. K. Jørgensen, *J. Compos. Sci.* **2021**, *5*, 28.
[337] X. Zhao, K. Copenhaver, L. Wang, M. Korey, D. J. Gardner, K. Li, M. E. Lamm, V. Kishore, S. Bhagia, M. Tajvidi, H. Tekinalp, O. Oyedeji, S. Wasti, E. Webb, A. J. Ragauskas, H. Zhu, W. H. Peter, S. Ozcana, *Resour., Conserv. Recycl.* **2022**, *177*, 105962.
[338] P. Peças, H. Carvalho, H. Salman, M. Leite, *J. Compos. Sci.* **2018**, *2*, 66.
[339] M. Milosevic, D. Stoof, K. L. Pickering, *J. Compos. Sci.* **2017**, *1*, 7.
[340] K. Kemmochi, H. Takayanagi, C. Nagasawa, J. Takahashi, R. Hayashi, *Adv. Perform. Mater.* **1995**, *2*, 385.
[341] X. Tian, T. Liu, Q. Wang, A. Dilmurat, D. Li, G. Ziegmann, *J. Cleaner Prod.* **2017**, *142*, 1609.
[342] A. Sinisi, M. Degli Esposti, M. Toselli, D. Morselli, P. Fabbri, *ACS Sustainable Chem. Eng.* **2019**, *7*, 13920.

 

[343] A. Sinisi, M. Degli Esposti, S. Braccini, F. Chiellini, S. Guzman-Puyol, J. A. Heredia-Guerrero, D. Morselli, P. Fabbri, *Mater. Adv.* **2021**, *2*, 7869.
[344] J. Pakkanen, D. Manfredi, P. Minetola, L. Iuliano, in *Sustainable Design and Manufacturing 2017* (Eds: G. Campana, R. J. Howlett, R. Setchi, B. Cimatti), Springer International Publishing, Cham, Switzerland **2017**, pp. 776–785.
[345] C. Zhu, T. Li, M. M. Mohideen, P. Hu, R. Gupta, S. Ramakrishna, Y. Liu, *Polymers* **2021**, *13*, 744.
[346] A. Sola, A. Trinchi, in *Fused Deposition Modeling of Composite Materials* (Eds: A. Sola, A. Trinchi), 1st ed., Woodhead Publishing, Elsevier, Cambridge, MA p. 22.
[347] E. J. Hunt, C. Zhang, N. Anzalone, J. M. Pearce, *Resour., Conserv. Recycl.* **2015**, *97*, 24.
[348] J. Fries, A. Durna, in *18th Int. Multidisciplinary Scientific GeoConference SGEM 2018*, vol. *18*, Surveying Geology and Mining Ecology Management (SGEM), Bulgaria **2018**, pp. 153–160.
[349] W. Ahmed, S. Siraj, A. H. Al-Marzouqi, *Polymers* **2020**, *12*, 2579.
[350] M. Niaounakis, *Eur. Polym. J.* **2019**, *114*, 464.
[351] P. Azimi, D. Zhao, C. Pouzet, N. E. Crain, B. Stephens, *Environ. Sci. Technol.* **2016**, *50*, 1260.
[352] P. Byrley, B. J. George, W. K. Boyes, K. Rogers, *Sci. Total Environ.* **2019**, *655*, 395.
[353] J. Yi, R. F. LeBouf, M. G. Duling, T. Nurkiewicz, B. T. Chen, D. Schwegler-Berry, M. A. Virji, A. B. Stefaniak, *J. Toxicol. Environ. Health, Part A* **2016**, *79*, 453.
[354] J. Zhang, D.-R. Chen, S.-C. Chen, *Build. Environ.* **2022**, 109348.
[355] A. Cowley, J. Perrin, A. Meurisse, A. Micallef, M. Fateri, L. Rinaldo, N. Bamsey, M. Sperl, *Addit. Manuf.* **2019**, *28*, 814.
[356] C.-L. Tang, S. Seeger, *Indoor Air* **2022**, *32*, e13010.
[357] E. Alberts, M. Ballentine, E. Barnes, A. Kennedy, *Atmos. Environ.* **2021**, *244*, 117956.
[358] A. Y. Davis, Q. Zhang, J. P. S. Wong, R. J. Weber, M. S. Black, *Build. Environ.* **2019**, *160*, 106209.
[359] P. M. Potter, S. R. Al-Abed, D. Lay, S. M. Lomnicki, *Environ. Sci. Technol.* **2019**, *53*, 4364.
[360] P. M. Potter, S. R. Al-Abed, F. Hasan, S. M. Lomnicki, *Chemosphere* **2021**, *279*, 130543.
[361] A. Davis, M. Black, Q. Zhang, J. P. S. Wong, R. Weber, presented at 2016 ASHRAE Annual Conf., St Louis, MO, JUN **2016**.
[362] H. Sigloch, F. S. Bierkandt, A. V. Singh, A. K. Gadicherla, P. Laux, A. Luch, *J. Visualized Exp.* **2020**, *164*, e61829.
[363] S. Sittichompoo, S. Kanagalingam, L. Thomas-Seale, A. Tsolakis, J. Herreros, *Atmos. Environ.* **2020**, *239*, 117765.
[364] L. Stabile, M. Scungio, G. Buonanno, F. Arpino, G. Ficco, *Indoor Air* **2017**, *27*, 398.
[365] G. Tedla, A. M. Jarabek, P. Byrley, W. Boyes, K. Rogers, *Sci. Total Environ.* **2022**, *184*, 152622.
[366] M. E. Vance, V. Pegues, S. Van Montfrans, W. Leng, L. C. Marr, *Environ. Sci. Technol.* **2017**, *51*, 9516.
[367] ANSI/CAN/UL 2904: Standard Method for Testing and Assessing Particle and Chemical Emissions from 3D Printers, American National Standards Institute, Washington DC **2019**.
[368] ISO 16000-9:2006, Indoor Air – Part 9: Determination of the Emission of Volatile Organic Compounds from Building Products and Furnishing – Emission Test Chamber Method, International Organization for Standardization, Geneva **2006**.
[369] R. German, *Metal AM* **2019**, *5*, 127.
[370] J. Damon, S. Dietrich, S. Gorantla, U. Popp, B. Okolo, V. Schulze, *Rapid Prototyping J.* **2019**, *25*, 1319.
[371] C. Kukla, J. Gonzalez-Gutierrez, I. Duretek, S. Schuschnigg, C. Holzer, *AIP Conf. Proc.* **2017**, *1914*, 190006.
[372] Y.-L. Fan, K.-S. Hwang, S.-H. Wu, Y.-C. Liau, *Metall. Mater. Trans. A* **2009**, *40*, 768.
[373] S. Banerjee, C. J. Joens, in *Handbook of Metal Injection Molding* (Ed: D. F. Heaney), 2nd ed., Woodhead Publishing, Sawston, CA **2019**, pp. 129–171.
[374] S. Pekin, A. Zangvil, W. Ellingson, in *Proc. 1998 Int. Solid Freeform Fabrication Symp.*, The University of Texas at Austin, Austin, TX **1998**, pp. 661–669.
[375] S. Roshchupkin, A. Kolesov, A. Tarakhovskiy, I. Tishchenko, *Mater. Today: Proc.* **2021**, *38*, 2063.
[376] A. Sola, A. Trinchi, in *Fused Deposition Modeling of Composite Materials* (Eds: A. Sola, A. Trinchi), 1st ed., Woodhead Publishing, Sawston, CA **2022**, p. 41.
[377] N. Cruz, L. Santos, J. Vasco, F. Barreiros, in *Euro PM2013 Congress and Exhibition - Proc.*, vol. *2*, The European Powder Metallurgy Association, Shrewsbury, Shropshire **2013**, pp. 79–84.
[378] S. Riecker, J. Clouse, T. Studnitzky, O. Andersen, B. Kieback, in *European Congress and Exhibition on Powder Metallurgy. European PM Conf. Proc.*, European Powder Metallurgy Association, Shrewsbury, Shropshire **2016**.
[379] J. H. H. Ter Maat, J. Ebenhöch, H. J. Sterzel, in *4th Int. Symp. on Ceramic Materials and Components for Engines* (Eds: R. Carlsson, T. Johansson, L. Kalhman), Springer, Dordrecht **1992**, pp. 544–551.
[380] M. K. Agarwala, R. van Weeren, A. Bandyopadhyay, A. Safari, S. C. Danforth, W. R. Priedeman, in *1996 Int. Solid Freeform Fabrication Symp.*, The University of Texas at Austin, Austin, TX **1996**, pp. 451–458.
[381] M. K. Agarwala, R. van Weeren, A. Bandyopadhyay, P. J. Whalen, A. Safari, S. C. Danforth, in *1996 International Solid Freeform Fabrication Symp.*, The University of Texas at Austin, Austin, TX **1996**, pp. 385–329.
[382] T. F. McNulty, I. Cornejo, F. Mohammadi, S. C. Danforth, A. Safari, in *1998 Int. Solid Freeform Fabrication Symp.*, The University of Texas at Austin, Austin, TX **1998**, pp. 613–620.
[383] T. F. McNulty, F. Mohammadi, A. Bandyopadhyay, D. J. Shanefield, S. C. Danforth, A. Safari, *Rapid Prototyping J.* **1998**, *4*, 144.
[384] Y. Abe, T. Kurose, M. V. Santos, Y. Kanaya, A. Ishigami, S. Tanaka, H. Ito, *Materials* **2021**, *14*, 243.
[385] J. Abel, U. Scheithauer, T. Janics, S. Hampel, S. Cano, A. Müller-Köhn, A. Günther, C. Kukla, T. Moritz, *J. Visualized Exp.* **2019**, e57693.
[386] A. Arnesano, S. K. Padmanabhan, A. Notarangelo, F. Montagna, A. Licciulli, *Ceram. Int.* **2020**, *46*, 2206.
[387] A. Boschetto, L. Bottini, F. Miani, F. Veniali, *J. Manuf. Processes* **2022**, *81*, 261.
[388] N. D. Ebrahimi, Y. S. Ju, *Addit. Manuf.* **2018**, *24*, 479.
[389] A. S. Egorov, M. V. Bogdanovskaya, D. S. Aleksandrova, V. S. Osipchik, A. S. Anokhin, V. S. Ivanov, E. V. Ivanov, *J. Phys.: Conf. Ser.* **2021**, *1758*, 012010.
[390] S. Esslinger, A. Grebhardt, J. Jaeger, F. Kern, A. Killinger, C. Bonten, R. Gadow, *Materials* **2020**, *14*, 156.
[391] D. Godec, S. Cano, C. Holzer, J. Gonzalez-Gutierrez, *Materials* **2020**, *13*, 774.
[392] H. Gong, D. Snelling, K. Kardel, A. Carrano, *JOM* **2019**, *71*, 880.
[393] J. Gonzalez-Gutierrez, I. Duretek, F. Arbeiter, C. Kukla, C. Holzer, presented at SPE ANTEC 2017, Anaheim, CA May **2017**.
[394] J. Gonzalez-Gutierrez, F. Arbeiter, T. Schlauf, C. Kukla, C. Holzer, *Mater. Lett.* **2019**, *248*, 165.
[395] L. Gorjan, R. Tonello, T. Sebastian, P. Colombo, F. Clemens, *J. Eur. Ceram. Soc.* **2019**, *39*, 2463.
[396] L. Gorjan, C. Galusca, M. Sami, T. Sebastian, F. Clemens, *Addit. Manuf.* **2020**, *36*, 101391.
[397] S. Iyer, J. McIntosh, A. Bandyopadhyay, N. Langrana, A. Safari, S. C. Danforth, R. B. Clancy, C. Gasdaska, P. J. Whalen, *Int. J. Appl. Ceram. Technol.* **2008**, *5*, 127.

 

[398] C. Kukla, S. Cano, D. Kaylani, S. Schuschnigg, C. Holzer, J. Gonzalez-Gutierrez, *Powder Metall.* **2019**, *62*, 196.
[399] T. Kurose, Y. Abe, M. V. A. Santos, Y. Kanaya, A. Ishigami, S. Tanaka, H. Ito, *Materials* **2020**, *13*, 2493. dv.
[400] B. Liu, Y. Wang, Z. Lin, T. Zhang, *Mater. Lett.* **2020**, *263*.
[401] A. C. Marsh, Y. Zhang, L. Poli, N. Hammer, A. Roch, M. Crimp, X. Chatzistavrou, *Mater. Sci. Eng.: C* **2021**, *118*, 111516.
[402] A. Pellegrini, M. E. Palmieri, M. G. Guerra, *Int. J. Adv. Manuf. Technol.* **2022**, *120*, 7951.
[403] C. M. Pistor, *Adv. Eng. Mater.* **2001**, *3*, 418.
[404] R. Prathumwan, K. Subannajui, *RSC Adv.* **2020**, *10*, 32301.
[405] C. Schumacher, E. Moritzer, *Macromol. Symp.* **2021**, *395*, 2000275.
[406] Y. Thompson, J. Gonzalez-Gutierrez, C. Kukla, P. Felfer, *Addit. Manuf.* **2019**, *30*, 100861.
[407] Y. Thompson, M. Polzer, J. Gonzalez-Gutierrez, O. Kasian, J. P. Heckl, V. Dalbauer, C. Kukla, P. J. Felfer, *Adv. Eng. Mater.* **2021**, *23*, 2100380.
[408] Y. Zhang, S. Bai, M. Riede, E. Garratt, A. Roch, *Addit. Manuf.* **2020**, *34*, 101256.
[409] D. A. Anderegg, H. A. Bryant, D. C. Ruffin, S. M. Skrip Jr, J. J. Fallon, E. L. Gilmer, M. J. Bortner, *Addit. Manuf.* **2019**, *26*, 76.
[410] C. Hopmann, W. Michaeli, in *Extrusion Dies for Plastics and Rubber* (Eds: C. Hopmann, W. Michaeli), 4th ed., Hanser, Munich, Germany **2016**, pp. 9–48.

**Antonella Sola** is the science leader in active materials at the Commonwealth Scientific and Industrial Research Organization (CSIRO, Clayton, VIC). She is driving innovation in additive manufacturing and processing technologies for the development of new materials and systems with improved functionalities. At CSIRO, Dr. Sola is leading the Fused Filament Fabrication Facility (4F), a dedicated centre for the design and production of bespoke feedstock materials for 3D printing by fused filament fabrication. She has published more than 100 papers and presented her research at numerous international conferences, with contributions regarding composite materials, biomaterials, advanced coatings, and additive manufacturing.